APPLICATION OF 2D ELECTRICAL RESISTIVITY TOMOGRAPHY TO ASSESS THE INFLUENCE OF GEOLOGY AND GEOLOGICAL STRUCTURES ON GROUNDWATER OCCURRENCE AND POTENTIAL IN KONZA AREA, KENYA

IRUNGU W.G MARGARET

I56/70284/2011

A DISSERTATION SUBMITTED IN FULFILMENT FOR MASTER DEGREE IN GEOLOGY IN THE DEPARTMENT OF GEOLOGY, UNIVERSITY OF NAIROBI

NOVEMBER, 2015

Declaration

This dissertation is my original work and has not been presented for a degree in any other University

Signature _____ Date _____

Margaret Wanjiru Gicheha Irungu

Department of Geology

School of Physical Science

University of Nairobi

This dissertation has been submitted for examination with my approval as University supervisor

Signature _____ Date _____

Dr. Edwin W. Dindi

Department of Geology

School of Physical Science

University of Nairobi

Signature _____ Date _____

Dr. Josphat K. Mulwa

Department of Geology

School of Physical Science

University of Nairobi

Declaration of Originality Form

University of Nairobi

Name of the student:	Margaret Wanjiru Gicheha Irungu
Registration number:	I56/70284/2011
College:	College of Biological and Physical Sciences
Faculty of Science:	School of Physical Science
Department:	Department of Geology
Course Name:	Master of Science in Geology
Title of the work:	Application of 2D Electrical Resistivity Tomography to Access the Influence of Geology and Geological Structures on Groundwater Occurrence and Potential in Konza Area, Kenya.

Declaration

1. I understand what plagiarism is and I am aware of the university's policy in this regard.
2. I declare that this project dissertation is my original work and has not been submitted elsewhere for examination, award of degree or publication. Where other people's work or my own work has been used, this has properly been acknowledged and referenced in accordance with the University of Nairobi's requirements.
3. I have not sought or used the services of any professional agencies to produce this work.
4. I have not allowed, and shall not allow anyone to copy my work with intention of passing it off as his/her own work
5. I understand that any false claim in respect of this work shall result in disciplinary action in accordance with University Plagiarism Policy

Signature:

Date:

Acknowledgements

My sincere thanks go to my supervisors, Dr. E. W Dindi and Dr. J. K Mulwa for guidance and advice during my studies. You helped me shape my thought.

I am grateful to Dr. Z. Kuria for the support he provided me through the application techniques of Electrical Resistivity Tomography equipment, I learnt a lot from his experience. My sincere thanks go to C. Atonya for the guidance he granted me through the application of GIS. My gratitude also goes to Chairman Department of Geology and the entire staff for all the encouragement during my studies.

I thank the Ministry of Water and Irrigation for awarding me a Scholarship to pursue a Masters Degree course and allowing me to use available information and equipment. I thank Director Water Resources, Mr. C. Juma and Deputy Director/ Ground Water, Mr. M. Munyao. Am also grateful to Water Resource Management Authority staff, especially Ms. Agatha Njuguna and Mr. B. Ngoruse for all the assistance they offered me during my studies.

I want to recognize with pleasure the team that I worked with in the field Ms. E. Njeri, Mr. R. Kamau, Mr. G. Mwaura, Mr. C. Mundunyi and Machakos assistance team.

I wish to thank my family members, especially my Father, Mother, Husband and my three children for the encouragement and understanding during my studies.

Last, but not the least am grateful to the Almighty God for giving me his grace to accomplish my studies.

Abstract

Groundwater occurrence in metamorphic rocks is highly influenced by geological structures. These geological structures, unless mapped with precision, groundwater exploration may end up with low yielding or dry boreholes. Konza area herein referred as study area; is dominated by metamorphic rocks and geological structures in the area are less known.

Geologically, the study area is underlain by metamorphic rocks covered by black soils. The crystalline nature of igneous and metamorphic rocks in study area lack permeability zones for groundwater occurrence and transmission, except in weathered or fractured condition.

This dissertation attempts to advance knowledge of groundwater occurrence, improve techniques of hydrogeological survey within the Mozambique Metamorphic belt terrain and reveal geological structures undetected in the area.

An integration of geophysical techniques was applied. Electrical Resistivity Tomography (ERT) was used to provide 2D sections to outline the geological structures. This method was complemented with Vertical Electrical Sounding (VES) and borehole data to depict groundwater occurrence in the study area.

This study delineated groundwater potential regions for future groundwater exploration. A general understanding of the influence of geological structures to groundwater occurrence in the study area was achieved through the study. The depth of bedrock and geological structures was estimated with high accuracy. The problem related to low yield and dry borehole of groundwater drilled within the study area was identified. This is mainly due to the dominance of clay material filled within fracture zones. The Shallow unweathered formation was also noted to be related to this problem.

Fracture lines cutting through in a north west – south east direction running parallel to each other was mapped in the area.

Table of Contents

List of Appendices

LIST OF FIGURES

CHAPTER ONE

1.1 Introduction

Water is one of the most basic components of human existence and socio-economic development, but its availability is usually taken for granted. This study focuses on groundwater characteristics in Konza area, herein referred to as study area; of southeast Kenya. The study area lies within Mozambique Metamorphic belt. The occurrence of groundwater within these rocks in the area is limited to fracture zones. This study attempts to isolate these fracture zones in order to improve the quality of future groundwater exploration in the study area. The proposed Konza Technology City is expected to be developed within the study area and water will play a vital role, especially during the initial construction of the city. Initial water demand of 10,000 cubic meters per day is projected by the Government of Kenya, for the technology city (Ministry of Information and Communication, 2012).

Groundwater is a key natural resource in many parts of the world. Equally groundwater is important in specific climate and hydrological contexts such as arid and semi-arid areas, where it is commonly the only safe source of water. In Konza area groundwater is the only reliable source of water supply for domestic and animal use. Kilimanjaro water supply through Nor Turesh Water supply is unreliable and inadequate.

Groundwater exploitation has the potential for boosting water supplies in Kenya, its use is limited by poor water quality, over exploitation, saline intrusion along the Coastal areas and inadequate knowledge of the occurrence of the resource (Mumma et al., 2010).

The hydrogeology and structural geology of the study area is less known, thus siting of boreholes in the area in the past has been poor making groundwater exploitation expensive. Metamorphic rocks dominating the study area, make groundwater resource exploration difficult, thereby affecting the socio-economic activities of the inhabitants. In this complex geological setting, there is need to understand the groundwater occurrence in relation to geology and geological structures.

The study focuses on the complex Mozambique Metamorphic belt within the study area which has undergone several tectonic deformations. The study also endeavors to determine any relationship between geological structures and groundwater occurrence within the study area using geophysical 2D groundwater investigation techniques and hydrogeological data.

1.2 Literature Review

This literature review provides an overview of the occurrence of groundwater and geological structural control of groundwater mainly within metamorphic systems. The review outlines commonly applied geophysical techniques in groundwater prospecting and subsurface geological structures in different areas.

In a number of researches, it is noted, groundwater in metamorphic rocks is limited to fracture zones. Davis and DeWest (1966) in their hydrogeological book stated that few tasks in hydrogeology are more difficult than locating drilling sites for water boreholes in igneous and metamorphic rocks. They recognize a well-established concept that boreholes located in geological faults or fracture zones can produce high yields. These zones of broken rock material and deep weathering usually have high transmissivity, providing avenues for groundwater flow.

Geological mapping of the study area started in 1952. Baker (1952) carried out the geological mapping of the area. He suggests detailed geological mapping in the area was not possible due to lack of exposures. This made it difficult to relate borehole results with geological structures. He further states that, geological structures must be considered when siting boreholes in the area.

During a recent hydrogeological survey by Njoroge (2013) in the study area, it is observed, the area is located in a region that has poor groundwater potential. Particular boreholes have high yields of upto 26 cubic meters per hour. According to Njoroge (2013), this exception is because of the possible location of the boreholes on a fault line.

Many researches undertaken in various areas have evaluated groundwater zones in different regions. Olayinka et al. (2004) assessed and located groundwater in crystalline metamorphic rock terrains in Igbeti, southwest Nigeria, using electromagnetic profiling and resistivity sounding. In their results, they identified three main targets for groundwater; these include weathered zone, fractured zone and vertical dykes.

Studies of the behaviour of groundwater in crystalline rocks usually point out that one factor or a set of factors are responsible for high well-productivity, although no conclusive evidence is available in some studies. Neves (2006), in the study of well productivity controlling factors in crystalline terrains of southeastern Brazil, has outlined some of these factors, to include faults and joints. In conclusion, it is noted in the study that the fundamental structures for obtaining high well yields from crystalline rocks are faults and joints that were originally open to extensional stress during tectonic reactivations.

Wanjohi (2013), during the study of characterization of structural control on groundwater in Enderit area, Kenya, established that faults have two effects. They may facilitate flow by providing channels of high permeability or they may prove to be barriers to flow by offsetting buried structures. The results of the study showed Enderit area has numerous faults and fractures buried at shallow and deep depths.

In the study of evaluating geological and structural influence on groundwater in El Obeid area, western Sudan, Elhag and Elzien (2013) notes that two types of folds (anticline and syncline) act as accumulation and drainage channels of groundwater flow in the study area. They note, the area is affected by tectonics that has caused faulting, folding and fracturing. The four main structures investigated during the study include faults, fractures, folds and veins. They note, the structures are responsible for the dryness of wells in parts of the area.

Boreholes can be recharged by faults found near the boreholes. Mulwa et al (2005) carried out investigation of how faults influence the occurrence of groundwater through distribution, flow and yield in Ngong area, Kenya. They noted, when filled with

weathered material, faults act as excellent aquifers. The yield from boreholes drilled into such faults is high. Mulwa (2001) mapped and delineated geological structures using electrical resistivity method in Kiserian-Matathia area in Kenya. Fault influence to borehole yield and flow direction of groundwater was determined during the study. In conclusion, it is noted, fractured and weathered formations are excellent aquifers. Boreholes with highest yield in the area, are those located in areas immediately recharged by faults.

Henriksen and Braathen (2006) observed in Sun fjord, western Norway that where there is a high fracture density and connectivity with negligible fracture fillings, potential largest abstraction of groundwater occurs. They note the effect of fracture lineaments and in-situ rock stresses on groundwater flow. Due to fracture heterogeneity, well yield in crystalline hard rocks possessing only secondary porosity, permeability is difficult to predict. They concluded that this concept may differ from one rock type to another, and even for a given rock type. The yields of adjacent wells may also differ by many orders of magnitude.

Al-Taji (2008) evaluated geologic and structural influence on groundwater in Irbid area in north Jordan. Joints and faults act as drainage channels of groundwater flow and aquifers in the Irbid area. The influence of faults and joints occur as barriers to groundwater flow. Clay layers and dense compact rock units underlying the aquifers often act as controls to the downward migration of groundwater.

Ahmadov et al. (2007) noted that fault rock extent and permeability are crucial for determining the fault-perpendicular flow component. They assessed the role of small-scale features on upscaled fault zone permeability in the valley of Fire State Park of Nevada. They developed a conceptual model for upscaling of fault zone permeability at the end of the study. Field observation and laboratory analysis revealed, during the study in Nevada, the complicated nature of slip bands.

To better understand groundwater flow through fracture zones in the northern desert of Israel, Weiss et al (2006) developed a groundwater flow model through a generated

network of fractures. It was, however, noted during the study in Israel that, often during modeling, it was impossible to get close enough to clearly examine the discontinuity planes.

Kuria (2000) used SCHINV program Barongo (1989) during the study of Naivasha area in Kenya and it was noted that in this program, the “sensitivity” matrix is decomposed into a parameter eignenvector matrix.

Billing (2008) pointed out that electrical methods employed in geophysical prospecting are many and vary, both in technique and in the properties measured. Some methods utilize natural electrical currents, whereas other methods use artificial currents introduced into the rocks by direct contact or induction. Electrical methods in general are effective for shallow depths not exceeding 450m. Consequently, they are more useful in the search for shallow ore deposits or water supply than in the search for petroleum.

Vertical Electrical Sounding (VES) is a commonly used geophysical technique of water prospecting in areas of deep weathering bedrock. Sabet (1975) used VES to locate groundwater in southeastern Virginia. The objective of using VES in the study area in Virginia was to obtain a true resistivity log, similar to induction log well without drilling of well. VES is a non invasive technique used for a long time in groundwater exploration. Resistivity variation property in small changes in water salinity makes VES a low cost technique suitable for groundwater exploration.

Chikwelu and Udensi (2013) applied direct current resistivity in Minna, Nigeria, to study groundwater potential in metamorphic structure, using conventional VES method. The results obtained from interpreting the data collected, showed the efficiency and suitability of electrical resistivity method in probing for geological subsurface structures and underground water in the basement complex area in Nigeria.

In delineating groundwater potential zones in Ibadan, Nigeria, Coker (2012) used VES to create longitudinal conductance map. In the map, groundwater zones classification of good, moderate and poor is outlined. From the study, weathered and fractured horizons

were revealed. In conclusion, from the study results, the electrical resistivity data give reasonably accurate results among other methods used to understand subsurface layers and basement configuration in groundwater prospecting.

The Electrical Resistivity Imaging (ERT) is a survey technique developed to investigate areas of complex geology where the use of vertical resistivity sounding and other techniques is unsuitable (Griffiths and Barker, 1993). They note that in many situations, particularly for surveys over elongated geological bodies, the imaging technique gives a clearer picture of the cross-section of the body. They conclude by pointing out that, with ERT and the software so far developed, in areas of modest subsurface geological complexity where some control is available and where the structures are two-dimensional, estimates of the true geoelectric sections can be obtained down to depths of between 100 to 200 meters.

In modern survey, resistivity imaging is the preferred tool to characterize productive lineaments. Chandra et al. (2006) used magnetic, Self Potential and resistivity imaging in Karnataka, India, to characterize lineaments and locate groundwater potential zones in a hard rock area. They noted that improvement in resistivity methods using multi-electrode arrays leads to an important development in electrical imaging for subsurface surveys.

In their studies on integrating geophysical techniques, VES and ERT, Mohamed et al. (2011) mapped groundwater aquifers in Nuba Mountain, Sudan, on complex geological settings, in crystalline metamorphic terrain. The data acquired from the two techniques in the study area overlapped to provide better interpretation of the hydrogeological setting of the aquifer under study. They inverted VES data smoothly and merged it with ERT in three-dimensional resistivity grid.

Githinji (2013) integrated electrical resistivity and seismic methods to characterize geological formation of Maira dam site, Nambale area in Kenya. The 2D electrical resistivity method used in the study area measured the electrical property of the

subsurface materials. Seismic refraction method enabled the interpretation of morphology of the bedrock and depth to the bedrock.

In delineating lineaments in a typical hard rock in west Bengal, India, Acharya (2013) used a methodological approach of ERT and VES. In conclusion, it is established, integrating geological and electrical resistivity data are necessary in hard rock areas to ascertain the subsurface features of lineament. It was concurred, for delineation of lineaments in the study area, ERT is the preferred tool to characterize the lineaments with their correlation to fractures.

In the methodological approach on subsurface characteristics of active fault, Kuria (2011) integrated geophysical techniques (electrical resistivity- ERT and ground magnetic survey) to evaluate axial rift fault in Magadi area, Kenya. The method adopted in the study area established fault geometry, characterized faulting activity and determined constituents within local active faults. In conclusion of the study higher resistivity showed sheared sediments characteristic of active deformation.

Driscoll (2005) stated that, hydrogeologists now know that well yields depend on the presence of joints and fractures and how well these features interconnect. It is further noted, fracture traces represent zones of increased porosity and hydraulic conductivity in igneous and metamorphic rocks.

It is from the reviews mentioned above that current research in the study area is directed toward expanding the applications of resistivity sounding survey to resistivity tomography. This is to advance the technique to determine geological structure features that influence the occurrence of groundwater in the study area. This will improve better site identification for drilling thus increase the success rate of boreholes drilled in the area.

This study attempts to relate geological structural elements acquired from Electrical Resistivity Tomography (ERT), Vertical Resistivity Sounding (VES) and borehole data. The data will assist to identify these fracture zones and lines where groundwater yields are high in the study area.

1.3 Problem Statement

Limited structural knowledge in the study area has made groundwater exploration difficult and groundwater exploitation expensive. Better understanding of groundwater systems and the occurrence go a long way in increasing the success rate of drilling boreholes in the area.

Groundwater investigation in the area has earlier been carried out using electrical sounding technique. This technique does not consider horizontal changes in the subsurface resistivity. Developing subsurface imaging using electrical resistivity tomography survey to map areas with complex geology has made it possible to delineate subsurface fractures. These fractures influence the occurrence, distribution and flow pathways of groundwater in the area. This research has, therefore, improved our understanding of groundwater occurrence in the study area through geophysical techniques.

1.4 Aim and Objectives

The aim of the study is to investigate how geological structures influence the occurrence of groundwater in the study area. This will enable identification future drilling sites of boreholes for water use.

The specific objectives include;

1. Identify and delineate geological structural elements from Electrical Resistivity Tomography techniques
2. Assess the inter-relationship between geological structures and borehole yield
3. Assess the role of geological structural framework on variability of groundwater occurrence

1.5 Justification and Significance of the Research

The study area is expected to provide huge opportunities after the construction of the Technological City within the region. These prospects will raise the water demand in the area, especially during the initial construction of the city. Although Thwake dam located along Thwake river, some 20 km from the area, is projected to serve the area with sufficient water supply. Immediate interventions require availability and access to water for domestic and productive use. Groundwater is the only reliable water supply in the area. Therefore, better understanding of groundwater occurrence will lead to productive aquifers in the area.

The results from this study in conjunction with other studies can aid in the selection of site for borehole drilling. In the context of this study, therefore, it is expected availability of groundwater will improve and thus underpin socio-economic development in the area.

CHAPTER TWO

2.1 The Study Area

This chapter provides a general introduction to the study area with emphasis on geology and groundwater resources. Groundwater is the only reliable source of water in the study area. Surface water only occurs within seasonal rivers during rainy periods. Boreholes earlier sited with vertical resistivity sounding technique alone, provide low success rate in the study area.

2.2 Location and General Description

The study region describes an area of about 110 square kilometres in eastern Kenya. It is bounded by latitudes $1^0$38'S and $1^0$45'S and longitudes $37^0$07'E and $37^0$12'E. The area covers east of Makueni County. Figure 2.1, shows a sketch map of the study area in Kenya.

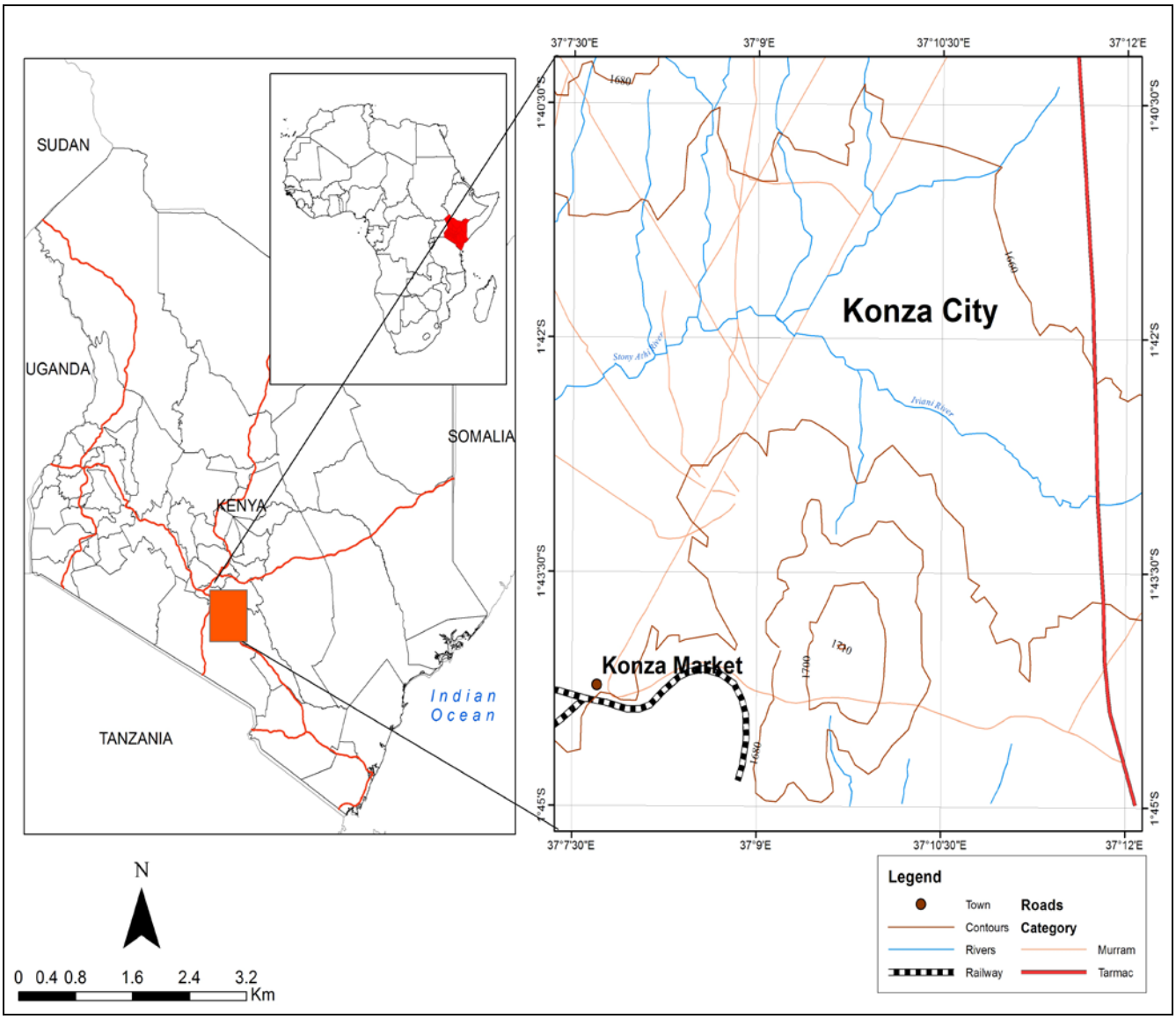

Figure 2.1: Map of the location of the study area

The area is well served by roads. The Nairobi-Mombasa railway and a tarmac road pass through the area. In the farmlands, tracks are numerous with dry-weather roads servicing the area. The weathered roads become impassable during the heavy rains, due to the rain water washing away the latarite material used to construct the roads.

2.3 Climate and Vegetation

The study area is characterized by an arid climate with two distinct rainy seasons. March-May occur as the long rains and October – December as the short rains seasons. The mean annual temperature is about 21^0C while the maximum temperature is about 35^0C. The mean annual precipitation is about 650mm. Due to high temperatures; the mean annual evaporation is high reaching around 1800 mm/d. The vegetation cover comprises; grass, shrubs and scattered indigenous trees.

2.4 Land Use and Land Resources

The availability of water is often a key factor in determining the patterns of human settlements and socio-economic development. Within the study area, there is a critical limitation on water resources availability.

The study area has predominant rural characteristics. Rural and scattered settlements with varying population density and small-scale subsistence economic activities and livestock occur in the area. Most of land development is low, probably due to lack of essential facilities such as water supply. However, increase development, especially in Malili centre, south, and Konza market, west of the area, by groups who include farmers, pastoralists and commercial entrepreneurs.

2.5 Physiography and Drainage

The physiography of the area divides into two, undulating Waami hills and Iviaini river valley. The valley is the lowest point on the Kapiti plain. The topography gently slopes to the west with altitudes ranging from 1880 to 1660 meters above sea level as shown in figure 2.2.

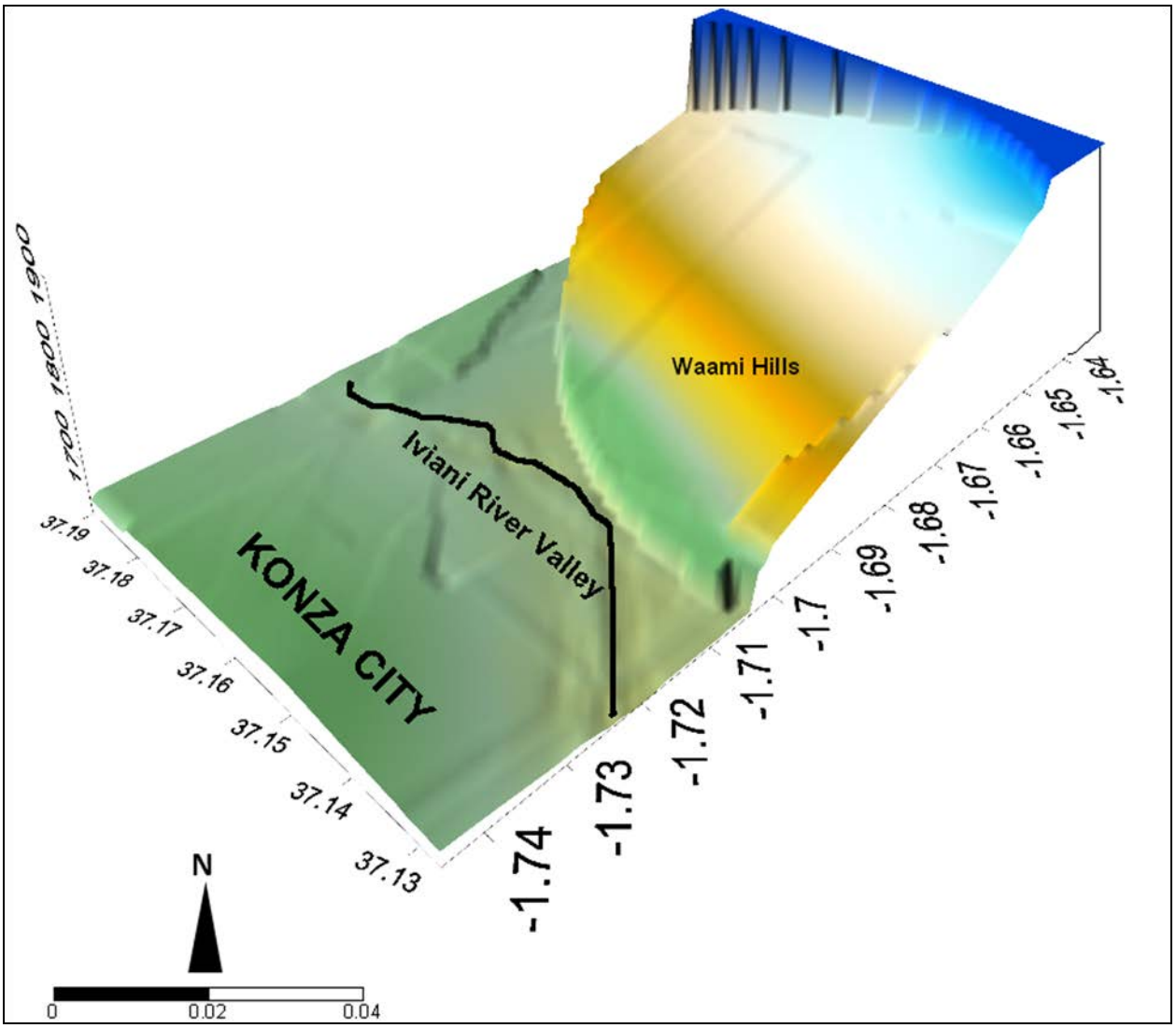

Figure 2.2: Physiography of Study Area

2.6 Regional Geology of the area

Geological works of the area carried out by Baker (1952) covered the southern part of Machakos region. It consists of, intensively folded Metamorphic System gneiss and schists which include amphibolites and quartzes as well as the predominating biotite granitoid gneisses. According to Baker (1952) these rocks are metamorphosed and granitized to a considerable degree. Overlying the Metamorphic System in the western part of the area is the Kapiti phonolite lava of Miocene age. In the south and south-eastern parts, there are seven olivine basalt vents of late Pleistocene age. Much of the

area in the west is covered by black cotton soil. In the east, sandy and brown earths, murrams and local iron **l**atarite predominate.

Baker (1952) states, the rocks of Metamorphic System were originally sedimentary rocks. These rocks are metamorphosed and some granitized to a greater or lesser extent. The rocks are invaded by basic igneous rocks before metamorphism. Because of an east-west, compression the original sediments were folded and depressed into the lower parts of the earth's crust. They are metamporphosed, partly granitized and had a foliation impressed on them. Due to granitization, the heterogeneous rocks are converted to uniform granitoid gneisses. The granitoid gneisses represent the end products of the metasomatic process.

2.7 Detailed Geology of the study area

The main formations are not conspicuous in the field area. They are covered by black peneplain soils. The formations are described below in their stratigraphical order. The geological sketch map in figure 2.3 shows the main formations in the study area.

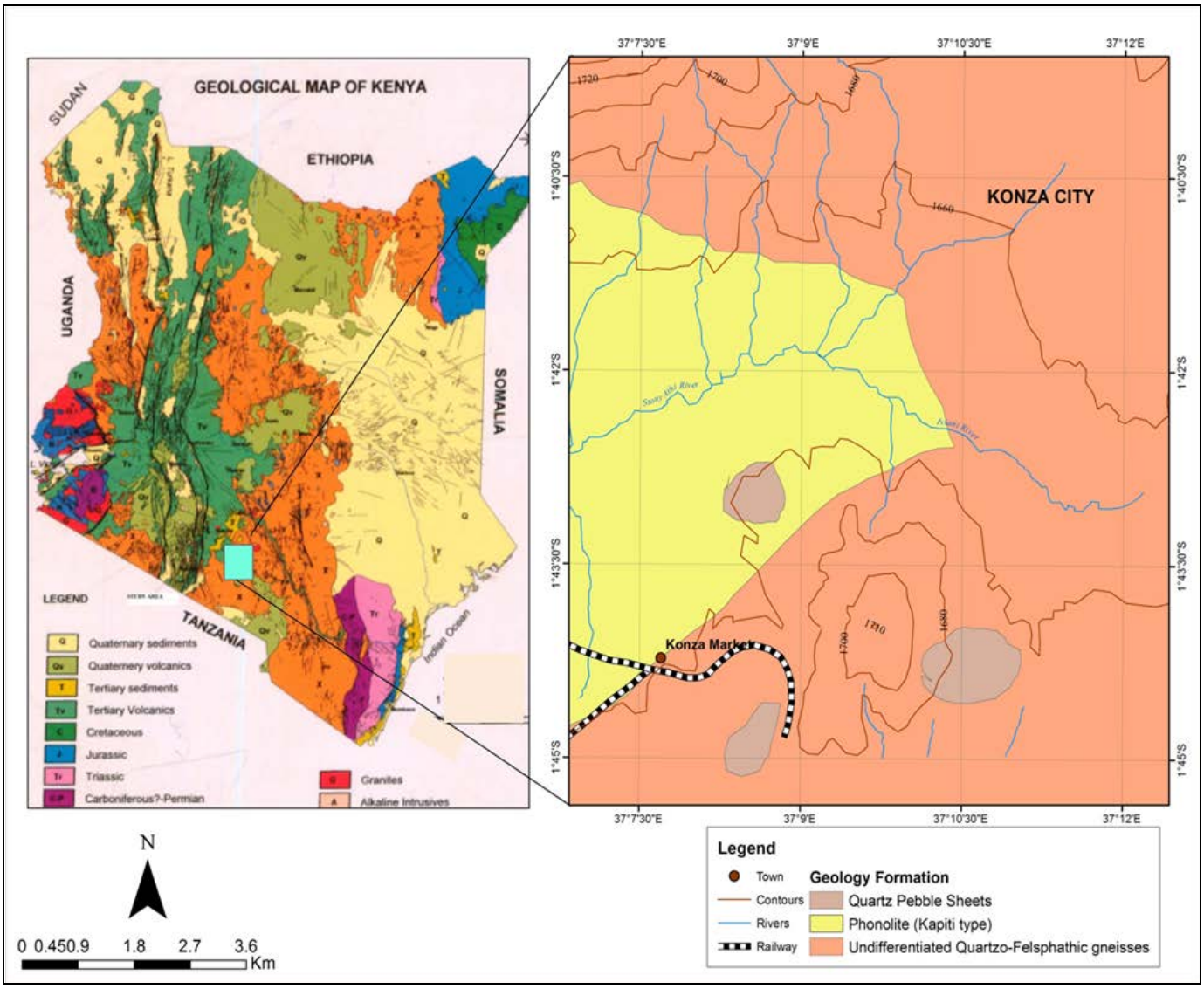

Figure 2.3: Map of Regional and Local Geology, modified from Baker (1952)

2.7.1 Recent Sediments

Black cotton soils cover much of the area. Recent events give rise to soils and laterites of various types. Quartz pebble sheets occurs on the south-west and eastern part of the study area. The pebble sheets found in the area are of late Pleistocene age (Baker, 1952).

2.7.2 Tertiary (Miocene)

Overlying the Metamorphic rocks in the western part of the area is the Kapiti phonolite, lava of Miocene age. Black cotton soil covers the Kapiti plains, where bands of quartz pebbles and calcrete horizons occur.

The Kapiti plains of the area are extremely level, cut only by seasonal stream channels. Inselbergs breaks and slopes becoming more undulating until it amalgamated into mountainous areas (Baker, 1952).

2.7.3 Undifferentiated quartzo felspathic gneisses

The area lies within the Mozambique belt of which forms the Precambrian rocks of eastern and central Kenya. The metamorphic rocks of the area consist of folded rocks metamorphosed and granitized. The shape and relationship of the large bodies of granitoid gneiss occur as granitiod domes resulting from upwelling of granitic material. Baker (1952) has outlined various groups of metamorphic rocks in the area. He suggests that much of the metamorphic rocks are bedded. Regular sequences of the beds can be traced for considerable distances. He further states that, the granitoid gneisses are homogeneous and unbedded. They often outcrop as large slabs or blocks on the summits of hills or form more or less flat exfoliation pavements.

2.7.4 Geological Structures

Geological structures are not easy to identify, especially within the study area as there are no rocks exposed. This is due to the thick black soils covering the surface.

2.8 Soils

Black cotton soil covered most of the area. There are small patches of local iron lateritic soil. The black cotton soil overlies weathered sediments characteristic of metamorphic system rocks.

2.9 Surface and Groundwater Resources

2.9.1 Water Resources

The poor water supply is alarming. There is inadequate surface water due to seasonal rivers. Groundwater is available for domestic use. It is unevenly distributed mainly because of the rock formation. Figure 2.4 shows surface drainage and borehole distribution in the area.

2.9.2 Surface Water Resource

There are ephemeral tributaries to include Iviani river which drains into the main river Stony Athi during flash floods. There are inadequate storage structures to collect and regulate the flow. This can be explained by the fact that there are occasional flash floods. Very little percolation occurs due to the formation.

2.9.3 Groundwater Resource

Many boreholes sunk on account of lack of perennial surface water provide low yields or occurs dry in the area. The borehole yields range from 26 cubic meters per hour to dry.

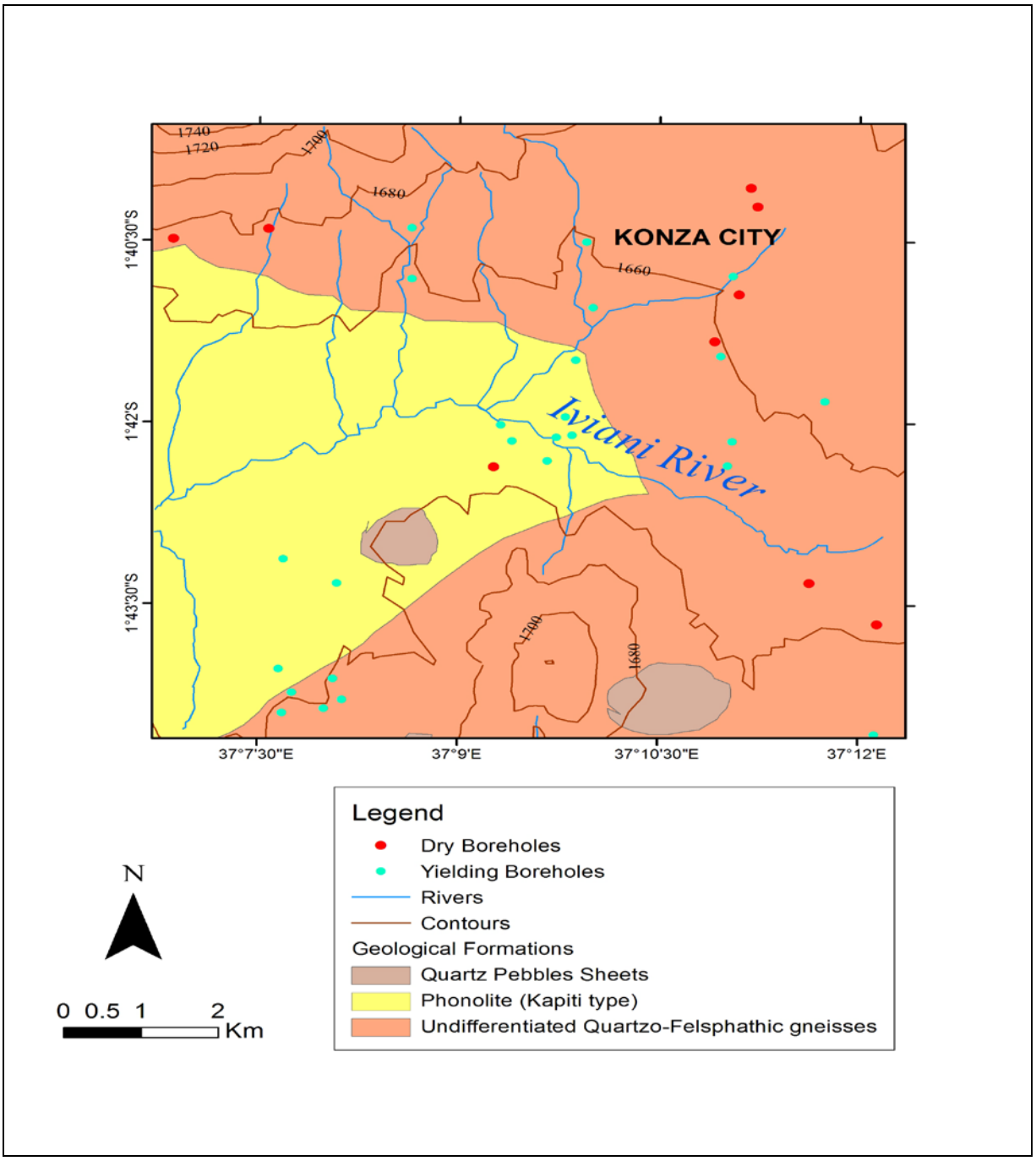

Figure 2.4: Surface drainage and borehole distribution in the Study Area, (modified from Baker, 1952)

CHAPTER THREE

3.1 RESEARCH METHODOLOGY

3.1.1 Introduction of methods

This research adopted an integrated hydro-geophysical approach where data was analyzed simultaneously to determine the relationship between any geological structures and groundwater occurrence in the study area. The ERT method was used to improve the understanding of the hydrogeological setting in the area. Vertical electrical resistivity sounding technique was used to approximate the extent of geoelectrical and weathering process, in terms of depth.

The methodological approach applied in this research commenced with desktop studies. Data from Ministry of Environment, Water and Natural Resources especially the borehole data was reviewed. This gave insight into obtaining the general understanding of the geology and hydrogeological of the study area. Review of other information during desktop studies includes topographic maps, satellite data and available literature of the study area.

During desk top studies, the geological report of the study area was reviewed to understand the geological formation of the area. Boreholes data were compiled in excel sheet and later overlaid on the geological map. This enhanced representation of boreholes in relation to geology of the area. Borehole logs of some boreholes were also reviewed to determine the type of geological formations at different depth.

Pre-existing work was also assessed to understand its relevance to the current research. During these reviews, gaps were identified and new ideas conceptualized.

The methodological approach in this research involves the integration of electrical resistivity tomography together with vertical resistivity sounding, common geological exploration methods. These methods are used to obtain information on the character of formations and on the presence of groundwater during field work. Several studies have integrated various methods to assess geological structures and groundwater zones.

VES is commonly useful in water prospecting in areas of deep in-situ weathering of fresh bedrock (US Department of Energy, 2000). Presence of horizontal or gently dipping beds of different resistivity is best detected by this technique. Kearey et al. (2002) explains this method in detail. They illustrate different processes of interpretation of VES including curve matching of simple layer case and multilayered structures. They indicate that, interpretation of VES data suffers from non-uniqueness arising from problems known as equivalence and suppression.

Electrical Resistivity Tomography (ERT) allows to conduct fast data acquisition and to obtain underground two-dimensional images with high resolution suitable for fracture identification (Qarqori et al., 2012). Modelling of data, acquired using this technique is carried out through inversion. Inversion is geophysical data processing procedure. It is applied to the electrical potentials measured between the electrode pairs to obtain the resistivity structure along the current flow lines. The inversion computation is both complex and intense. It yields a two-dimensional or three-dimension vertical cross-section of the true subsurface resistivity beneath the electrode array (Loke, 2001).

A pseudosection is a diagram presenting plot of data along a profile traverse line. The pseudosection contouring method is for use in 2-D imaging survey. The pseudosection gives a very approximate picture of the true subsurface resistivity distribution. It enables the presentation of the measured apparent resistivity values in a pictorial form. It is useful as an initial guide for further quantitative interpretation Loke (1999). This approach seeks to elucidate the relationship between geological structures in the study area and groundwater occurrence using high resolution. This method was used to process data acquired from the study area. Section 4 in this dissertation has highlighted some of the steps used when applying this method.

Faults and igneous rock intrusions are common structural elements located and defined using geophysical methods in the study area. This study further asserts the effectiveness of an integrated approach to fracture and fault characterization. This approach is useful in groundwater exploration, especially in terrain, previously classified as difficult, hydro geologically.

Geophysical techniques are useful in detection of contrasts in different physical properties of materials. Surface geophysical methods are non-intrusive and non-invasive. Thus avoiding the disruption caused by intrusive investigative methods such as drilling and pitting. Electrical methods utilize direct currents or low-frequency alternating currents to investigate the electrical properties of the subsurface. ERT works well in both the vadose and saturated subsurface zones. As earlier pointed out, VES and ERT geophysical methods were used in acquiring data in the field within the study area. It is noted that both methods are equally important as they complemented one another during the collection and analysis of data.

3.2 Theory of the methods

3.2.1 Vertical Electrical Sounding (VES)

VES technique is also referred to as 'electrical drilling' or 'expanding probe'. It involves increasing electrode separations around a mid-point. The technique is useful in hydrogeology to define horizontal zones of porous strata. Thus making it the most commonly used geophysical technique in water prospecting. It is also useful in geotechnical surveys to determine overburden thickness and depth, structure and resistivity of metamorphic rocks (Telford et al., 1990) and flat-lying sedimentary beds.

Extrapolation of geological information in the study area was achieved from earlier surveyed and drilled boreholes along two profiles. VES technique was earlier applied as a geophysical survey method to acquire the geological information in the area for boreholes BH 10 and BH VES 2.

3.2.2 Electrical Resistivity Tomography (ERT)

This is a geophysical technique known as electrical imaging or electrical tomography. It is useful in describing resistivity structure of near-surface. In the study area, the technique was used complementarily with VES data to describe the nature and geometry of the formations. Features that govern groundwater occurrence, resistivity

property of the ground and structural feature in the area are also described using this technique.

ERT allows to conduct fast data acquisition and to obtain underground two-dimensional images with high resolution suitable for fracture identification (Qarqori et al., 2012). Resistivity imaging is particularly useful in clayey ground where methods such as the ground penetrating radar (GPR) are less effective. It helps define translational boundaries that are difficult to detect using other geophysical methods (Griffiths and Barker 1993).

Direct Current (DC) technique entails injecting an electrical current in the ground between two electrodes and then measuring the induced potential between two potential electrodes. Two electrical resistivity methods, applying DC technique, were useful in investigating the study area during field work; the vertical electrical sounding and electrical resistivity tomography methods. This section outlines the basic principles of direct current electrical resistivity methods. In the resistivity method, artificially-generated electric currents are introduced into the ground and the resulting potential differences are measured at the surface. The resistivity of a material is defined as the resistance in ohms between the opposite faces of a unit of the material (Kearey et al., 2002).

For a conducting cylinder, Figure 3.1, of resistance δR, length δL and cross-section area δA the resistivity ρ is given by equation 3.0;

$$\rho = \frac{\delta R \delta A}{\delta L} \qquad \text{----------3.0}$$

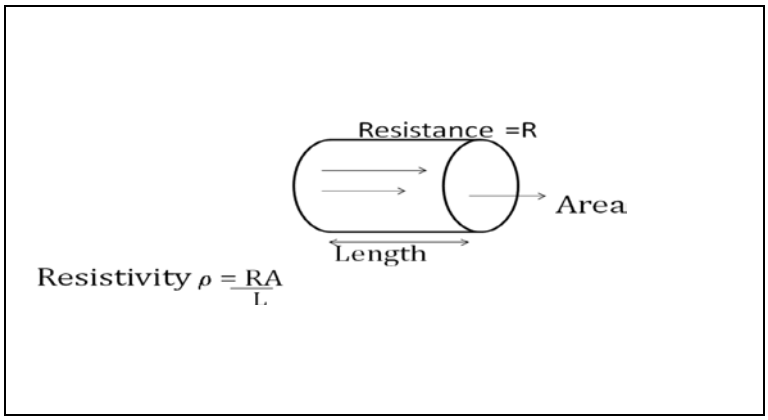

Figure 3.1: Parameters used in defining resistivity

Resistivity measurements of the surface of the earth (an infinite half space below) seen in Figure 3.2 can be resolved using equation 3.1. Where V is the potential at distance r from current source I and ρ is the resistivity. The SI unit of resistivity is ohm-m and the reciprocal of resistivity is conductivity.

$$V = \frac{\rho I}{2\pi r^2} \quad \text{---------- 3.1}$$

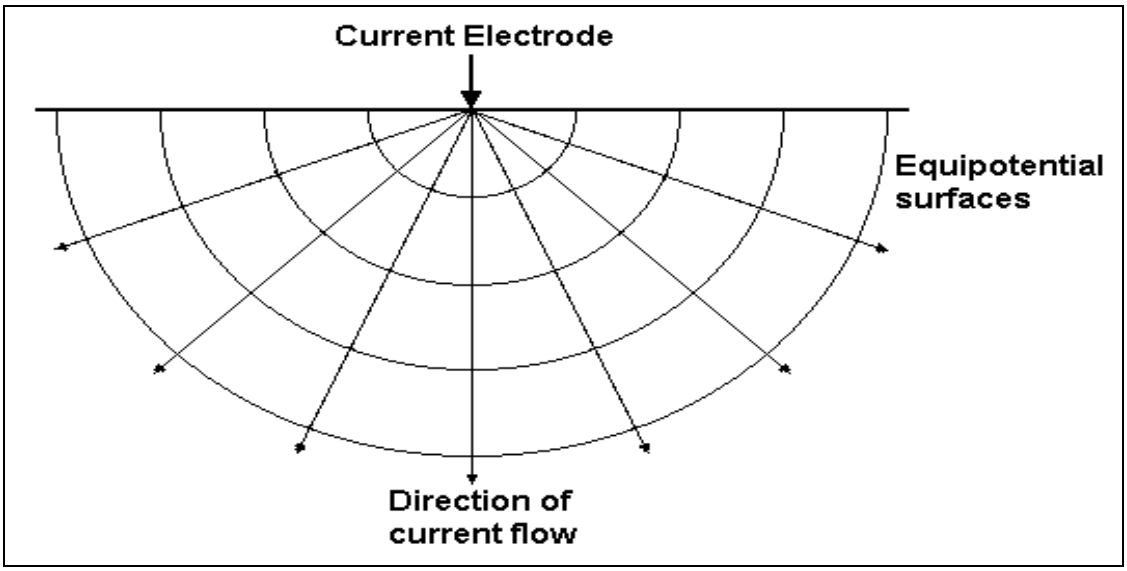

Figure 3.2: Potential and Current Distribution (after Loke, 2001)

Figure 3.3 shows the general four electrode configuration. Where C1 and C2 are the current electrodes as source and sink respectively. P1 is the detection point of potential due to source C1 and potential due to sink C2 is P2. The generalized form of electrode configuration is shown under Figure 3.4.

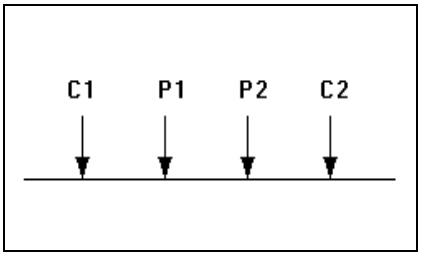

Figure 3.3: Conventional array with four electrodes (after Loke, 2001)

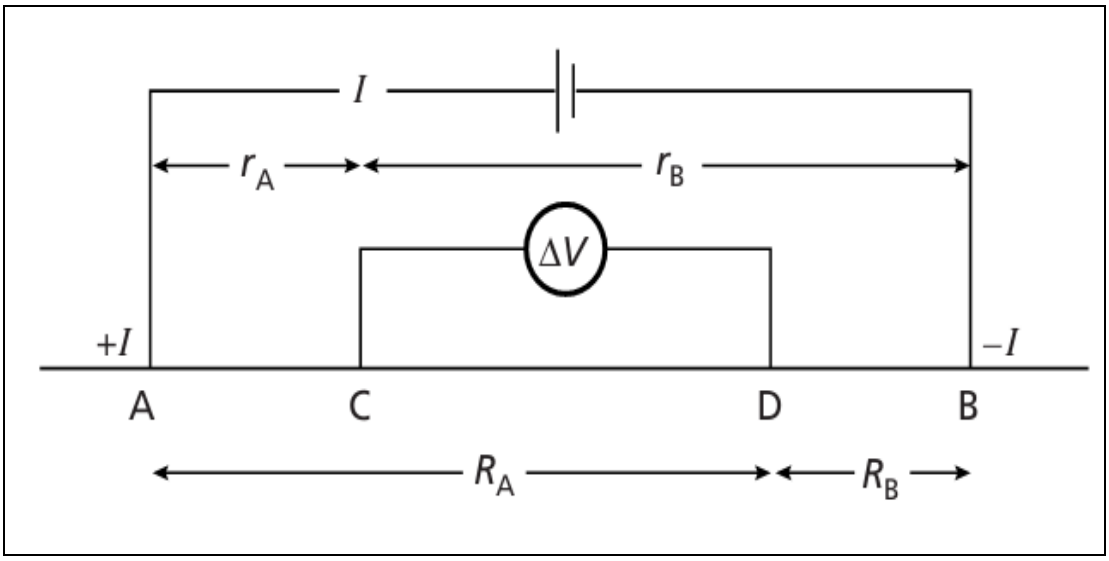

Figure 3.4: Generalized form of electrode configuration (after Kearey et al., 2002)

The current electrodes A and B act as source and sink, respectively. At the detection C the potential due to the source A is $+\rho I/(2\pi_{AC})$, while the potential due to sink B is $-\rho I/(2\pi_{CB})$. The potential different measured Lowrie (2007) connected between C and D is;

$$\Delta V = \rho I/2\pi r \{(1/^{r}AC - 1/^{r}CB) - (1/^{r}AD - 1/^{r}DB)\} \quad \text{----------3.2}$$

Thus;

$$\rho = 2\pi r\Delta V/ I\{(1/^{r}A - 1/^{r}B) - (1/R_A - 1/ R_B)\} \quad \text{----------3.3}$$

The mathematical demonstration for deriving the equation is given by Keller et al. (1966).

Any computed value of resistivity is then known as apparent resistivity ($\rho_{a)}$ because it is not true resistivity of a layer and will be a function of the form of in-homogeneities. Apparent resistivity values computed from the resistance measurements using the formula relevant to the electrode configuration is used (Lowrie, 2007). The apparent resistivity is then a function of the measured impedance (ratio of potential to current) and the geometry of the electrode array. Depending upon the survey geometry, the

apparent resistivity data plot is in form of one dimensional model or 2D cross-sections in order to define anomalous regions. The current electrode separation must be chosen so that the ground energizes to the required depth.

DC resistivity methods can be divided into various subcategories depending on the geometrical arrangement of electrodes. The most common are Schlumberger sounding and dipole sounding. The main disadvantages of these methods are their sensitivity to lateral in-homogeneities and limited capacity of depth prospection (<1500 m) (Lopez, 1995). The Schlumberger configuration was used for acquisition of data in the field for this research. Kearey et al., (2002) have explained various electrode spreads in relation to their formulas.

The equation for Ohm's law in vector form for current flow in a continuous medium (Loke, 2001) is given by;

$$\mathbf{J} = \sigma E \qquad \text{----------} \qquad 3.4$$

where σ is the conductivity of the medium, **J** is the current density and **E** is the electric field intensity. The relationship between the electric potential and the field intensity is given by;

$$\mathbf{E} = -\nabla\phi \qquad \text{----------} \qquad 3.5$$

Combining equations (3.4) and (3.5), we get

$$\mathbf{J} = -\sigma\nabla\phi \qquad \text{----------} \qquad 3.6$$

For the 1D case, where the subsurface is restricted to several horizontal layers, the linear filter method is more useful. For 2D and 3D cases, the finite-difference and finite-element methods are the most versatile. Loke (2001) has explained more on the use of forward modeling computer program for 2D structures.

Actual field surveys are invariably conducted over an in-homogeneous medium where the subsurface resistivity has a 2D distribution. The resistivity measurements are still made by injecting current into the ground through current electrodes (in Figure 3.4), and measuring the resulting voltage difference at potential electrodes. From the current (I) and potential ($\nabla\phi$) values, an apparent resistivity (ρ_a) value is calculated. This is the weighted resistivity. Loke (2001) has given the mathematical steps to this formula.

$$\rho_a = k\nabla\phi / I, \quad \text{---------- 3.7}$$

where;

$$k = \frac{2\pi}{\left(\frac{1}{r_{C1P1}} - \frac{1}{r_{C2P1}} - \frac{1}{r_{C1P2}} + \frac{1}{r_{C2P2}}\right)} \quad \text{---------- 3.8}$$

k is a geometric factor that depends on the arrangement of the four electrodes. Resistivity measuring instruments normally give a resistance value, $R = \nabla\phi I$. In practice, the apparent resistivity value is calculated by;

$$\rho_a = k\,R \quad \text{----------3.9}$$

In modelling one dimensional data, the assumption is that, the subsurface consists of horizontal layers. In this case the subsurface resistivity changes only with depth, but does not change in the horizontal direction (Loke, 1999). The number of layers is determined by the computer software. Editing of the layers can be carried out either to increase or decrease the number of layers. Two to five layers were used to model VES data in the study area.

On the other hand, a two dimensional model takes into consideration resistivity changes, both in the vertical direction as well as in the horizontal direction, hence making it more accurate while modelling the data.

3.3 Inverse modelling

This is the application of mathematical problems in science to transform a set of observed data to reconstruct a model. In the 2D resistivity inversion modelling applied during modelling of the study area data, the aim was to model data to present images in order to view the distribution of resistivity horizontally and laterally and relate the resistivity with groundwater occurrence.

According to MacInnee and Zonge (1996), forward modelling algorithms such as finite element is useful in calculating resistivity data. Loke (2001) explains, from RES2DINV software, used to model the study area data, one can choose the finite-difference (Dey and Morrison, 1979a) and finite-element (Silvester and Ferrari, 1990) method to calculate the apparent resistivity. (Loke, 1999) further explains, this program divides the subsurface into a large number of small rectangular cells as seen in figure 3.5. This modelling yields a two-dimensional or three-dimensional vertical cross-section of the true resistivity beneath the electrode array.

The 2D model used by the software divides the subsurface into a number of rectangular blocks. The inverse modelling carried out during data processing, enables identify anomalous regions by interpreting pseudosections which were the end result of modelling. Figure 3.5 shows the division of subsurface into a number of rectangular blocks during the modelling process.

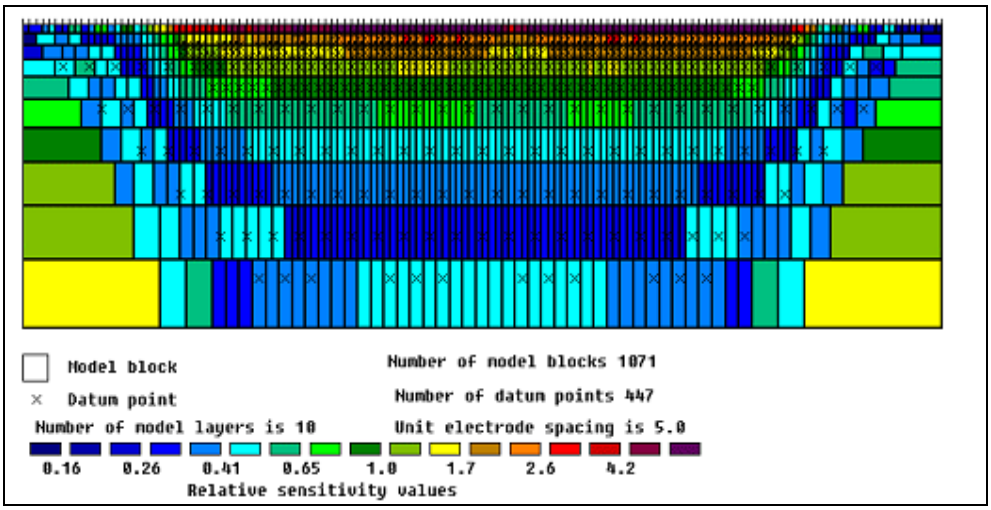

Figure 3.5: Modelled Apparent Resistivity data in Rectangular Blocks (after Loke 1999)

The arrangement of the blocks is loosely tied to the distribution of data point in the pseudosection. Distribution and size of the blocks are automatically generated by the program using the distribution of the data points as a rough guide. The depth of the bottom row of blocks is set to be approximately equal to the equivalent depth of investigation (Loke, 1999).

In the determination of resolution limits of electrical tomography of the block model, Sumanovac and Dominković (2007) used 2D electrical modelling to analyse electrical tomography potentials in the detection of a higher resistivity block in a homogenous environment of lower resistivity. The detectable depth increases with the increased contrast and resistivity ratio, until it reaches a maximum detectable depth. The dipole-dipole array enables the highest resolution and the lowest by the Wenner array. Between them are the pole-pole and Wenner-Schlumberger arrays with very similar resolution. In conclusion, concrete investigations, environmental, geophysical, geological and urban noises influence decrease. As a result, electrode array sensitivity varies. They will also influence the decision on selecting the most optimal electrode array. In the study area, Schlumberger array was applied. The selection of this array for use in the study area is due to its effectiveness to reach deeper depths during probing of the ground. Lopez (1995) further noted in the geothermal field of El Salvador in

America that, the main obstacle of the Schlumberger sounding is the sensitivity to relatively shallow lateral resistivity variations.

Loke (2001) notes the l_2-norm smooth inversion method is not the optimal method for data with sharp boundaries. No major sharp boundaries were encountered during data processing of the study area. Only modelling of profile 13 on the western part of the study area occur to have two sharp boundaries. Lopez (1995) notes that, interpretation based on 1D inversion programs is inadequate when high resolution and detection of sharp resistivity boundaries is required.

According to Narayan et al. (1994), a good inversion method must minimize the effects of data error and model parameter. Loke (1999) outlines guidelines for data inversion as he demonstrates the fact that inversion normally tries to reduce the square of difference between the measured and calculated apparent resistivity values.

Data error is usually due to data misfit between observed and calculated data. The data misfit is characterized by an objective function, which is minimized by a proper optimization algorithm. To reduce the error, optimization method is applied during inversion process.

Geophysical inversion in the context of optimization involves finding an optimal value of a function (Sen and Stoffa, 2013). The optimization problem involves equality and inequality constraints (Barhen et al., 2000). In all optimization methods (Loke, 2001), an initial model is modified in an iterative manner so that the difference between the model response and the observed data values is reduced. The set of observed data is written as a column vector **y** given by;

$$y = \text{col}\,(y_1, y_2, \ldots\ldots, y_m), \quad \text{----------} \quad 3.10$$

where m is the number of measurements. The model response **f** is written in a similar form

$$f = \text{col}\,(f_1, f_2 \ldots\ldots f_m) \qquad \text{----------} \qquad 3.11$$

For resistivity problems, it is a common practice to use the logarithm of the apparent resistivity values for the observed data and model response, and the logarithm of the model values as the model parameters. The model parameters are represented by the following vector

$$q = \text{col}\,(q_1, q_2, \ldots\ldots, q_n), \qquad \text{----------} \qquad 3.12$$

where n is the number of parameters. The difference between the observed data and the model response is given by the discrepancy vector g that is defined by

$$g = y - f \qquad \text{----------} \qquad 3.13$$

In the least-squares optimization method, the initial model is modified such that the sum of squares E of the difference between the model response and the observed data values is minimized

$$E = g^T g \qquad \text{----------} \qquad 3.14$$

To reduce the above error value, the following Gauss-Newton equation is used to determine the change in the model parameters that should reduce the sum of squares (Lines and Treitel, 1984)

$$J^T J \Delta q_i = J^T g, \qquad \text{----------} \qquad 3.15$$

where, Δq is the model parameter vector and J is the Jacobian matrix (of size m by n) of partial derivatives. The elements of the Jacobian matrix are given by

$$\frac{J_{ij} = \delta f_i}{\delta q_j} \qquad \text{----------} \qquad 3.16$$

That is the change in the *i*th model response due to a change in the *j*th model parameter.

CHAPTER FOUR

4.1 DATA ACQUISITION, PROCESSING AND INTERPREPATION

This chapter outlines the principles of electrical resistivity data acquisition, processing and interpretation of data within the study area.

Introduction

Field survey and Instrumentation

The method of direct-current resistivity is readily adapted to electrical resistivity equipment.

4.1.1 VES data acquisition

As earlier indicated VES Schlumberger survey was previously carried out for two boreholes. In acquiring VES data, site area was identified through physical, avoiding buried cables and pipes. SAS 300 terremeter Abem equipment was used to acquire the VES data. Centre of two cables laid on the site area was identified and equipment placed at the centre. Potential electrodes made of stainless steel were driven into the soil at measured position. Two current electrodes were also driven into the ground and connected to the voltage receiver at the centre. Taping of distances was carried out on both sides of the machine and current electrodes moved to the required spread.

Readings were taken at the machine position every time the current electrodes were moved. The frequency used, current sent to the ground, voltage received and distances within the current electrodes and potential electrodes were recorded.

4.1.2 ERT data acquisition

Instead of deploying a single pair of current-electrodes and a single pair of potential electrodes, an array of regularly spread electrodes is deployed and a linear arrangement of electrodes is used. This section is dedicated to highlighting field

procedures and instruments used during 2D electrical resistivity field survey, in acquiring data in Konza area. Figure 4.1 shows the general arrangement of electrodes, the instruments used and the sequence of measurement.

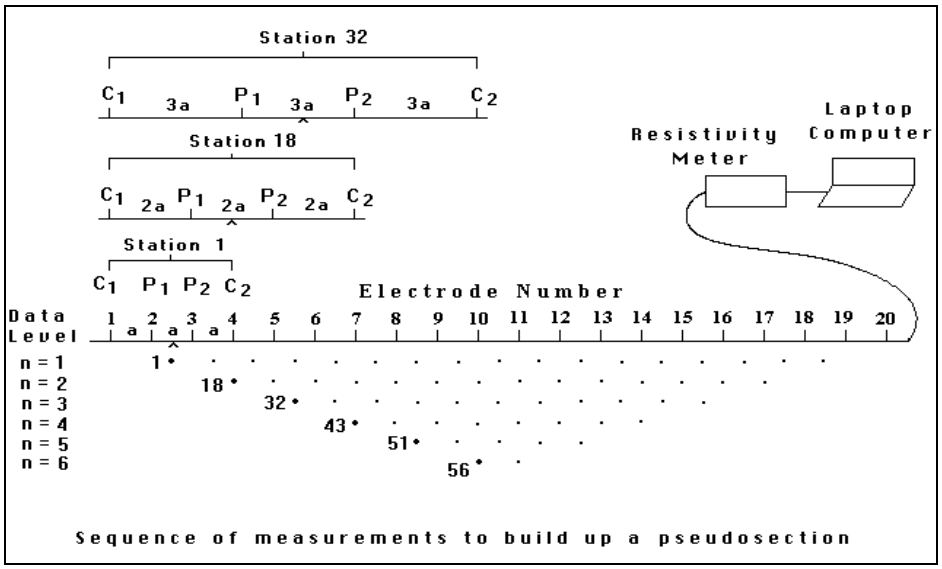

Figure 4.1: Arrangement of electrodes for 2D electrical resistivity survey (after Loke 1999)

Electrodes along a straight line are attached to a multi-core cable, which is attached to an electronic switching unit connected to a lap top computer. After setting the program text file, the measurements are automatically read and stored in the computer.

Field work was carried out during August and December 2013 followed by November 2014, for further data verification. ABEM SAS 1000 Terrameter geophysical instrument together with accessories: LUND, electrode system enabled the acquiring of resistivity data from the field. Figure 4.2 shows the Terrameter machine connected to the LUND system on the ground.

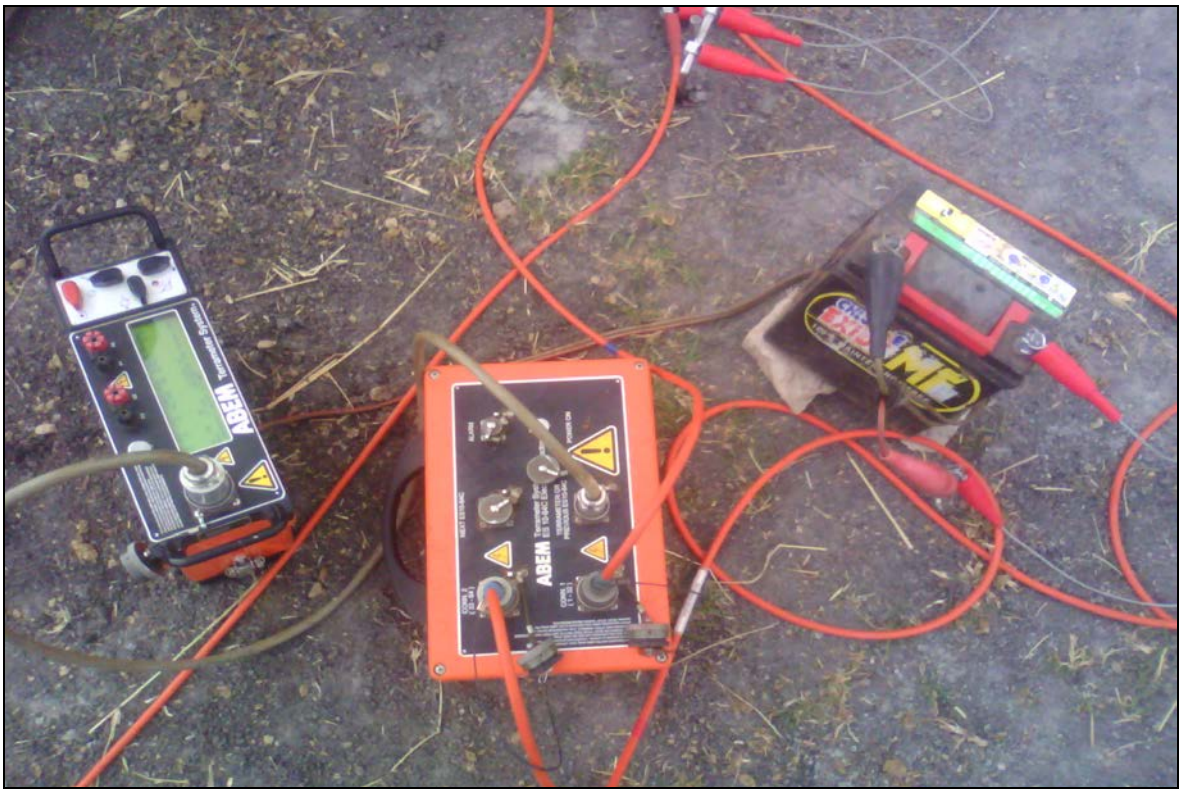

Figure 4.2: Connection of Terrameter SAS 1000 and LUND system

The survey was carried out with the system. During the first field work, set of four cables, each measuring 200 meters with 21 electrode take-outs were arranged along different selected positions. A set of two 200 meter cables was used during the second field work. Identification of specific sites for laying down the cables had been carried out through satellite images of the study area and later confirmed on the ground. Electrodes were hammered into the ground at each contact on the cables with a spacing of 5 and 10 meters. The small electrode spacing was necessary to achieve high resolution on the ground. As in many standard resistivity methods, the resolution of investigation depends on separation of the electrodes (Lowrie, 2007). The multi-core cables were then connected to the electrodes using cable jumpers. The terrameter which acted as a switch system and a measuring device was connected to the laid cables. The terrameter was later connected to the battery source.

Setting up the system was accomplished as explained and the terrameter switched on. Set-up on the terrameter was undertaken and the survey reading started.

The field work research site was observed under various conditions, dry and wet periods. During the field work, negative resistivity readings were encountered, this was caused by poor grounding. This resulted to low transmission due to dry ground. To enhance the ground contact, water was dispensed at electrodes with poor contact. During the wet period of undertaking the survey the ground contact was also poor due to the contraction of clay material, in this case changing of electrodes to a firm position was done to enhance the ground contact. Global Positioning System (GPS) points were recorded at points of electrodes and saved in the GPS equipment.

To extend the area of coverage along the profile lines, a roll-along technique was carried out during the field work. In this technique, extensions of cables are further connected using a connector garget.

Apparent resistivity values were acquired at different positions on the ground corresponding to each lateral location and approximate depth of investigation. The survey activity was completed and measurement stored in the terrameter.

Out of the data acquired in the field, a total number of fourteen tomography profiles were produced. The profiles covered a good segment of the study area. Figure 4.3 shows the fourteen profiles overlaid on the geological map of the study area. The labeling of each profile is denoted by P (Profile) followed by a number of the profile. Profile 14 covered the extreme North West part of the study area while profile 13 covered the south western part of the area. Twelve profiles were concentrated in the middle part of the study area targeting Iviani river valley and boreholes drilled along the river valley. Figure 4.3 shows the locations of ERT profiles in the study area.

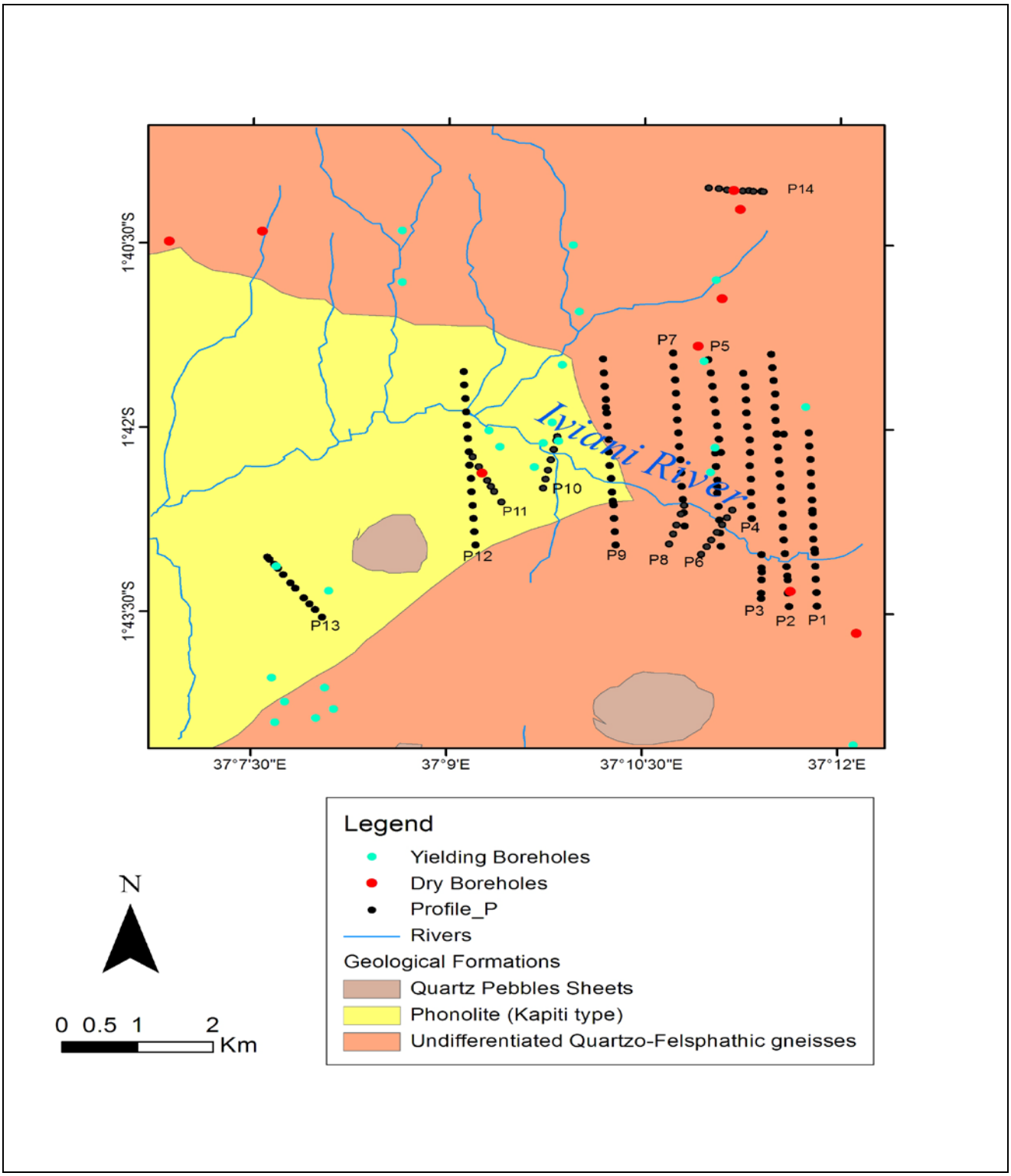

Figure 4.3: Map showing ERT Profiles in the study area

The profiles obtained, varied from 800 meters to 4160 meters in length generally laid in the North West – South East direction. Eight profiles were laid out across the Iviani river valley to identify the structural setting of the valley and to determine the influence of the valley to groundwater occurrence. Six profiles were laid on existing boreholes within the study area.

4.1.3 Data Processing

Data processing was the next step undertaken after acquiring data from the field. This process involves the use of computer programs to model the data.

IPI2win+IP software was used to model VES data of earlier drilled boreholes. From the data acquired, apparent resistivity P_a was calculated through feeding the recorded data to the computer program. The computer automatically generates model calculated apparent resistivity and matches with field curve generated from feeding field data. Curve matching results of VES data from the area are attached under Appendix II.

RES2DINV software enabled the processing of ERT data acquired from the area. ERT combines sounding and profiling techniques when acquiring data. Data processing is accomplished through applying computer software to control the data acquired from arrays of electrodes. Sophisticated computer algorithms to model 2D to image data are used.

Acquired data from the survey carried out in the study area was downloaded from the terrameter to a computer for processing purpose. Field data was downloaded using Erigraph software which recognizes the format of saved data. The data was saved into the computer in the form of a text file. Data was processed and the end results were presented as measured apparent resistivity, calculated resistivity and inverse model resistivity. These sections are the final results contoured to 2D inversion through the use of RES2DNIV version 3.56 software. Figure 4.4 illustrates the processes carried out within profile 1 laid in the study area. To identify influences of topography to the final 2D inversion model further processing of the model is undertaken with the same software, taking into account the elevation data. Figure 4.5 shows model resistivity with

topography data. This model has no masking effect since elevation of the profile is gently sloping. Elevation is only noted to rise gently at a distance of 800 meters.

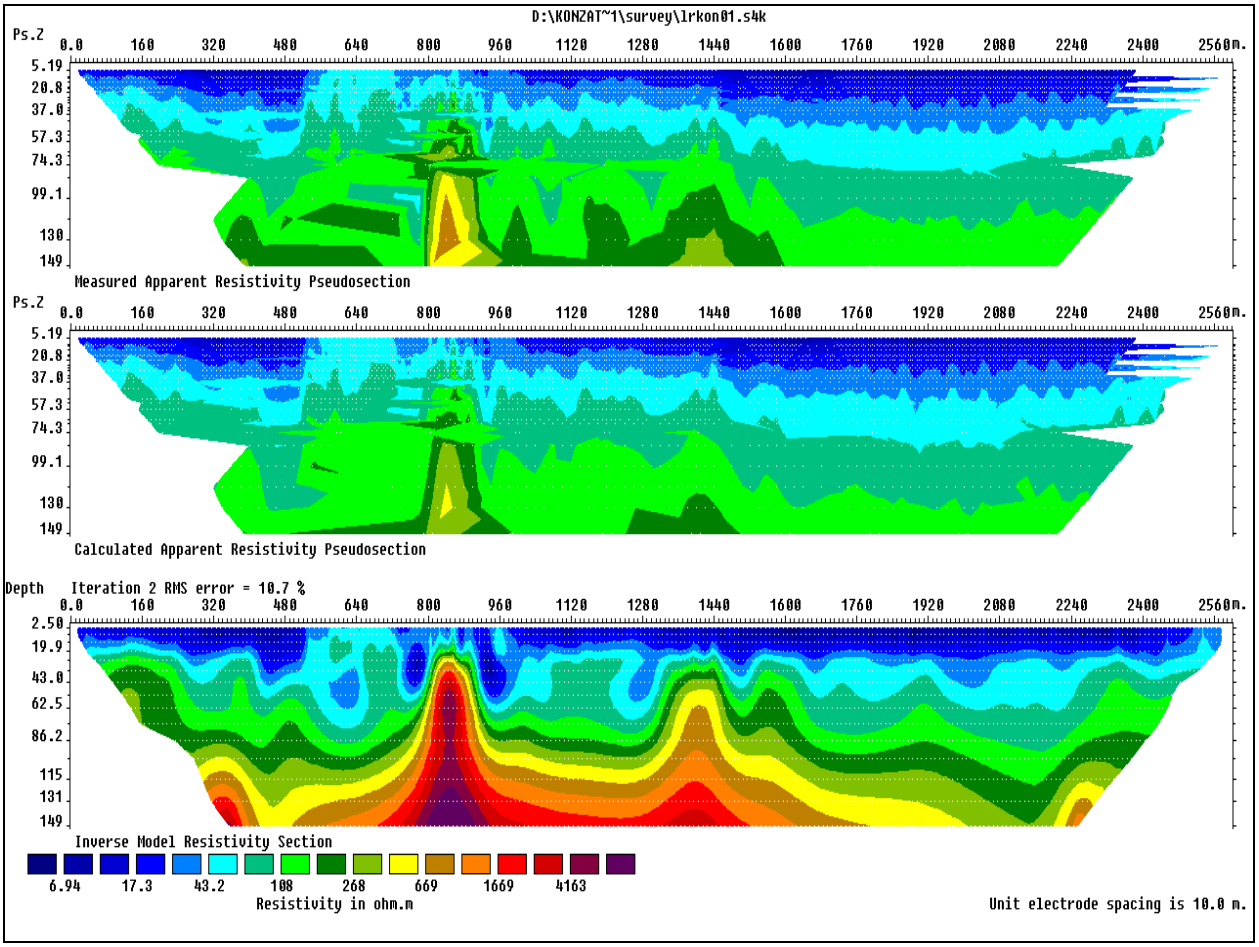

Figure 4.4: Shows measured apparent resistivity pseudosection, calculated apparent resistivity pseudosection, inverse model resistivity section of profile 1 in Konza area

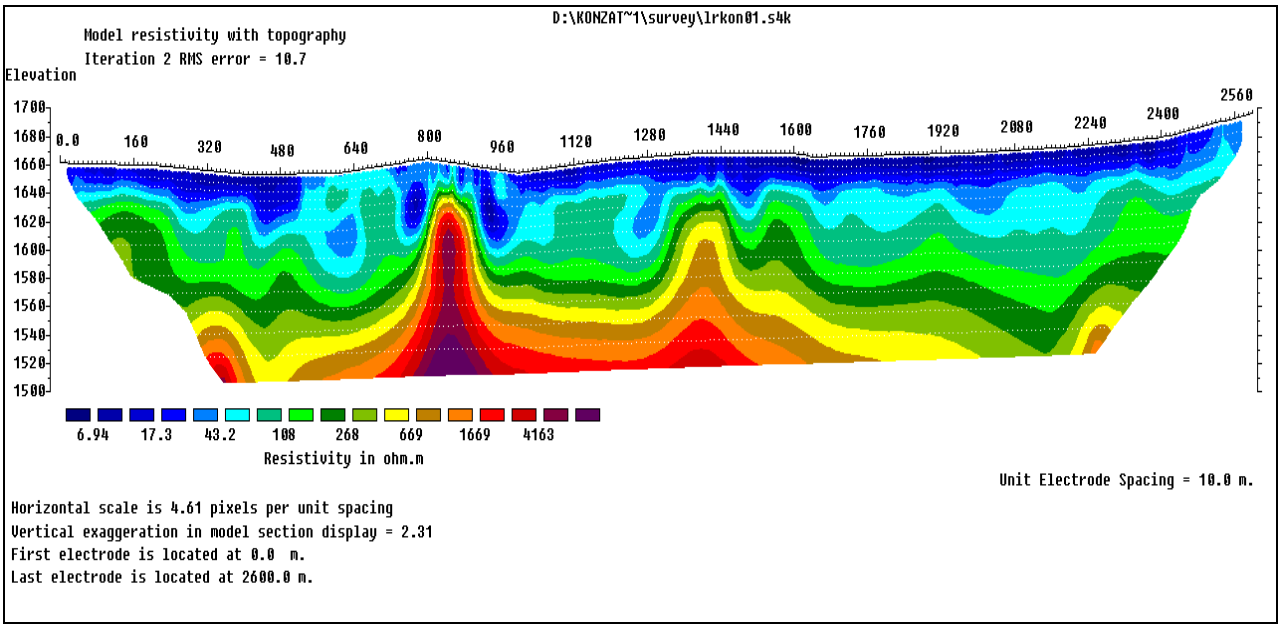

Figure 4.5: Illustrating modelled profile 1 with elevation data incorporated in the model

Optimization method tries to reduce the difference between calculated and measured apparent resistivity values by adjusting the resistivity of model blocks. A measure of this difference is given by the Root-Mean-Square (RMS) error. Maclnnes and Zonge (1996) in carrying out smooth-model inversion, attempts to simultaneously minimize the squared difference between observed and calculated data. However the model with the lowest possible RMS error can sometimes show large and unrealistic variations in the model resistivity values and might not always be the “best” model from a geological perspective (RES2DINV software manual 2007). The modelled data in the study area illustrates variations of lowest RMS of 1.3% to 54.6% high RMS error. Application of 2 to 5 iterations, during data processing of the data enabled to reduce the RMS within the final model.

During data processing of the resistivity data, optimization was performed through applying iterative algorithm based on finite element method. This method allows calculation of resistivity data with topographic data, where influence of topography

occurs. The program reads the data file with topographic data by selecting finite element method, to model pseudusection with topographical information.

The finite-element method used as an inversion method during processing of data, involves solving forward and inverse linearity problems. The solution to the forward linearity problem uses the finite-element method to compute the potential electrical response on the ground (U.S Department of Energy, 2000). The processed data produced pseudosections that have triangular features. Forward modelling algorithms, such as finite elements can be used to calculate resistivity data, given a particular model section and array configuration (Maclnnes and Zonge, 1996). Fourteen profiles from the study area were processed to produce the end results of 2D ERT in form of pseudosections. The end results of the inverse section were analyzed for any anomaly considering the resistivity values in the section.

SURFER and Arc GIS softwares were used to model and represent topographic and geological data. An optimization framework that creates a picture of spatially variable subsurface is produced.

4.1.4 Pseudosection Data Plotting Method

Pseudosection is a diagram presenting plot of data which was undertaken in the field, along a profile traverse line. Apparent resistivity data is represented as pseudosection to give an idea of 2D or 3D distribution of resistivity. Data from the study area is presented as 2D under section 5.0. According to Loke (1999) to plot the data from a 2D imaging survey, the pseudosection contouring method is normally used. The pseudosection gives a very approximate picture of the true subsurface resistivity distribution. However the pseudosection can give a distorted image of the subsurface because the shape of the contours depends on the type of array used as well as the true subsurface resistivity. In the study area the Schlumberger array was selected during collection of data in the field. This array is moderately sensitive to both horizontal and vertical structures. The area of coverage for data with this array is also normally wider than other arrays.

Figures 4.3 and 4.5 shows inversion results and pseudosection of profile 1 of the profile line laid for data collection during field work in the area.

Data analysis was carried out for the fourteen profiles acquired during the field work in the area. The end results achieved after data processing, assisted in the analysis of information contained within the fourteen profiles under section five.

The pseudosection is useful as a means to present measured apparent resistivity values in a pictorial form, and as an initial guide for further quantitative interpretation (Loke 1999). The resistivity tomography profiles used together with available geological maps, VES data, borehole yield and drill-core lithologic descriptions (under appendices) are presented under the following section. The information was used to determine the influence of geology and geological structures on groundwater occurrence and potential aquifer zones within the study area.

CHAPTER FIVE

5.1 RESULTS

5.1.1 Introduction

This section presents and interprets the 2D resistivity model of fourteen tomography profiles. Nine profiles (2, 3, 4, 5, 6, 7, 8, 10 and 12) present topographic information. Elevation in meters displays on the left side of the section margins. No topographic information occurs in the five profiles (1, 9, 11, 13 and 14). Since modelling of the sections did not in co-operate topographic data. Gentle slopes occur in areas where these profiles were laid. Thus, elevation had no influence to final modelled section of profiles. Depth in meters displays on the left side of the margins. Long profiles with distances more than 800 meters occur in two sections cut across A – B for ease of interpretation of the profile.

Borehole analysis occurs under six presented profiles. Three boreholes are dry while, three boreholes provide a yield of minimum 4.3m^3/hr to maximum of 25m^3/hr. Details of boreholes drilled within the area are under appendix I. Some data is missing within the borehole records but this did not affect the final results.

The general resistivity occurring within the fourteen profiles presents horizontal distance and lateral depth. Horizontally with a maximum distance of 4162 meters and laterally a maximum depth of 159 meters deep within the profiles. Different geological structures depicted from the profiles are fractures, occurring as major geological structures. F (Fracture) denotes the fracture zones and numbering of each fracture zone is specific to the profile.

5.2 Two Dimensional Resistivity Tomography Profiles

The results of two dimensional resistivity tomography profiles in this section allowed identification of strong variation of electrical resistivity values of about 0.3Ωm minimum to 4960Ωm maximum. Identification of fracture zones and other geological structures within the 2D resistivity tomography profiles is achieved. Presentation and a brief

description of each two dimensional resistivity tomography profile occur in the following section. White vertical lines outline the fracture zones.

5.2.1 Profile 1

The results gathered from this profile clearly shows fracture zones within the study area. High resistivity long fracture limbs, separates fracture zones F1 and F2. Less weathered high resistivity material of 4163Ωm, probably feldspathic gneiss formations characterize the fracture limbs. Figures 5.1, 5.1a and 5.1b illustrate Profile 1.

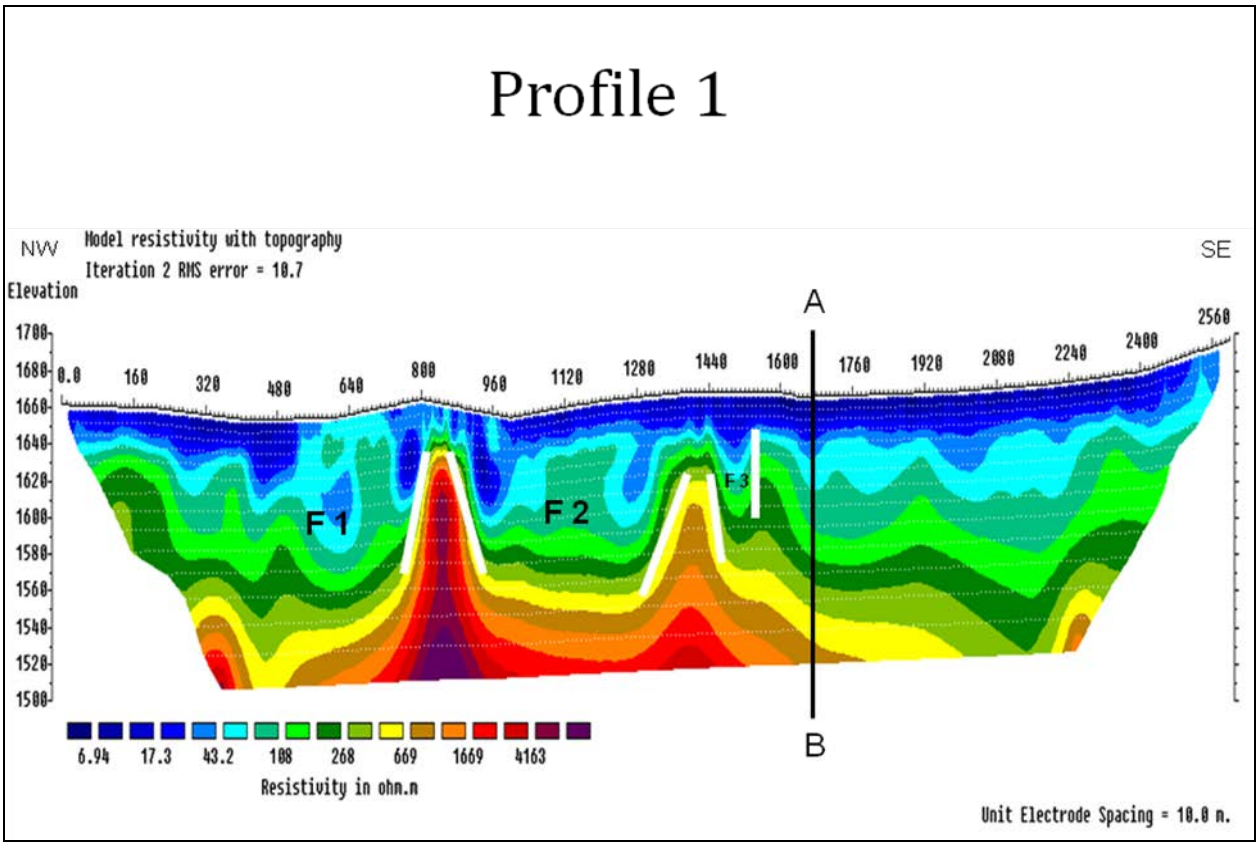

Figure 5.1: Results of 2D ERT along profile 1 showing fracture zones (F1, F2 and F3)

The different resistivity accounts for stratigraphical units within the area. The low resistivity of 6.94Ωm corresponds to sandy clay material found within the subsurface area. The bedrock of the profile demonstrates resistivity material of more than 4163Ωm.

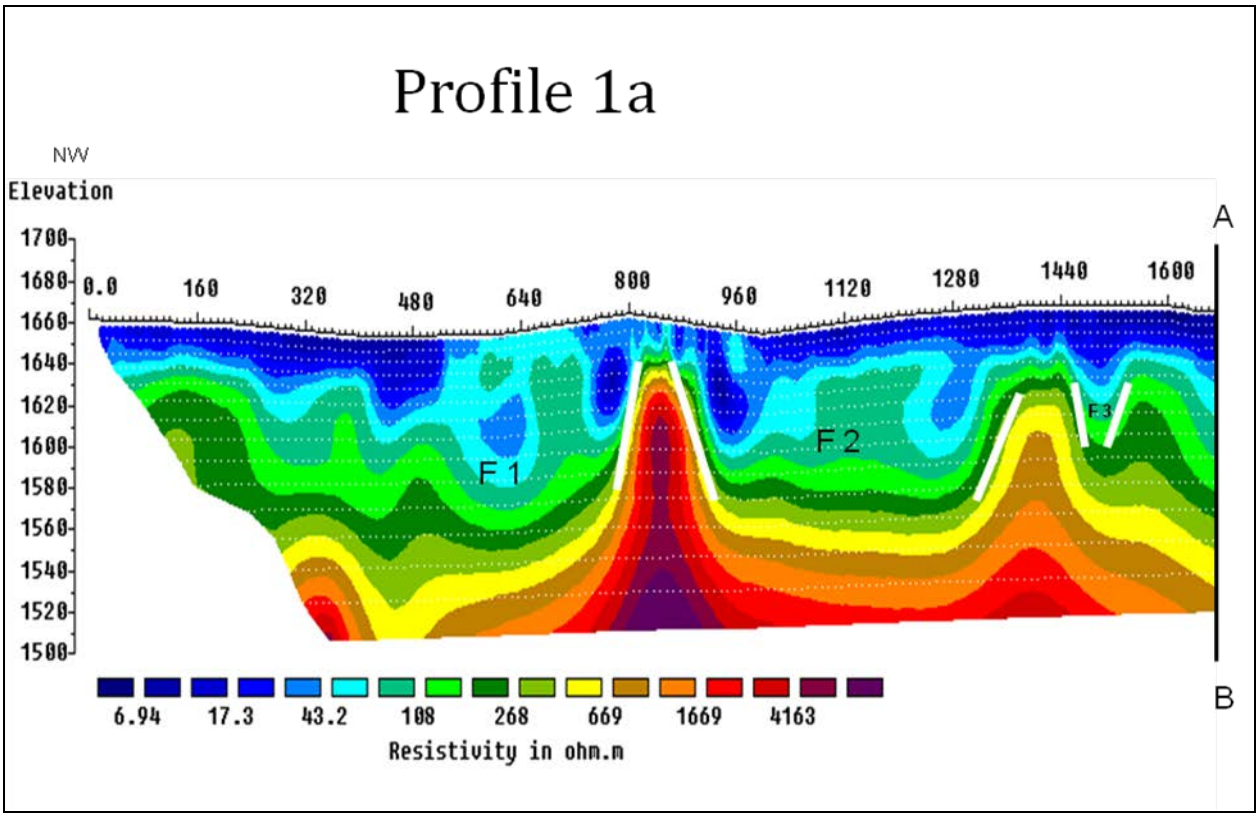

Figure 5.1a: 2D ERT North West Section along Profile 1

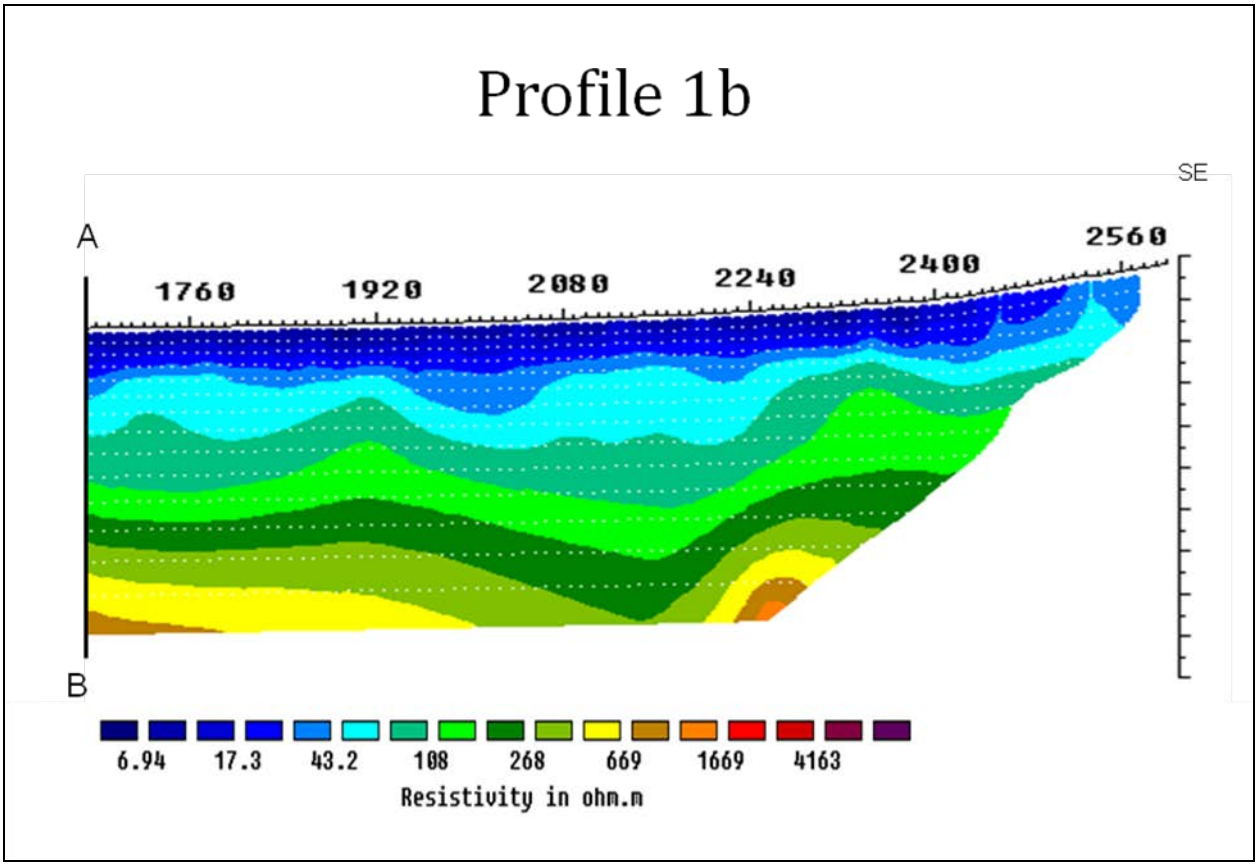

Figure 5.1b: 2D ERT South East Section along Profile 1

The profile provides productive extensive aquifer zone towards fracture zone F3 on the eastern part of the profile. This is evidenced by resistivity of between 10 to 100Ωm of water zone. The aquifer stretches to about 100 meters deep, although the horizontal extend of the fracture zone is only marked by one limb. Fracture zone 3 is the smallest in size, as compared to other fracture zones. No borehole mapping occurs within the profile. The formations were only analyzed through resistivity values to understand the influence of the Iviani valley on groundwater occurrence.

5.2.2 Profile 2

The inverted profile modelled with topographic data presents a varying elevation. The profile cuts across an existing borehole with a yield of $1m^3$/hr at a depth of 107 meters. The geological structures occurring in this section present system of fracturing zone. Due to saturation of water within the fracturing zones, weathering occurs. Figures 5.2, 5.2a and 5.2b show Profile 2

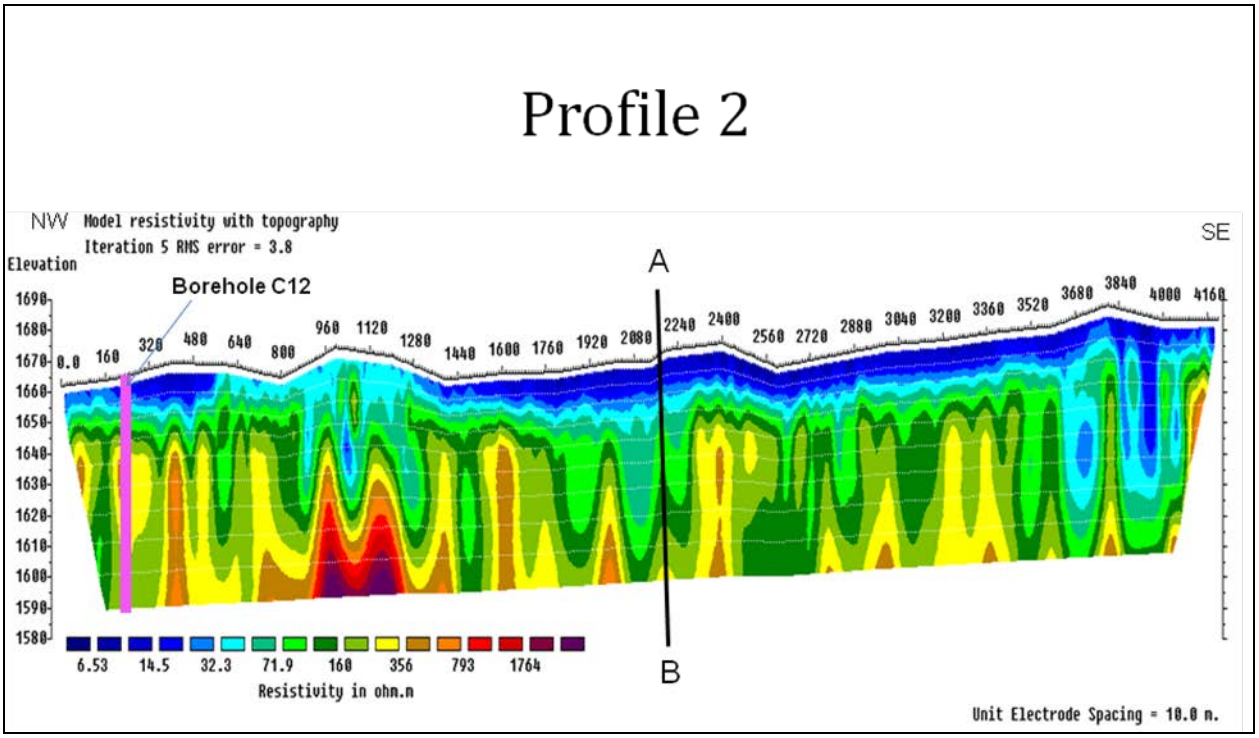

Figure 5.2: Result of 2D ERT along profile 2 showing borehole C 12

A sandy clay layer of about 20 meters deep with resistivity of 15Ωm overlay a medium resistivity zone of 40Ωm to 400Ωm across the profile. A high resistivity saddle structure occurs at the base of the profile with resistivity of about 1764Ωm.

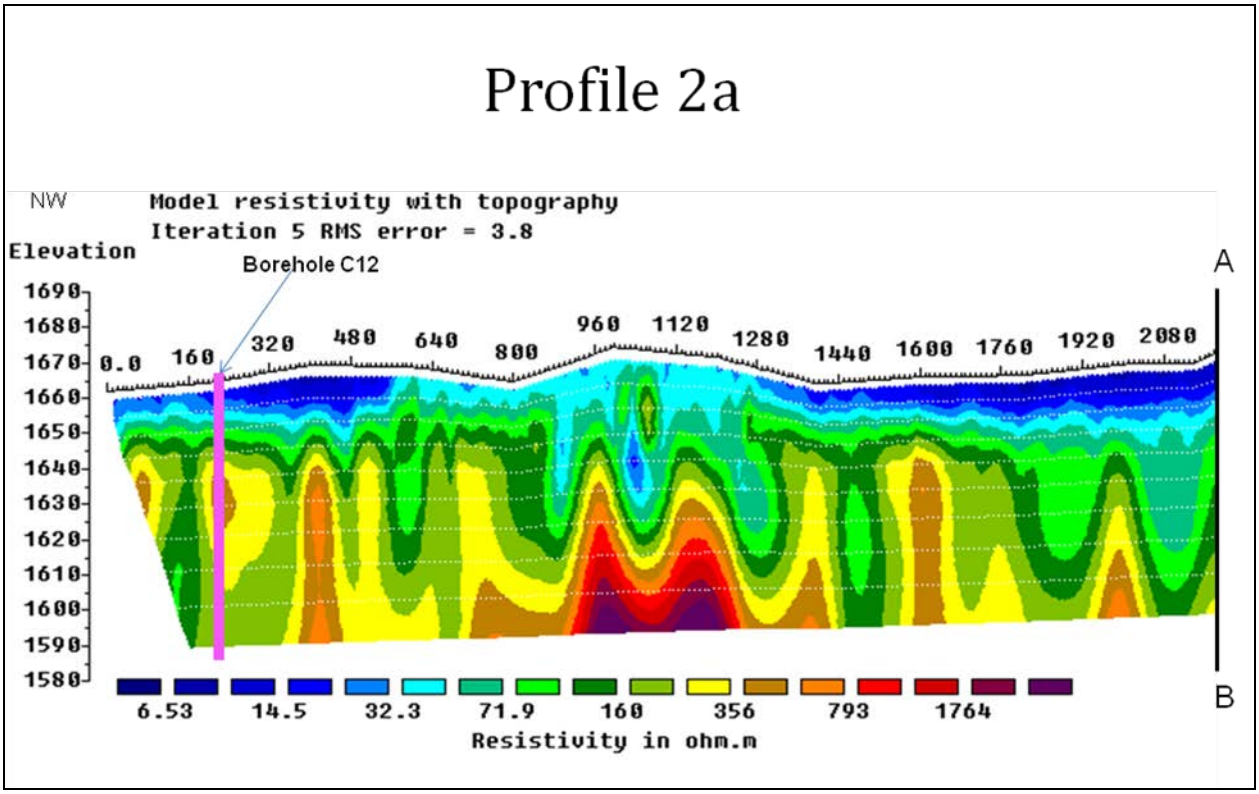

Figure 5.2a: 2D ERT North West Section along Profile 2

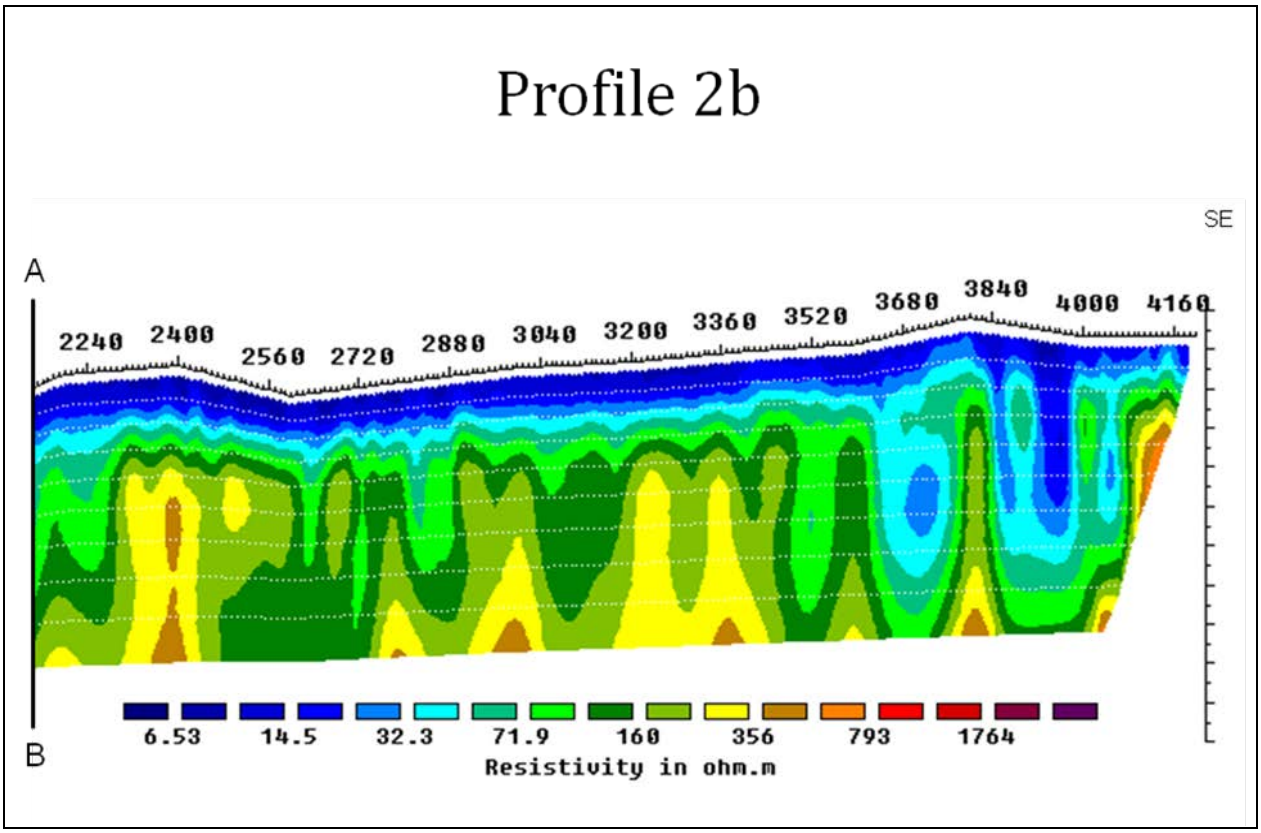

Figure 5.2b: 2D ERT South East along Profile 2

This section does not provide productive aquifer zone. A low yield borehole occurs within the section on the western part of the profile. Probably a borehole drilled on the eastern part of the section, at distance between 3560m and 4000m along the profile could probably be more productive. This is because of suitable resistivity values of groundwater of 10Ωm to 100Ωm occurring at a depth of 73 meters on the southeastern part of the profile.

5.2.3 Profile 3

The characteristic feature of profile 3 within the area shows horizontal geological layers with a saddle structure at the base (159m) of the profile under figure 5.3. The topography of the profile is relatively flat, indicating little or no influence of topography to the model. The saddle constrained structure, show the tendency of rupturing at the middle. This geological structure signifies a period of depositional, followed by a period of folding within the area.

Variation in resistivity highlight anomalous regions with low resistivity of 14Ωm, medium resistivity 128Ωm and high resistivity of 2464Ωm under figure 5.3. Sandy-clay formation occurs on the upper part of the profile. Feldspathic gneiss depicts the base of the profile. The weathering pattern within this profile appears to be in the downward direction. Low resistivity of 14Ωm indicates weathered zone on the upper part of the profile and high resistivity of 2464Ωm of unweathered zone occur at the base of the profile. Less fracturing within this profile occur, except little tendency of weathering on the eastern part, at a distance of 640 meters and 740 meters. The weathered zone shows a resistivity of 563Ωm. This resistivity is high, probably due to less fracturing process within the profile under figure 5.3.

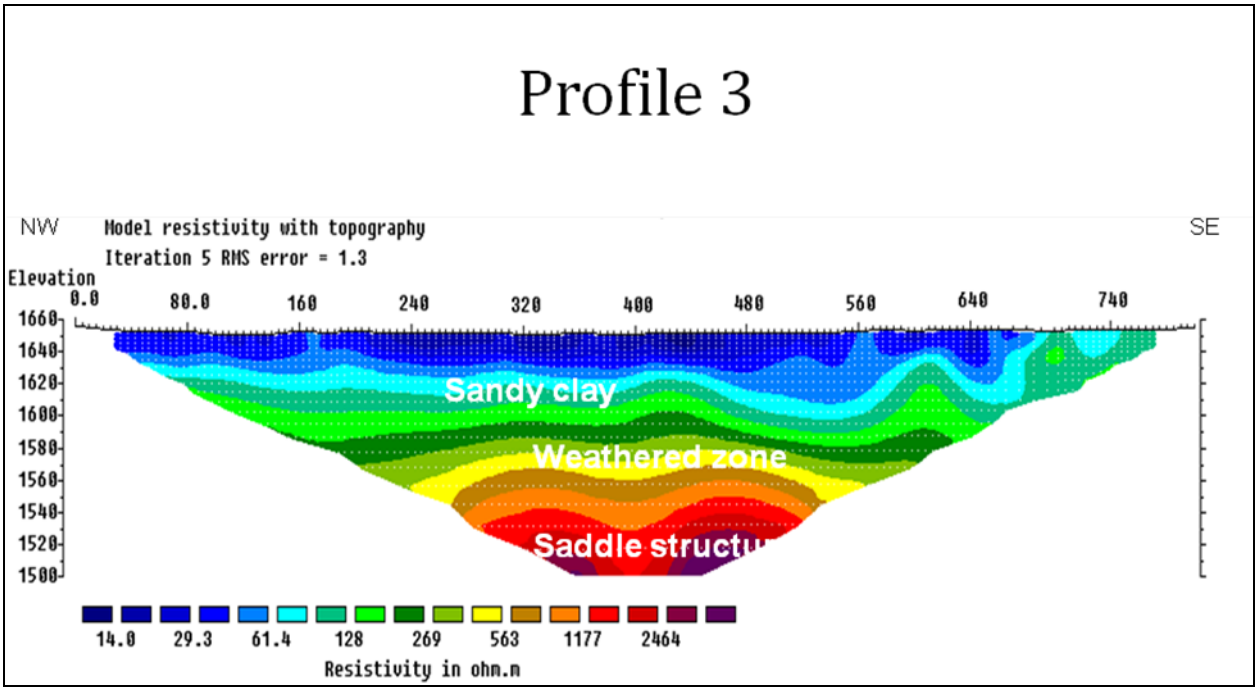

Figure 5.3: Result of 2D ERT along profile 3 showing horizontal geological formations

Sandy clay zone occurs at a maximum elevation of 1600 meters below ground level and a saturated zone at 1500 meters, indicating a shallow aquifer zone.

5.2.4 Profile 4

Profile 4 is characterized by a gently sloping topography rising from the western part of the profile to a maximum elevation of 1970 meters, figure, 5.4, 5.4a and 5.4b shows profile 4.

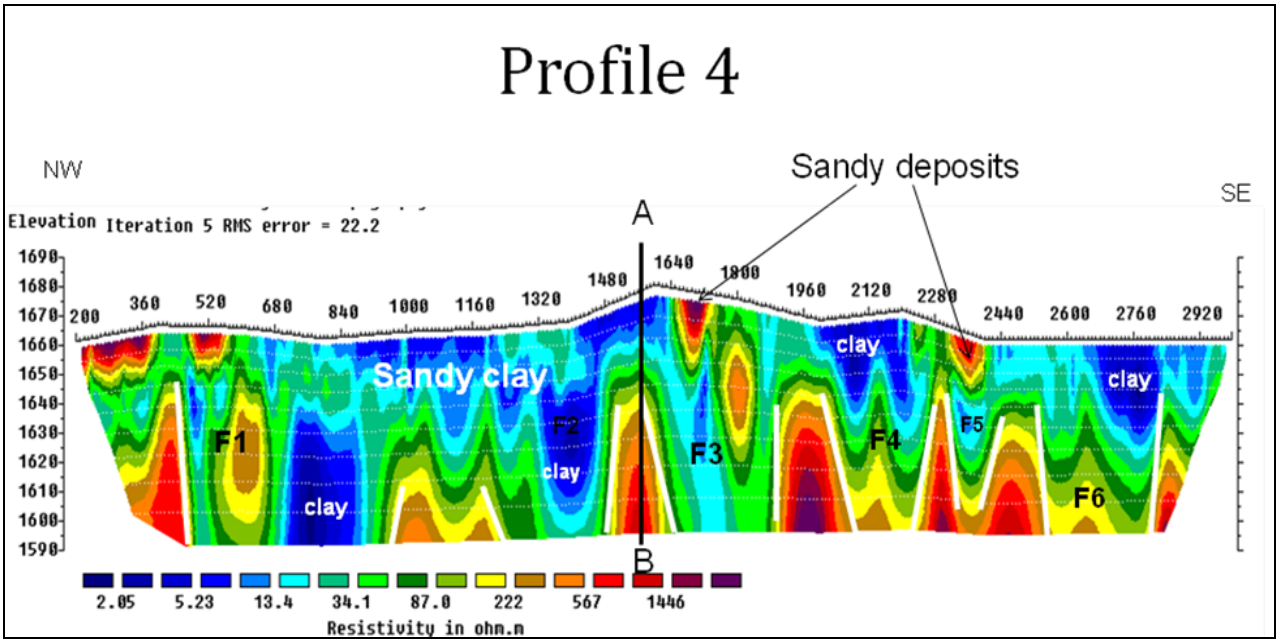

Figure 5.4: Result of 2D ERT along profile 4 showing system fracturing within the formations

This profile depicts a distribution of fracturing system across the section. The fracturing within this profile is more elaborate than in profile 3. Six fracture zones outlined fracturing within the profile. Fracture zone F1 occur as the widest zone. Some of the fractures are partly filled with clay material of resistivity between 2Ωm to 5Ωm except for fracture zones F3 and F5.

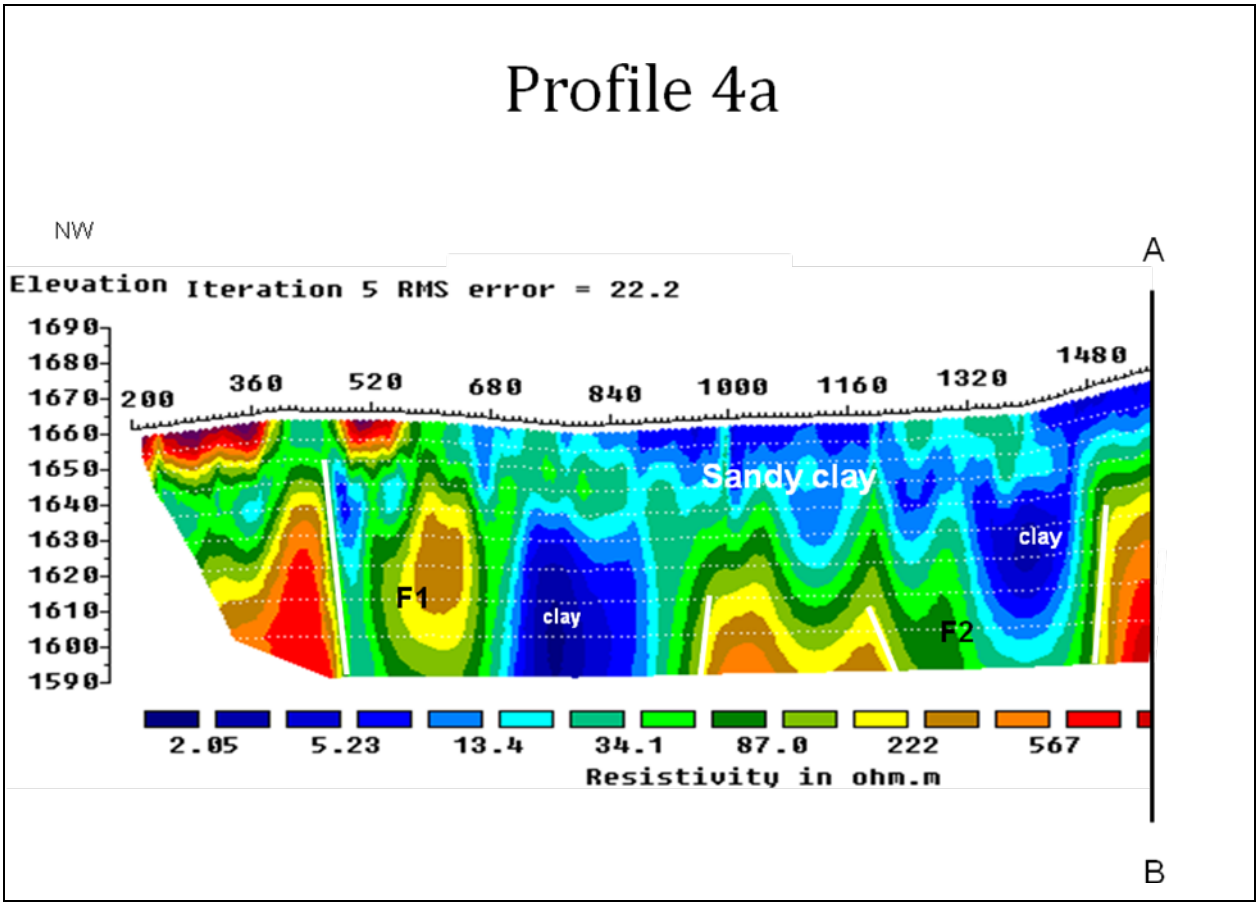

Figure 5.4a: 2D ERT North West Section along Profile 4

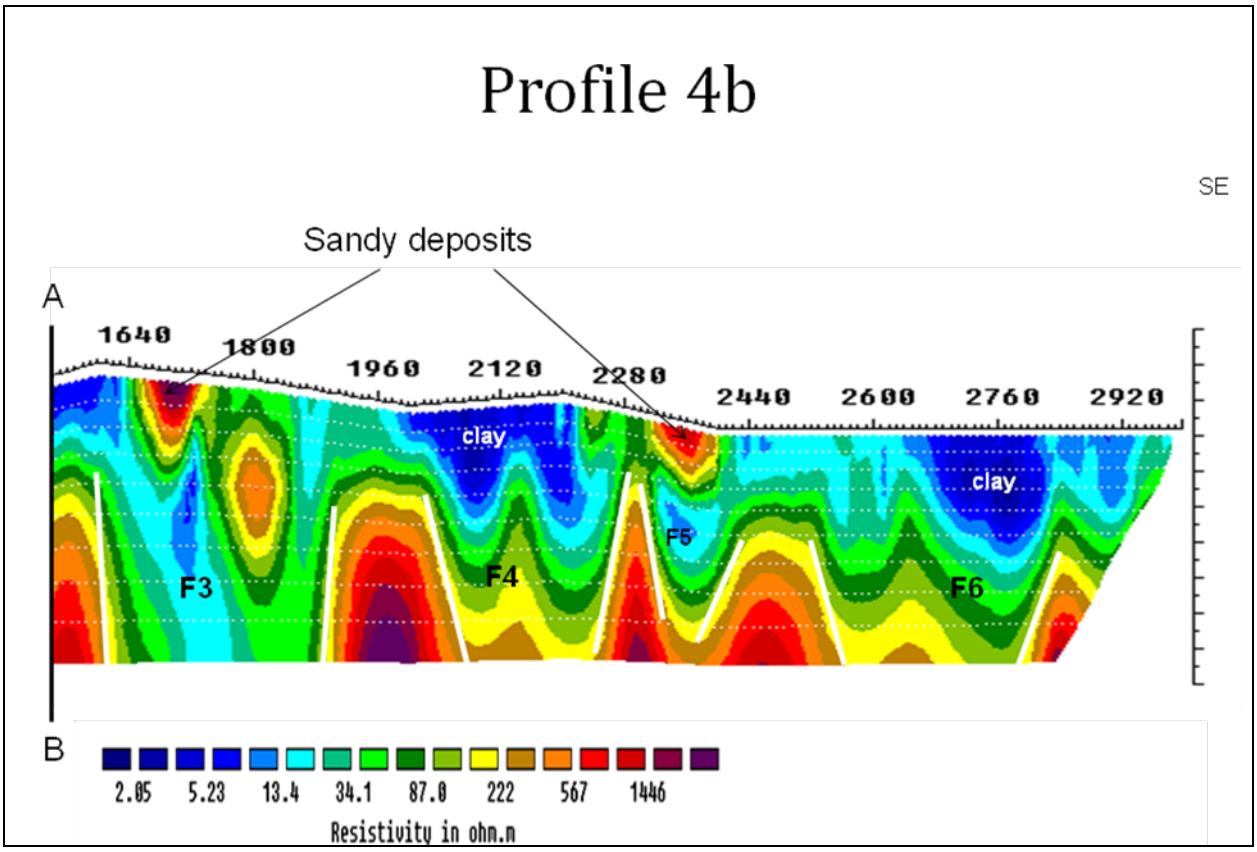

Figure 5.4b: 2D ERT South East section along Profile 4

Lenses of sandy formations observed at the surface of the profile illustrate a high resistivity of more than 1446Ωm. Varying resistivity of minimum 2Ωm to a maximum of more than 1446Ωm occur at the base of the profile.

Tomography results along this profile do not offer a good aquifer zone in most of the region except within the fracture zone F3 which occurs to provide a deep narrow aquifer zone.

5.2.5 Profile 5

Profile 5 is characterized by gentle sloping topography and a low altitude valley. A high resistivity formation probably of felspathic gneiss occurs within the traverse and it is cut by three fracture zones. The fracture zones cuts the formation in a downward thrust and later filled with less resistivity material. A material of resistivity 30Ωm to 80Ωm probably granitoid gneiss fills fracture zone F1 and F2. Fracture zone F3 is filled with material of resistivity 4Ωm to 20Ωm probably clay under figure 5.5, 5.5a and 5.5b demonstrate the profile.

Layering of geological formations appears to be interrupted at the fracture zones. This indicates fracturing formed after the formations. Fracture zone F1 occur to be shallower than fracture zones F2 and F3.

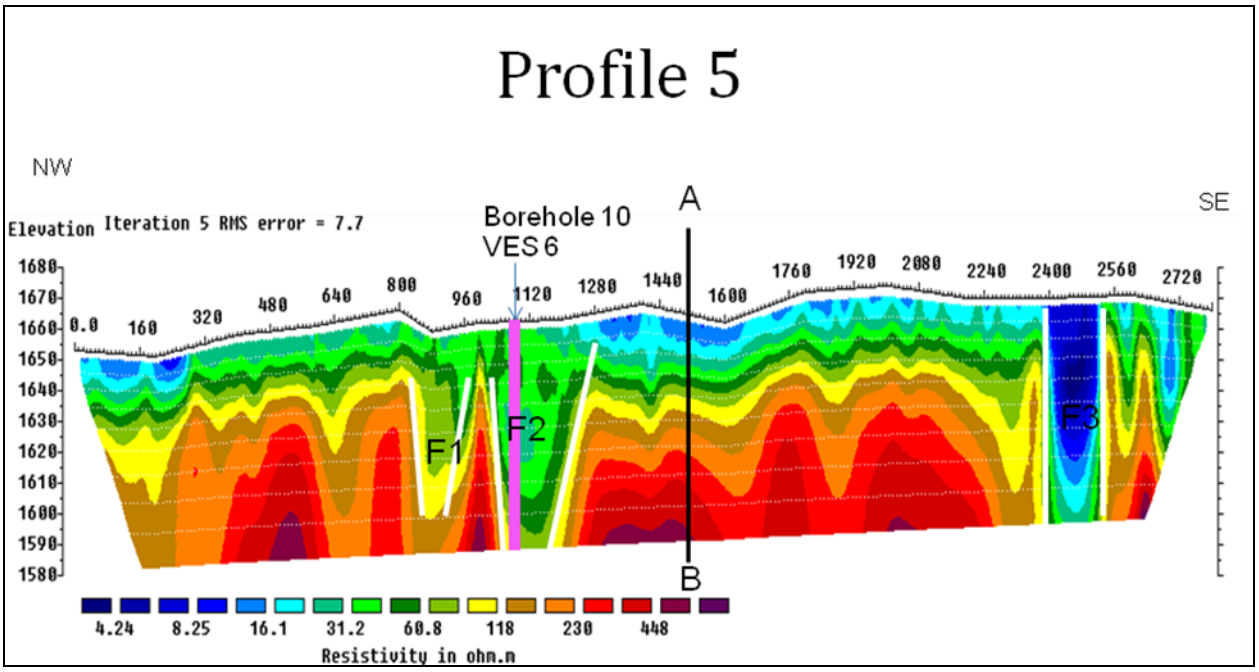

Figure 5.5: Result of 2D ERT profile 5 showing the geological formations interrupted by fractures

Fracture zone F2 presents a productive aquifer zone, although at shallow depth. Fracture zones F1 and F3 do not provide appropriate borehole site. Fracture zone F3 is partly filled with low resistivity material probably clay formation of resistivity 4Ωm to 5Ωm to a depth of 70 meters. The maximum depth achieved within this profile is 73.8 meters.

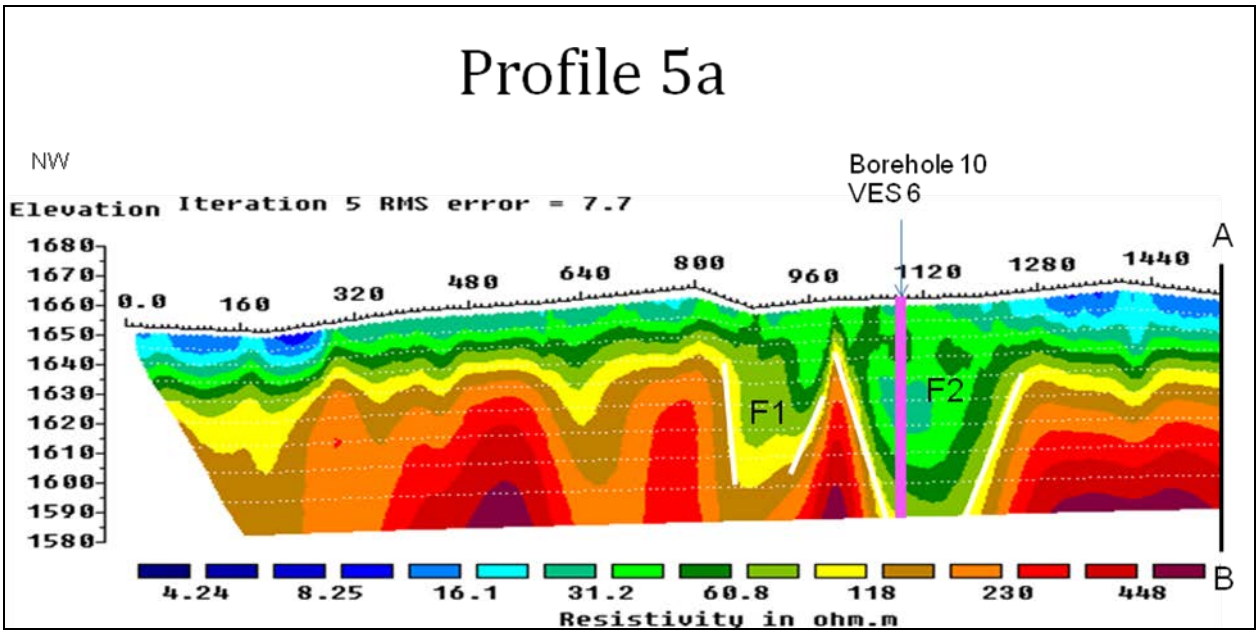

Figure 5.5a: 2D ERT North West Section along Profile 5

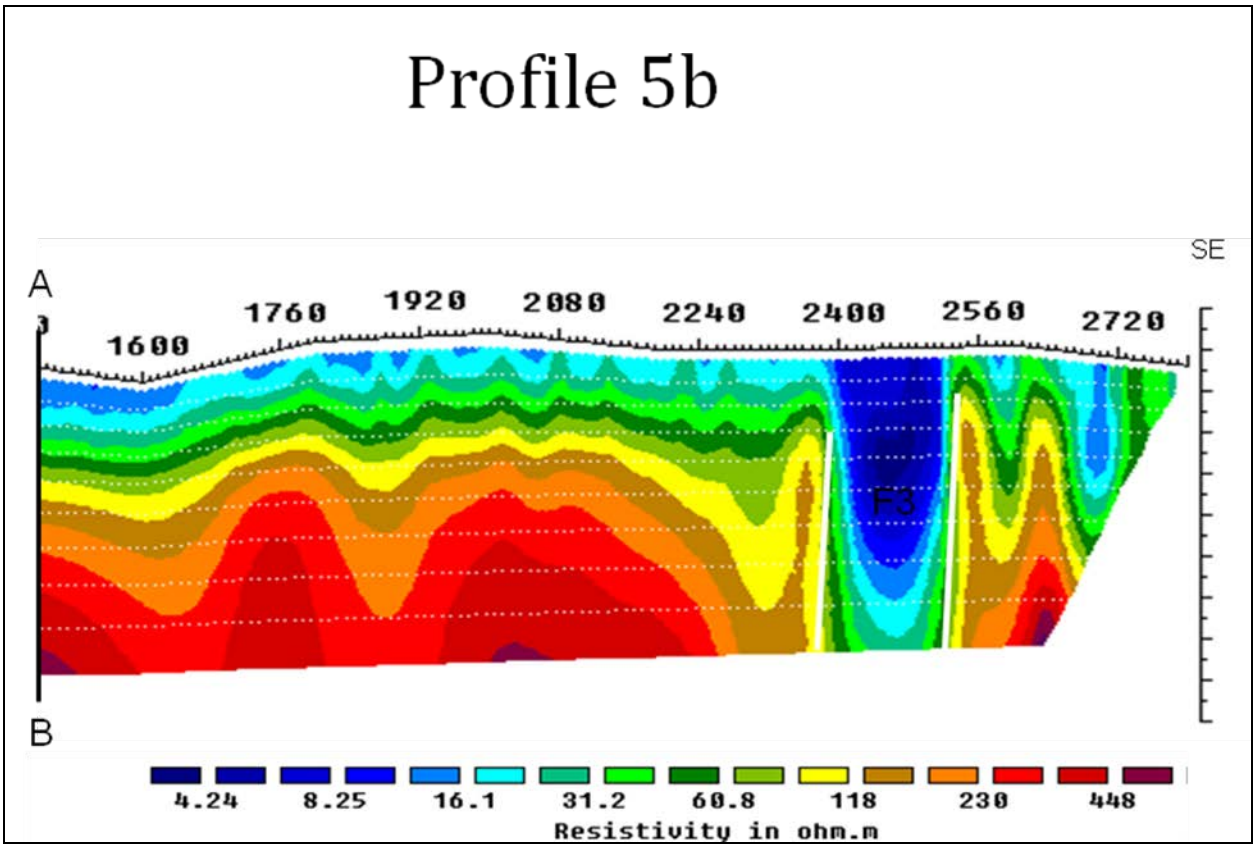

Figure 5.5b: 2D ERT South East Section along Profile 5

A borehole drilled within fracture zone F2 provide a discharge of about 4.3m^3/hr of water. VES data interpretation of borehole VES 6 indicates less fracturing at depths of more than 50 meters. The resistivity within this profile increases with depth, as observed under (Appendix II) VES analysis data. The borehole log of VES 6 under appendix III of this site also confirms slight weathering below a depth of 100 meters. Probable weathered felspathic gneiss formation continues to a depth of more than 110 meters.

5.2.6 Profile 6

Profile 6 laid 200 meters away from profile 5 although both profiles overlap at the initial point. The ERT clearly shows boundaries between different formations. Sequence of resistivity vary from low resistivity (15.1Ωm) probably sandy-clay, medium resistivity of 116Ωm probably fractured granitoid gneiss, 322Ωm probably weathered biotite gneiss

and high resistivity of greater than 537Ωm probably fresh biotite gneiss and felspthic gneiss respectively under figure 5.6.

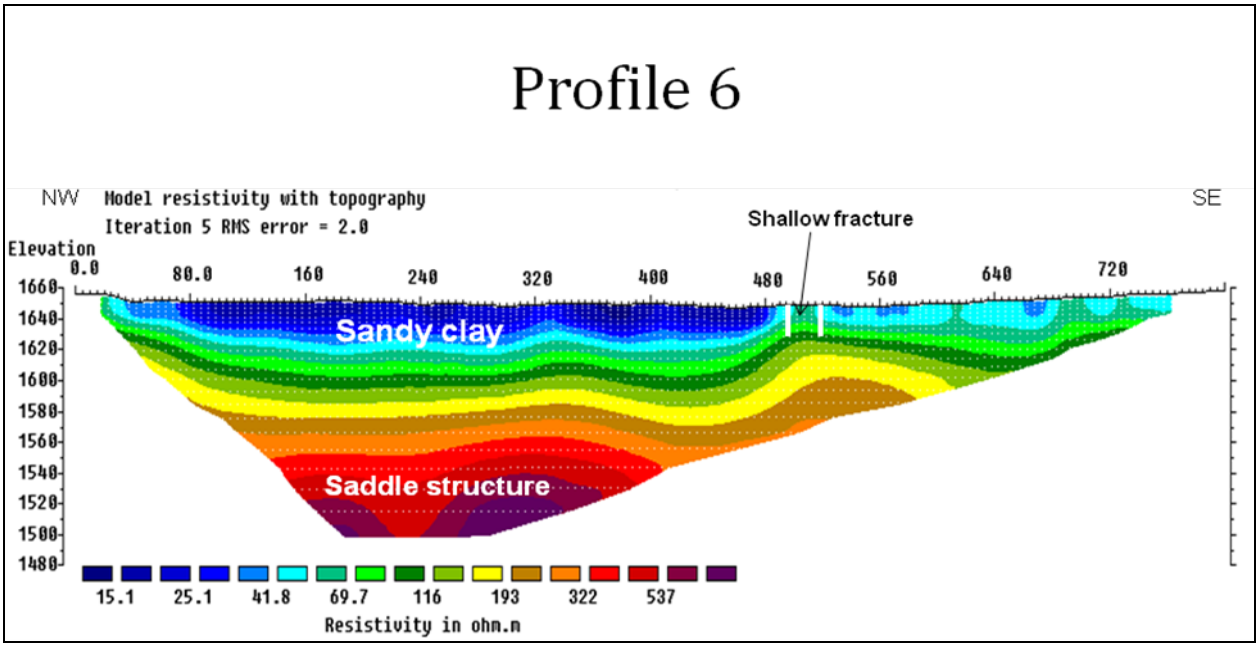

Figure 5.6: Result of 2D ERT along profile 6 showing saddle structure at the bottom

At the base of the profile, a saddle structure occurs at an elevation of 1620 meters. This structure is also observed within profile 3 and profile 8, although under profile 8, the structure ruptures completely and almost separate at the centre. A shallow forming fracture disconnects the sandy clay formation at a distance of 300 meters from the western part of the profile at an elevation of 1630 meters. A saturated zone occurs below sandy clay formation at an elevation of 1559 meters.

5.2.7 Profile 7

The resistivity tomography illustrated under figure 5.7, 5.7a and 5.7b shows fracturing within the profile. Across the profile three fracture zones are depicted. All fracture zones occur to be filled with clay formation at different depths.

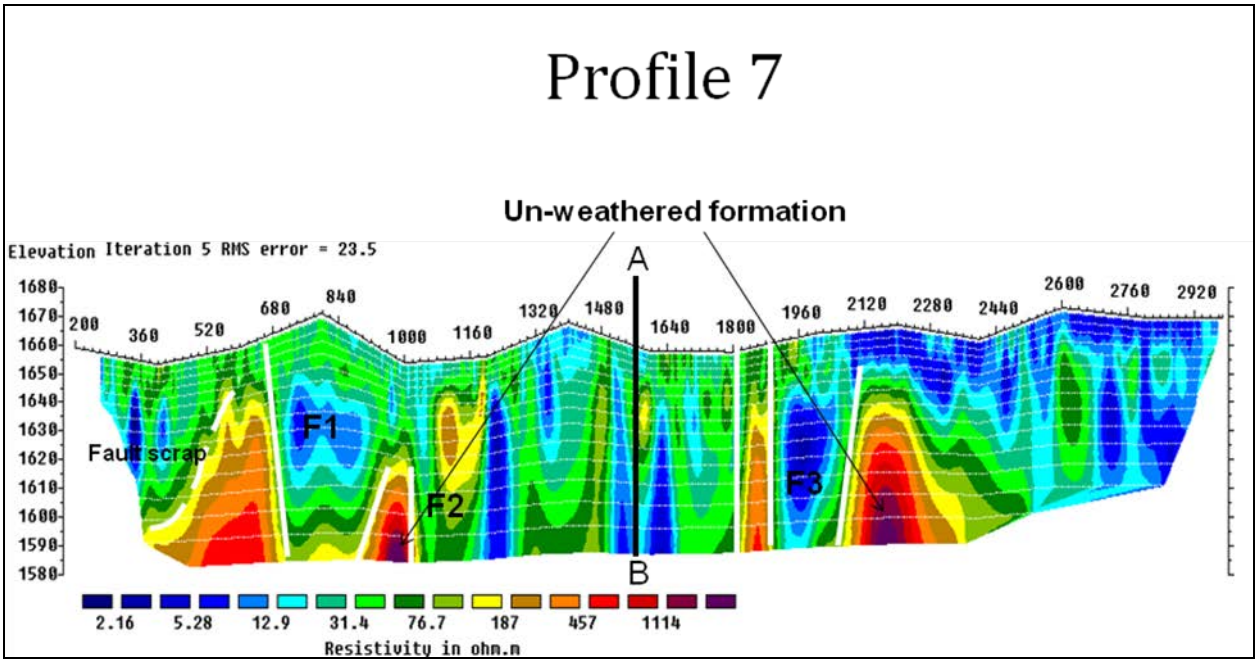

Figure 5.7: Result of 2D ERT along profile 7 showing three fracture zones

Topography of the profile varies, with the highest elevation noted at 1670 meters. A significant amount of clay- sandy formation occurs to the eastern part of the profile with resistivity of 2.16Ωm to 5.28Ωm. The moderately weathered regions occur in isolated sections at different position of the profile with resistivity of 187Ωm to more than 1114Ωm.

Within fracture zone F2 good sites for productive aquifer occurs. There is little clay formation observed at the bottom part of the fracture zone. No high resistivity material occurs within the fracture zone. This is an indication, high weathering process within the zone take place. The unweathered formation is probably felspathic gneiss.

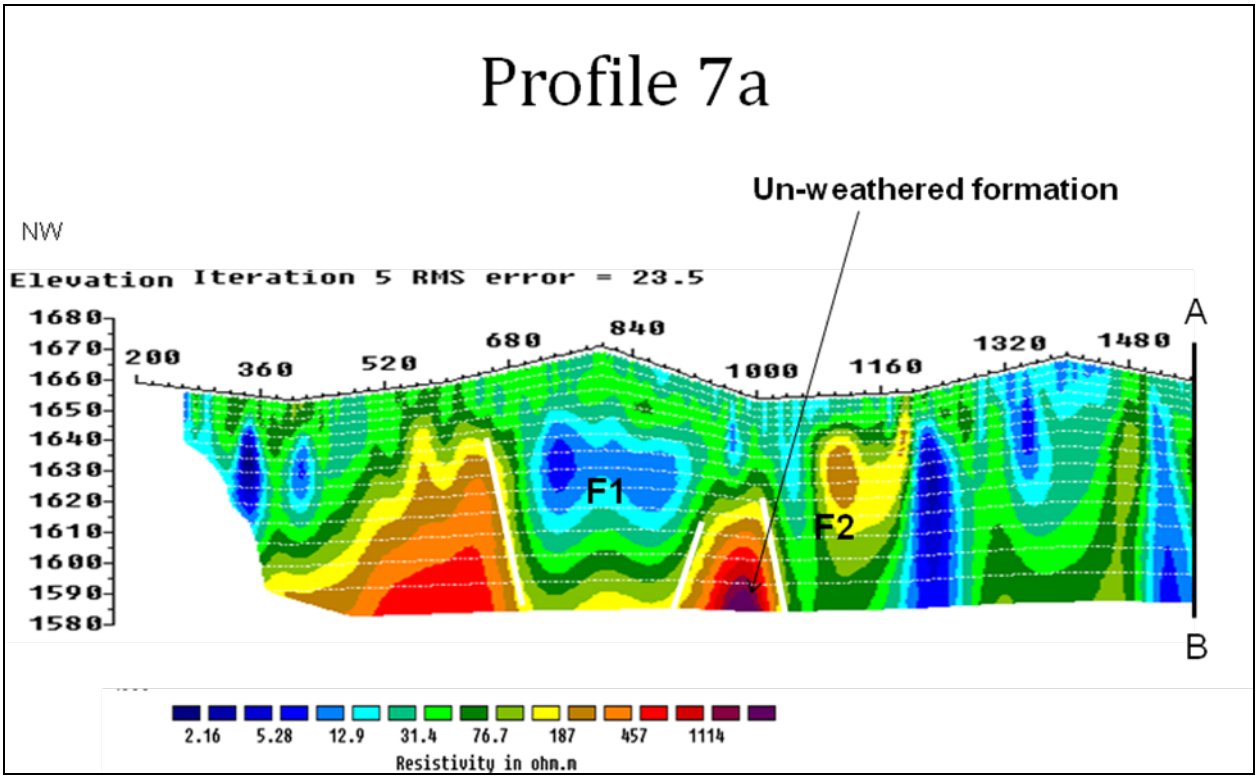

Figure 5.7a: 2D ERT North West Section along Profile 7

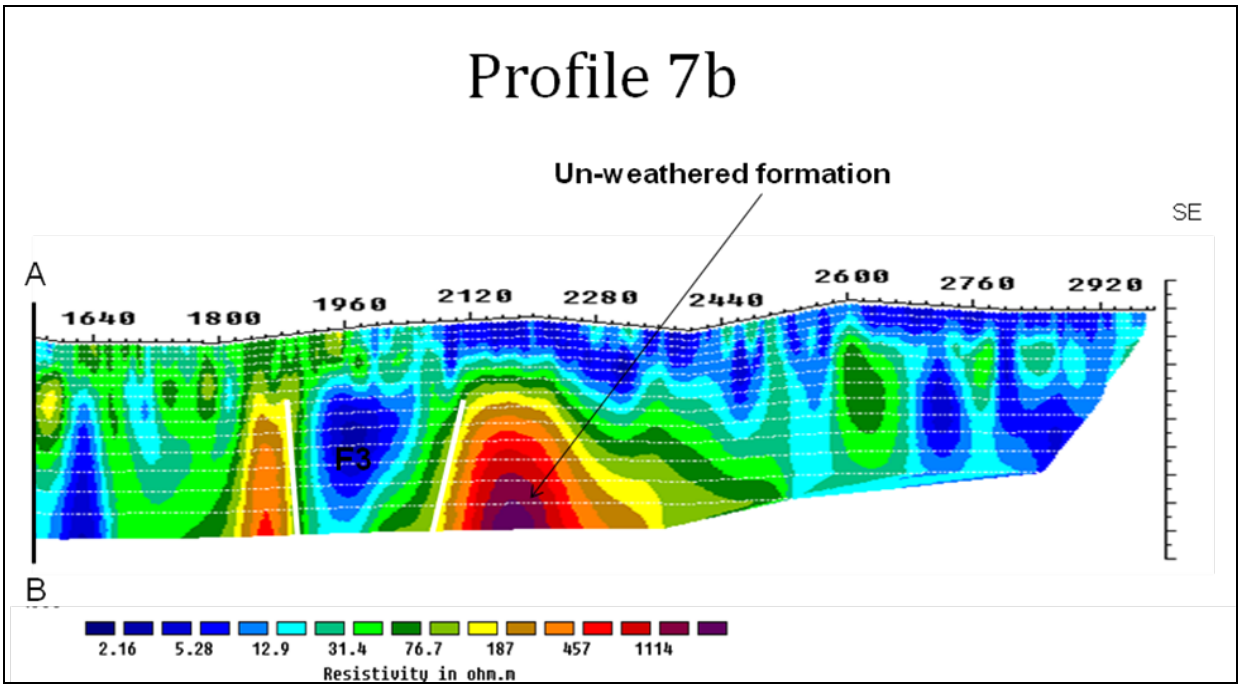

Figure 5.7b 2D ERT South East Section along Profile 7

5.2.8 Profile 8

Profile 8 was laid 900 meters away from profile 7. Same feature observed within profile 3 and 6 characterized Profile 8. Formations within Profile 8 appear to be more deformed than those within Profile 3 and 6. The deformation consists of folding and faulting. The saddle structure at the base of the profile occurs to have completely separated and the central part of the structure has widened. A fault scrap occurs on the eastern part of the profile completely separating the sandy clay formation from the eastern part as seen under figure 5.8.

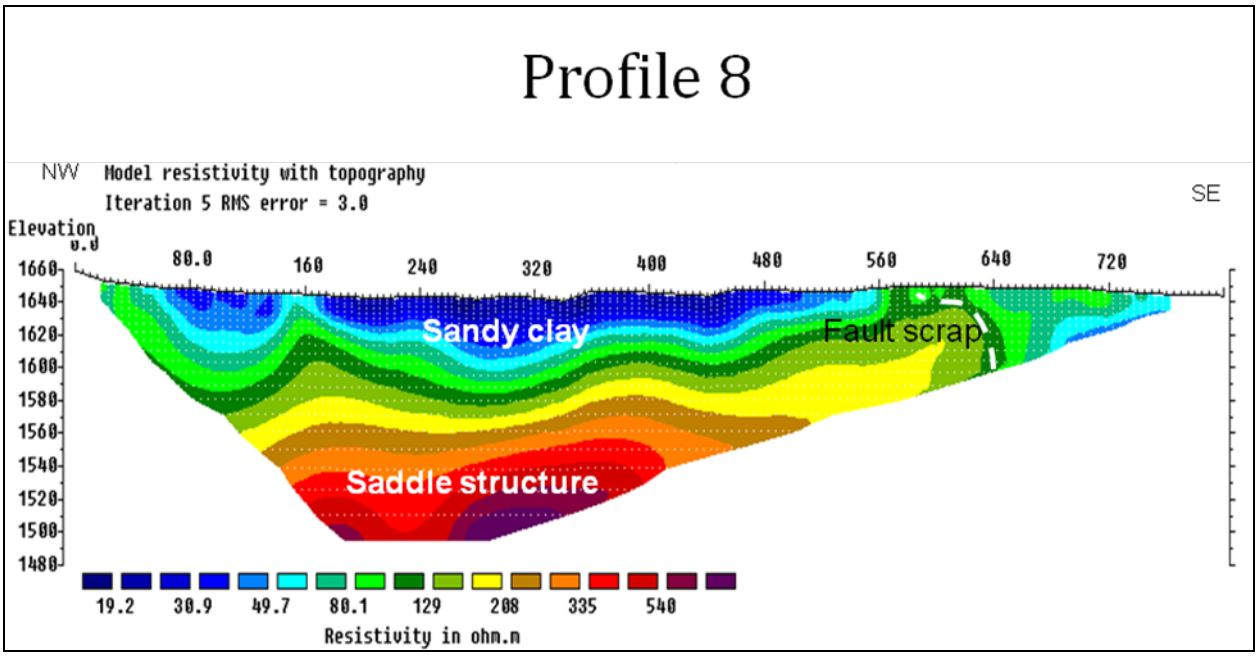

Figure 5.8: Result of 2D ERT along profile 8 showing saddle structure

The resistivity tomography clearly indicates change in thickness and geometry of the formations. The water-saturated zone varies with different depth to a maximum of 102 meters at 1560 meters. The upper layer is characterized by low resistivity of 19.2Ωm. The highest resistivity occurs with resistivity greater than 500Ωm probably felspathic gneiss formation.

5.2.9 Profile 9

Variation of resistivity characterizes Profile 9. The profile line indicates low resistivity formation probably clay formation of 4Ωm overlaid by a series of high resistivity formations seen under figure 5.9. A lithological section of this profile is illustrated under figure 6.4.

Fracture system of five fracture zones occurs across the profile. Fracture zone F1, F2 and F5 occur to narrow towards the base of the profile while fracture zone F3 widen at the bottom. Fracture zone F3 and F4 are partly filled with more sandy-clay formation.

Fracture zone F1, F2 and F5 provide good aquifer zones, although their depths are shallow with a maximum depth of 62.5 meters.

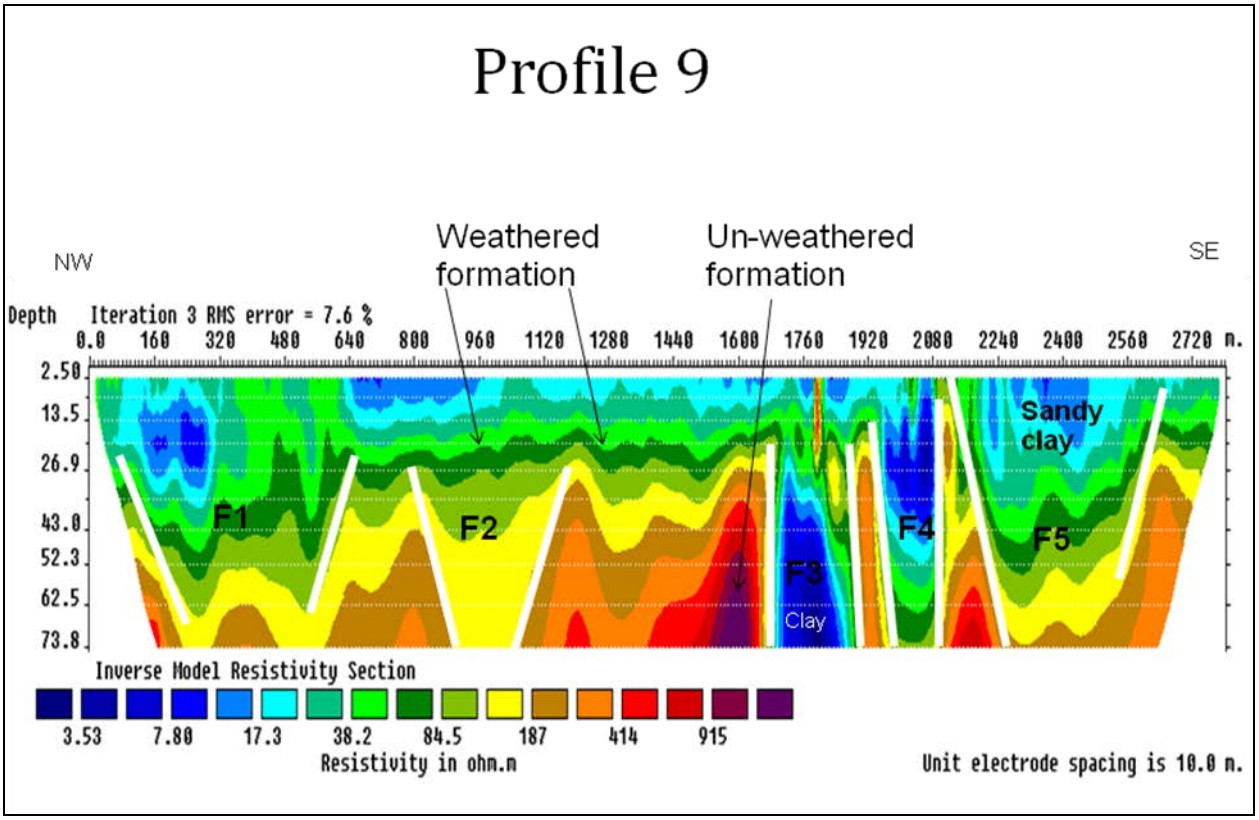

Figure 5.9: Result of 2D ERT along profile 9 showing weathered and un-weathered formations

5.2.10 Profile 10

The ERT profile line measuring a distance of about 800 meters along the profile provides a detailed variation of resistivity of more than 3581Ωm to low resistivity of 6.43Ωm. Maximum depth of the profile occurs at 159 meters deep. Lateral discontinuities of formations occur on both sides of the profiles with. Two fractures interrupt the continuity of the formations from the western and eastern part of the profile. This process of discontinuity is signified by a period of folding, uplifting and fracturing

within the area. The depositional of formation took place, followed by a period of folding of formations and later fracturing occurred.

Three zones are depicted from the profile with sandy-clay zone occurring on the upper part of the profile to a maximum of 10 meters deep. An aquifer zone is observed between the sandy-clay layer and the weathered layer see figure 5.10.

.

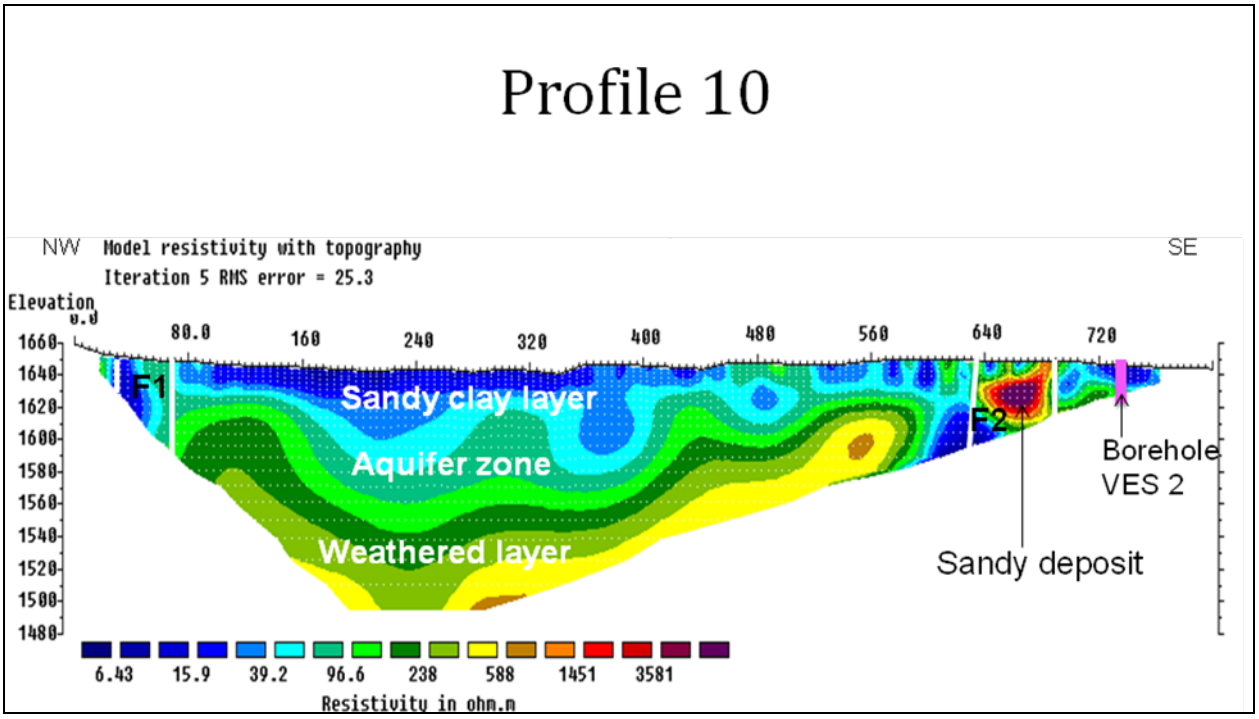

Figure 5.10: Result of 2D ERT along profile 10 showing isolated sandy deposit

Profile 10 laid at the confluence of Iviani river valley and one of its tributaries. An isolated sandy deposit occurs on the eastern part of the profile with high resistivity. The low resistivity of 6Ωm sand-clay formation overlies the aquifer zone of medium resistivity of 39.2Ωm to 96.6Ωm. The weathered layer occurs at the base and uplifted towards the eastern part of the profile with a resistivity of about 588Ωm (probably weathered biotite gneiss).

Clay formation partly fills two fracture zones as presented within the model. A borehole recorded as VES 2 with a depth of 185 meters discharges a yield of 25m^3/hr. VES data of the borehole, attached under appendix II, indicate weathering continues to depth of more than 150 meters.

5.2.11 Profile 11

This profile occurs about 50 meters from the west and 370 meters on the eastern part from profile 12. The purpose of laying this profile was to control a dry borehole earlier drilled within the area. The maximum depth achieved with this profile is 159 meters, see figure 5.11.

The profile presents horizontal beds as compared to profile 10, indicating little interference by folding and fracturing. The metamorphic formation occurs shallow, at a depth of less than 59.5 meters deep. The shallow and unfractured metamorphic rocks explain the dry borehole occurring along this profile.

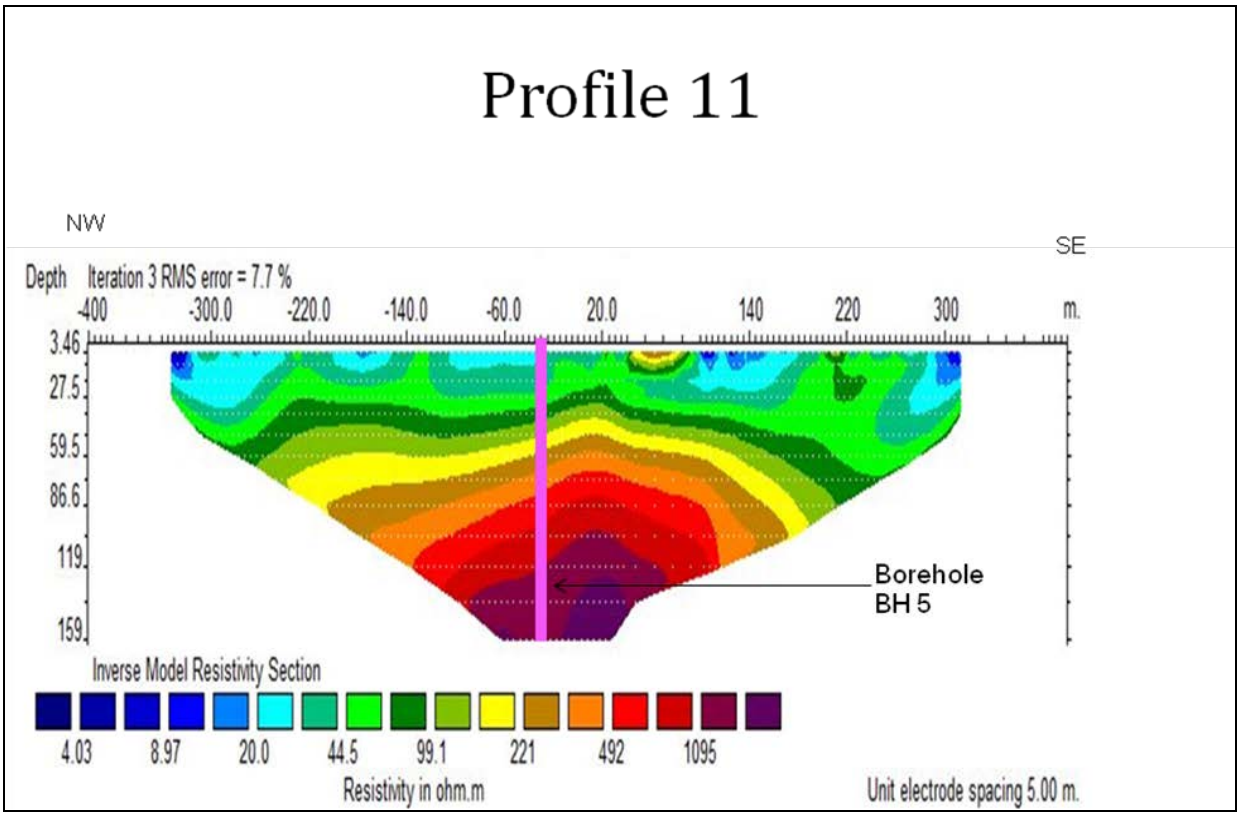

Figure 5.11: Result of 2D ERT along profile 11 showing occurrences of unweathered metamorphic rocks at shallow depth

Low resistivity of about 4Ωm formation probably sandy-clay occurs at the surface of the profile. The unweathered metamorphic rocks depict a high resistivity of more than 1095Ωm.

5.2.12 Profile 12

Resistivity varies within the model profile 12. The upper part of the profile depicts low resistivity of 1.50Ωm with sections of high resistivity, greater than 500Ωm. At the base of the model, medium resistivity of between 50Ωm to 500Ωm occurs see figure 5.12, 5.12a and 5.12b.

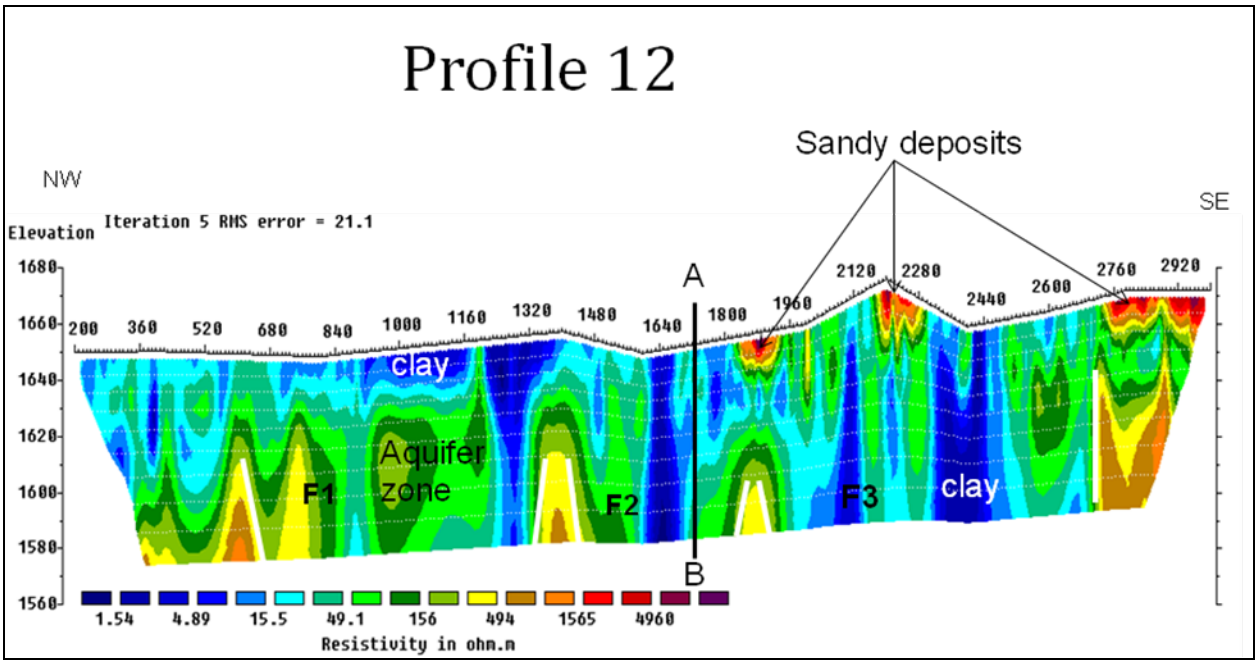

Figure 5.12: Result of 2D ERT along profile 12 showing occurrences of aquifer zone

The resistivity profile shows water saturated zones with clay infill sections. The presence of fracturing system is observed with different dimensions, shape and at different depths.

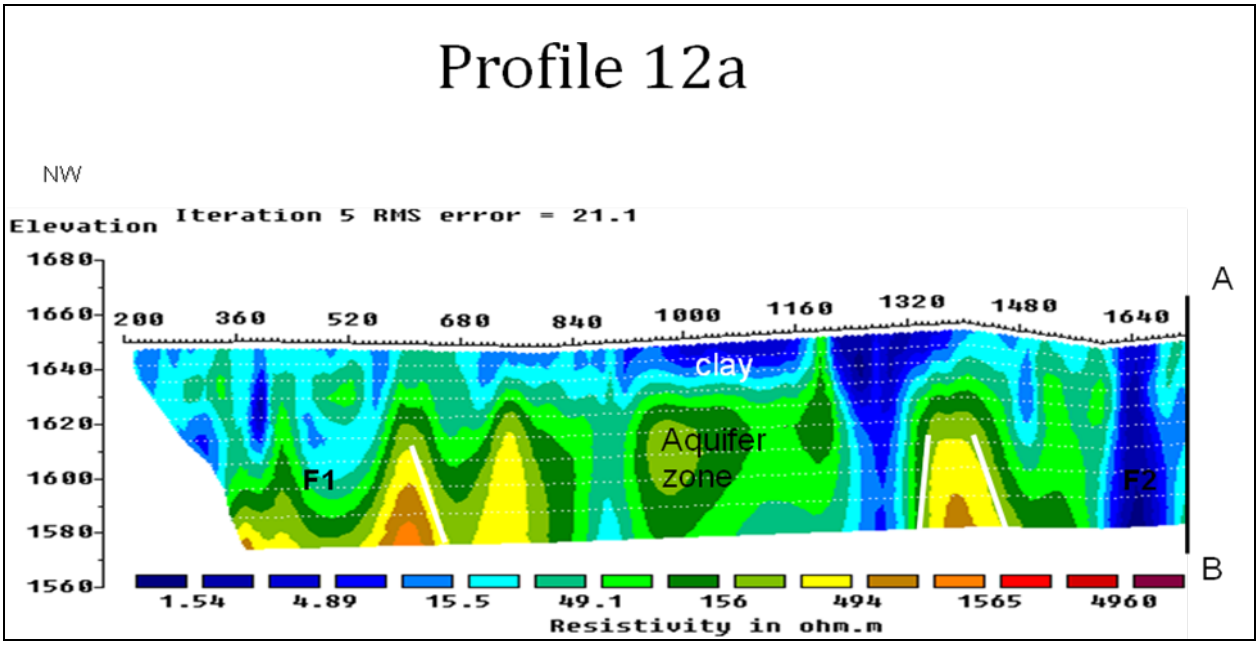

Figure 5.12a: 2D ERT North West Section along Profile 12

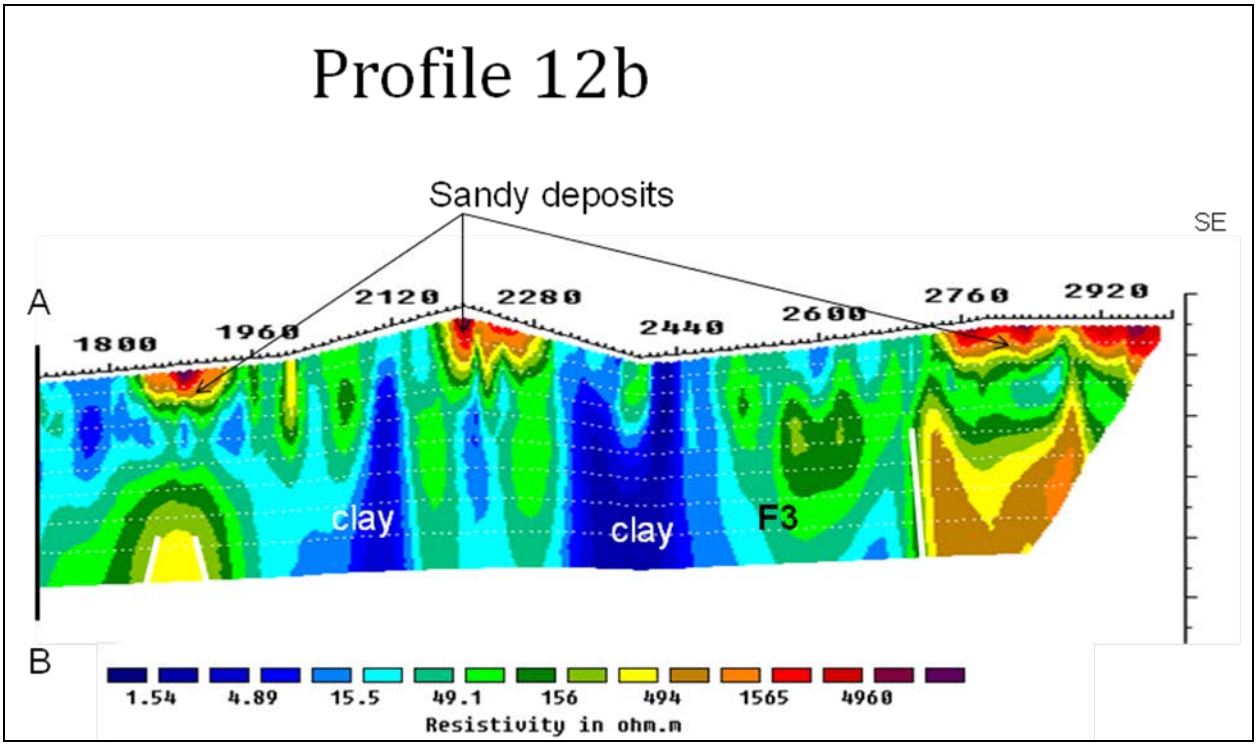

Figure 5.12b: 2D ERT South East Section along Profile 12

Three fracture zones occur across the profile and partly filled with clay material. The clay material act as barrier for aquifer zones boarding the fracture zones. This profile also occurs at the confluence of Iviani river valley and one of its tributaries.

5.2.13 Profile 13

Profile line 13 was laid on the western part of the study area. An elongated block of un-weathered formation probably a granitic rock of igneous intrusion of high resistivity strikes out within the profile which was modelled without topographic data. This elongated block of un-weathered formation could be a large geological structure probably a dome structure resulting from upwelling of granitic material within the study area. This geological structure acts as a barrier for the aquifer zone within fracture zone F1. Maximum depth achieved within this profile is 74.7 meters deep, see figure 5.13.

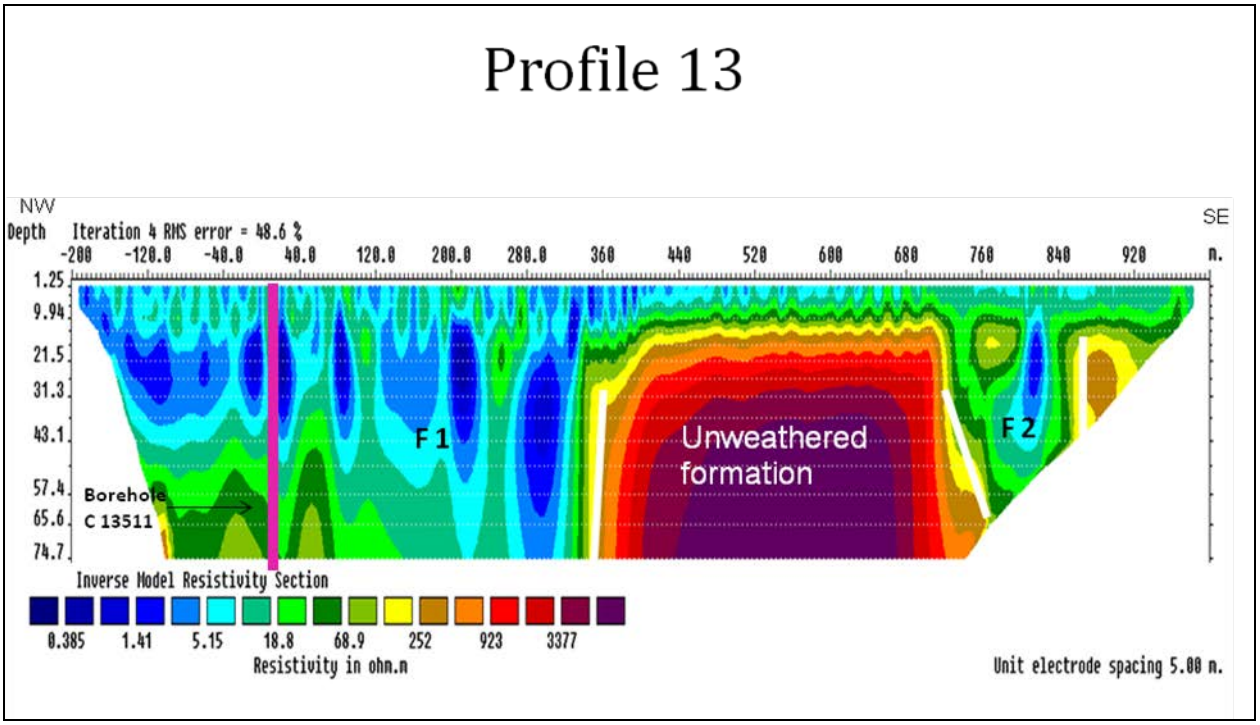

Figure 5.13: Result of 2D ERT along profile 13 showing a dome structure

Outstanding geological feature is the occurrence of two fracture zones along the profile. Fracture zone F2 extends to shallow depth while fracture zone F1 extends to a depth of 74.7 meters. Fracture zone F1 provides a region of better aquifer zone than fracture zone F2 due to its deeper depth. A borehole drilled on the western part of fracture zone F1 records a yield of 16m^3/hr, this yield implies that the fracture zone occurring on the western part of profile provides a productive aquifer zone. This profile was undertaken to control high yielding borehole C 13511 occurring within the model.

The high RMS error of 48.6% could be attributed to surrounding noise which was caused by pumping of the borehole during acquisition of data.

5.2.14 Profile 14

Profile 14 presents two isolated low resistivity parts within the model. Resistivity of 0.4Ωm (clay) to 11Ωm (sandy clay), high resistivity of a maximum of 1500Ωm probably felspthaic gneiss as observed at the base of the profile. Two shallow aquifers occur within the profile as isolated low resistivity zone see figure 5.14. A borehole drilled within this profile occur dry. This could be due to the shallow unweathered metamorphic rocks occurring within the profile or sitting of the borehole probably missed the target of the two isolated aquifers.

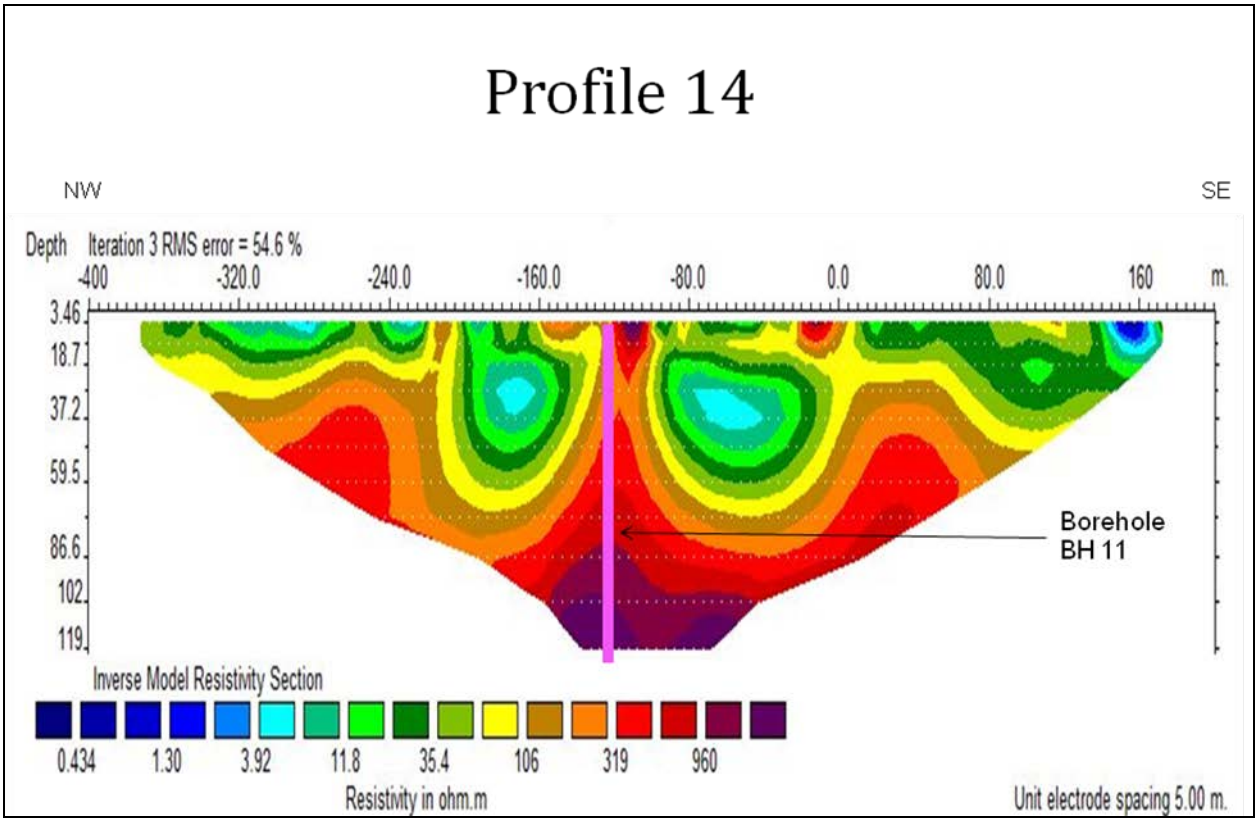

Figure 5.14: Result of 2D ERT along profile 14 showing isolated low resistivity

The RMS error within this model occur high to about 54.6%, this could be attributed to lose of data during acquisition due to faulty electrodes. Modeling of this profile did not

incorporate topographic data. Elevation within the profile varied gently therefore not influencing the model.

CHAPTER SIX

6.1 DISCUSSION

This discussion focuses around effort of advancing the understanding of groundwater occurrence in Konza area. A combination of geology, hydrogeology, and geophysics data was carried out and analyzed to identify the influence of geological structures to groundwater occurrence within the study area.

Generally the analysis of the obtained ERT images, VES and borehole data (under appendices) allowed the identification of strong variations of electrical values. The results clearly show the evidence of deep and shallow fractures within the study area. All images interpreted from data acquired from the study area shows resistivity of 0.03Ωm to 4960Ωm increasing with depth within presented 2D ERT profile. Low resistivity dominates the upper part of most profiles completely weathered zone associated with clay material. The bedrock of most of the profiles is depicted by high resistivity formation probably of igneous formation. The large variation of resistivity depicted from the profiles indicates that the formation in the area is not homogenous.

ERT method is useful in the study of horizontal and vertical discontinuities in the electrical properties of the ground. It is also useful in detection of three-dimensional bodies of anomalous electrical conductivity (Kearey et al., 2002). Although they indicate, one of the limitations of ERT survey method is that topography and its effects of near-surface resistivity variations can mask the effects of deeper variations, it will be important to note that the ERT takes into consideration topographic effect during modelling of data. Ten ERT profile data acquired were noted to have a high variation difference in elevations. These profile data were processed taking into account elevation data, thus addressing effect of masking of deep variation.

The metamorphic formation in the area occurs at different depths of the profiles. Although occurs deeper within profiles 10 and 12 in the western part of the area. Probably due to deep weathering within the region. Clay material is depicted within the profiles at different depths. This clay material is the product of weathering within the

area and the clay type is probably smectites clay or vermiculites clay. This is due to their swelling nature when in contact with water. Sandy material of high resistivity similar to the metamorphic formation occurs in patches on the surface of profiles 4, 9, 10, 12 and 14.

Overlying the bedrock basement formation is the weathered metamorphic formation, which is highly fractured except within profiles 3, 6, 8 and 11 which show little of no fracturing. Some of these fracture zones act as a structural control of groundwater infiltration for recharge zones of deeper aquifer zones. In filled fracture zones with clay material act as low permeability or barrier to groundwater.

The Kapiti Phonolite as explained by Baker (1952) occurs in the western part of the study area. He notes it outcrops as lavas in a few areas in the neighborhood of Stony Athi River. The interface between Kapiti Phonolite and metamorphic System is probably located on the extreme southern part of profiles 12 and 13. No Kapiti Phonolite formation occurs within any of the fourteen profiles laid within the area, although Baker (1952) indicates phonolite outflows to the study area.

(Sander 2007) in analyzing different types of maps and remotely sensed data to understanding groundwater occurrence, especially in areas with igneous and metamorphic rocks, reviewed the application and limitations of lineament approaches in groundwater exploration. It was noted that mapping and interpretation of lineaments need to be done with care and with proper understanding of maps and images.

Electrical resistivity of between 10Ωm to 100Ωm within the area depicts saturated zone of water bearing aquifers. Profiles 10 and 13 provide productive aquifer zones. This is evidenced by two high yielding boreholes BH VES 2 with a yield of 25m^3/hr and borehole C13511 of 16m^3/hr of yield. (BH and C are coding of the boreholes). These two boreholes are high yielding probably due to their location within fracture zones as indicated within the profiles. From the analysis of borehole water struck level two aquifer zones of 50 meters (shallow zone) and 100 meters (deep zone) deep occur within the area.

Profile 12 provides a good drilling site for a productive borehole although no borehole control is within this profile. The probable location of Profile 10 and 12 within confluence of Iviani valley and its tributaries also provide good drilling site for productive borehole. Profile 10 demonstrates less clay material as compared to other profiles. Clay material at the surface can probably act as an impermeable layer for groundwater recharge.

Profiles 5, 6, 8 and 11 encounter shallow metamorphic formation. Profile 4, 5 and 7 depict fracture zone in-filled with clay material at different depths. These characteristics of shallow unweathered metamorphic rocks and infill of clay material within fracture zones do not offer good regions for productive aquifers. Shallow unweathered metamorphic rocks implies shallow aquifer to a depth of 30 meters as observed within profile 11 which could easily contaminate with surface water. In-filled clay material within the fractured zone implies barrier of the aquifer. These regions are therefore not recommended site for drilling boreholes. It is also noted from the analysis of borehole logs appended under Appendix III, drilling, which encountered quartzite, feldspathic and fresh biotite gneiss formations at shallow depths of 15 meters end up with dry boreholes. This is because unless these formations are fractured or weathered, they have little or no porosity, thus low permeability.

Weathering process within the profiles is depicted from the surface towards the bedrock of the profiles. This illustrates clay and quartz materials at the surface of the profiles which are product of weathering. Less weathering process is noted within profiles, 3, 8 and 11. This depicts homogenous formations which are not disrupted by weathering process.

VES data presented under Appendix II indicate fracturing at different depths of the formations within the area. This data further indicate possible continuation of metamorphic formation to depths of more than 200 meters.

Two fracture lines were detected through the analysis of the profiles within the area. Figure 6.1a - b shows the delineation of fracture lines running parallel to each other on a NE-SW direction. Fracture line occurring on the North West direction cuts profiles 1, 2,

4, 7, 8, 10 and 12 at a distance approximately 640 meters within the outlined profiles. This fracture line is interrupted within profile 5. Fracture line occurring in the south east direction of the profiles cuts profiles 1, 2, 4, 5, 7, 8, 9, 10 and 12 at a distance approximately 2400 meters within all the stated profiles. Figures 6.1a, 6.1b and 6.1c show the fracture lines within the profiles. Figure 6.2 shows an inferred fracture line on a geological map of the study area.

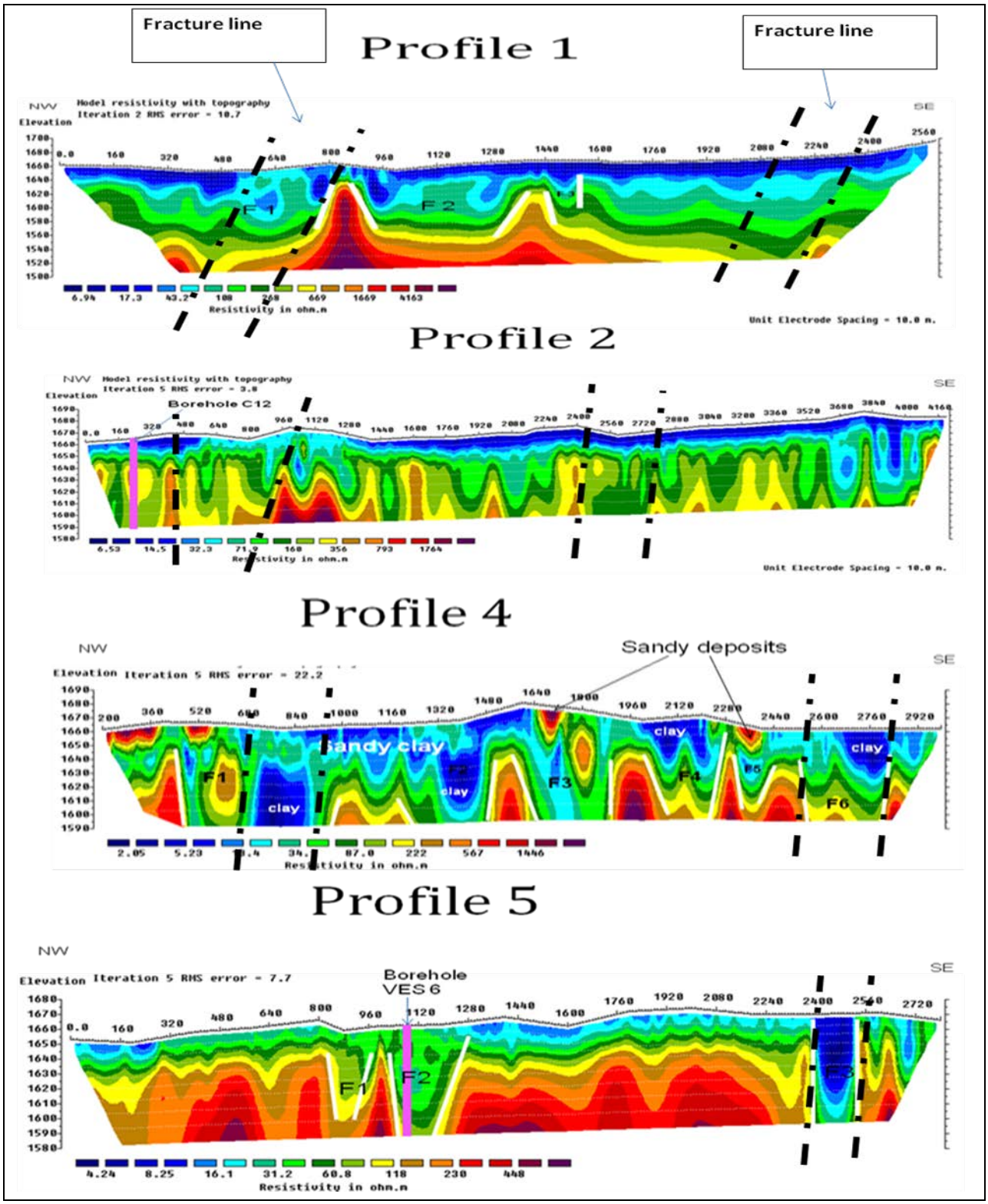

Figure 6.1a: ERT models Illustrating fracture lines (dash) cutting through in North West - South East directions in profiles 1, 2, 4 and 5 in Konza area

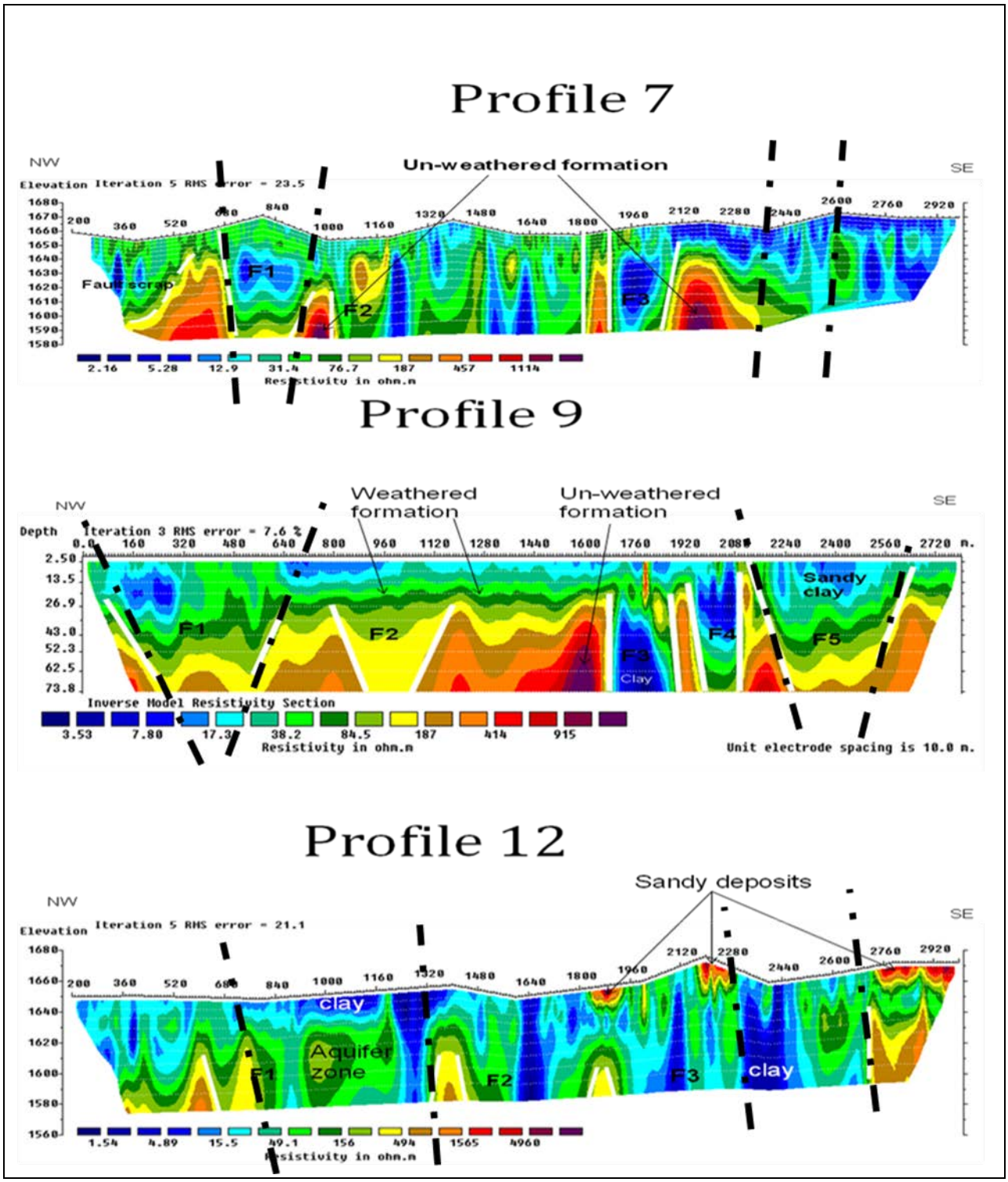

Figure 6.1b: ERT models Illustrating fracture lines (dash) cutting through in North West - South East directions in profiles 7, 9 and 12 in Konza area

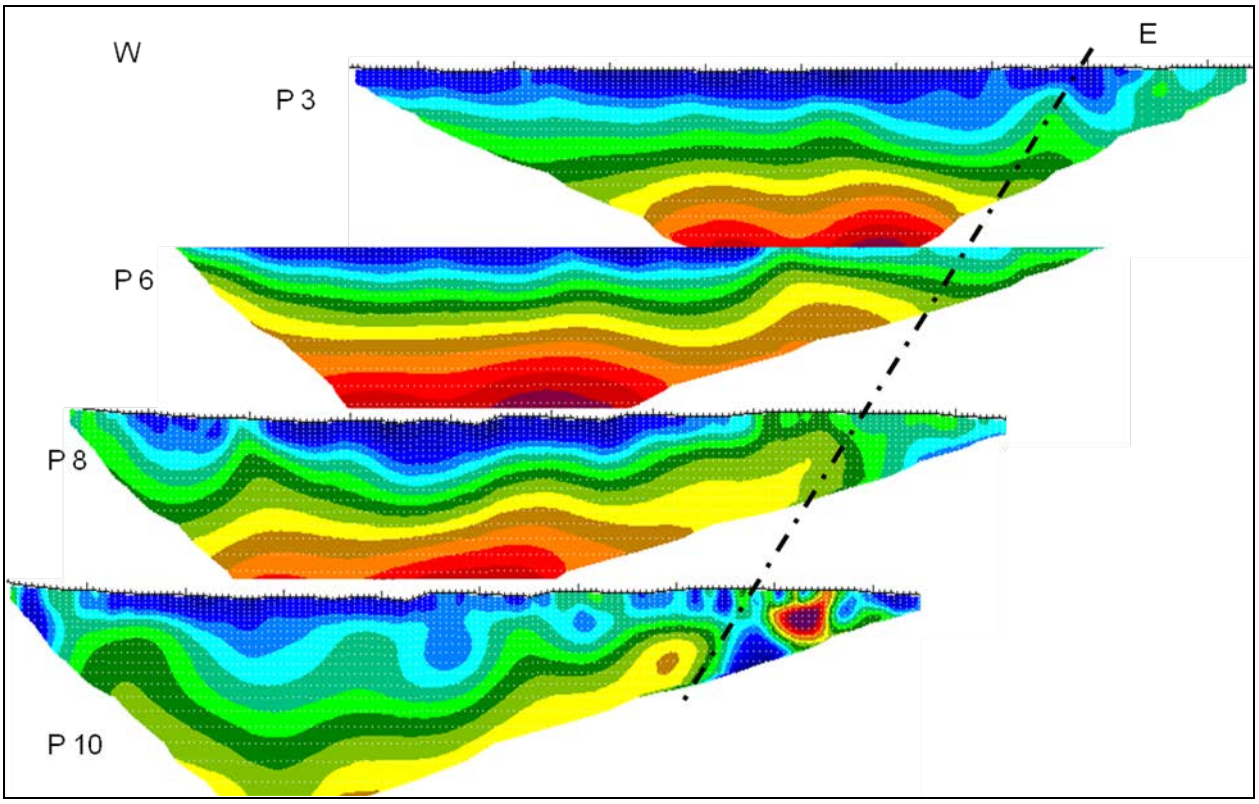

Figure 6.1c: ERT models illustrating fracture line (dash) cutting through in North East - South West directions in profiles 3, 6, 8, and 10 in Konza

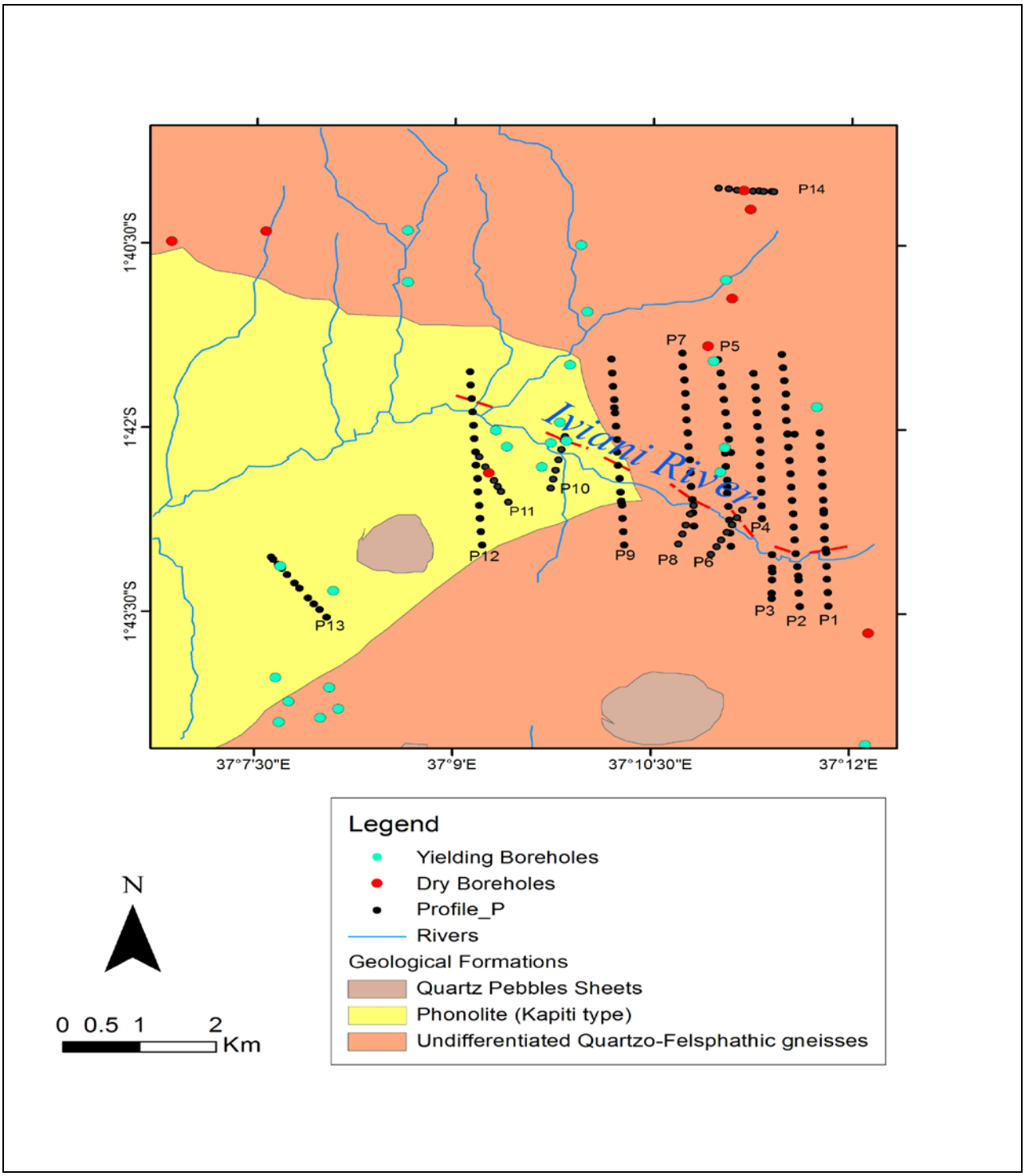

Figure 6.2: showing inferred fracture line on geological map parallel to Iviani river valley in Konza

A general lithological section of the area is outlined under figure 6.4 considering resistivity of different rocks under figure 6.3.Depth of the formations is estimated after the analysis of data acquired from the area.

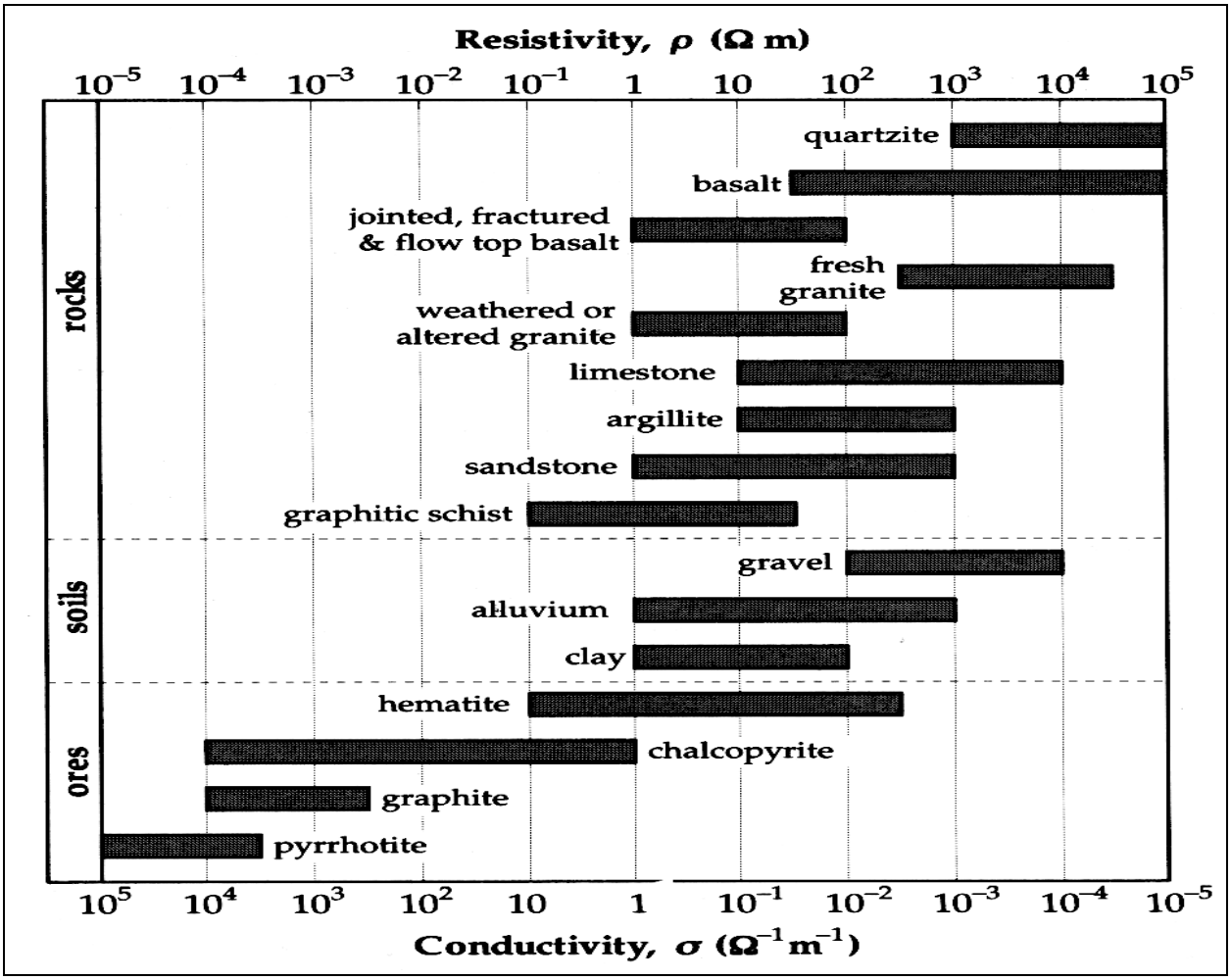

Figure 6.3: Typical ranges of electrical resistivity/conductivities of earth materials (after Ward, 1990a).

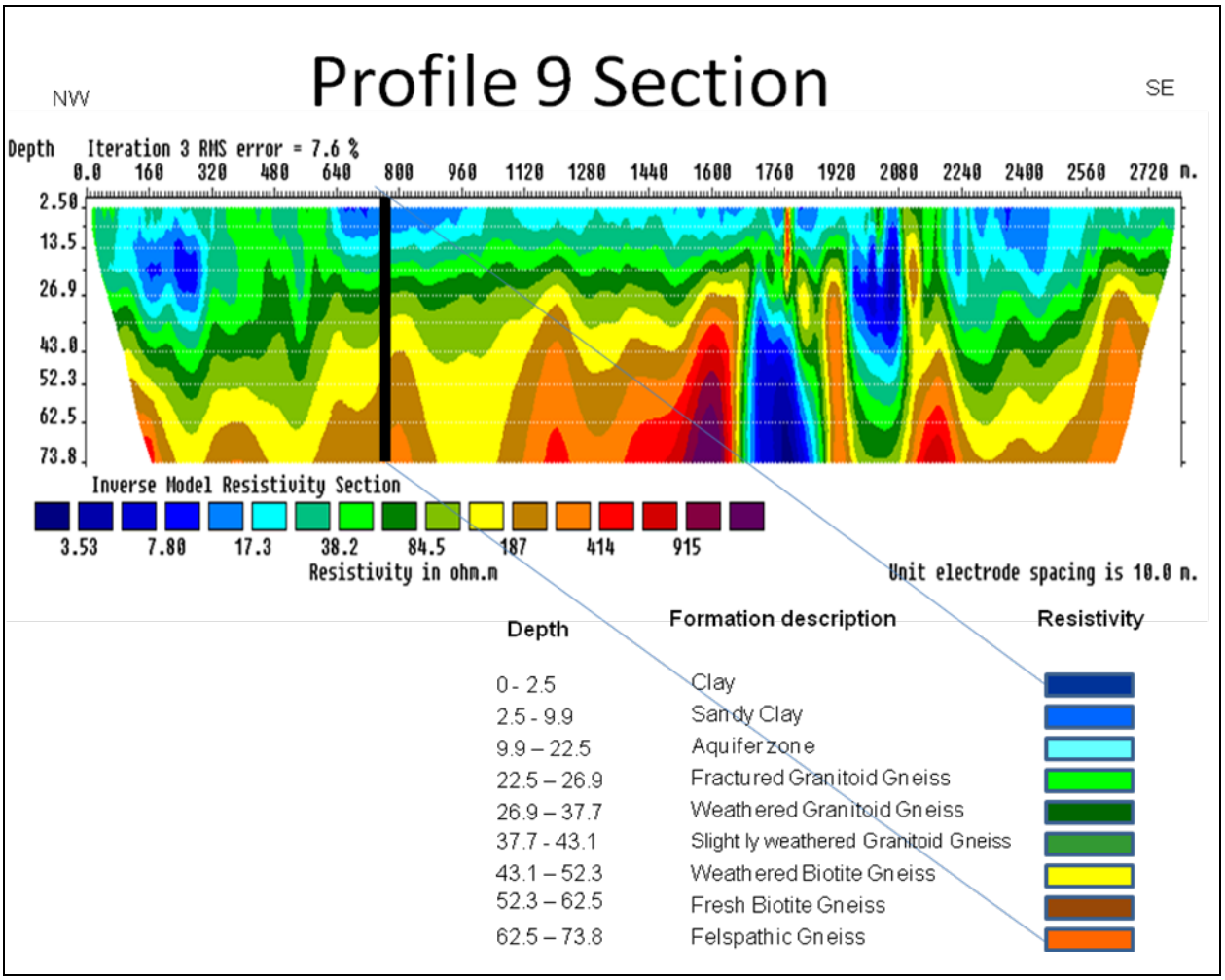

Figure 6.4: Showing lithological section in Konza area along profile 9

CHAPTER SEVEN

7.1 CONCLUSION AND RECOMMEDATION

7.2 CONCLUSION

Application of 2D ERT to access influence of geology and geological structures on groundwater occurrence and potential in the study area was achieved through this study. 2D ERT was used as an effective technique. VES technique and borehole data were also used in the study.

Use of ERT allowed confirmation of VES data to certain depths. Interpretation of wet weathered formation, earlier interpreted with VES as water bearing zones during hydrogeological survey, was interpreted through the use of ERT as fracture zones filled with clay material.

A general understanding of the influence of geological structures on groundwater occurrence is achieved. This was necessary for the selection of drilling site of productive boreholes within the study area. It is concluded from this study that fracture limbs of impermeable formation and clay material act as barriers or semi-barriers for groundwater flow. It is also noted from this study that some clay filled fracture zones act as aquiclude where water is absorbed, but no significant amount of water can be released from the same fracture zone. The problem related to low yield and dry borehole of groundwater drilled within the area is identified as due to dominance of clay material filled within fracture zone or thick clay material at the surface of the area. Shallow basement formation is also related to the problem.

The depth of bedrock within the study area was estimated with high accuracy. The profiles concur with Baker (1952), that rocks within the area were originally sedimentary before they were granitized and metamorphosed. Metamorphic formation is illustrated at different depths and generally observed at deeper depth on the western part as compared to the eastern region unless where outcrop occur.

The series of resulting tomography revealed the stratigraphic formations, fracture zones and water bearing zones. Modelled results indicate geological structures within the area are mapped at different depth and orientation.

Iviani river valley displays different geological structures within different profiles. Several sections within the river valley illustrate the high potential for productive aquifer, especially at the confluence of the valley and some of its tributaries.

Fracture lines running NE-SW parallel to each other are detected within the study area.

7.3 RECOMMENDATION

The following are recommended for future hydrogeological survey within the study area;

The use of geophysical and hydrogeological methods presented within this study is recommended for complex geological terrain.

It is recommended that drilling of boreholes in very low permeable rocks be undertaken along fracture zones which are not filled with clay material to avoid low yielding or dry borehole.

It is also recommended from this study that an attempt of estimating fracture-zone permeability introduced by geological structures be undertaken to optimize regions of high groundwater potential for sustainability of aquifers identified within the study area.

REFERNCES

Acharya, T., Basumallik , S., Nag, S. K.,Prasad, R., 2013: Study of Lineaments in Metamorphic Terrains Using Electrical Resistivity Tomography, Purulia District, West Bengal, (India). Journal of Engineering Geology and Hydrogeology 1(1):16-22

Ahmadov, R., Aydin, A., Karimi-Fard, M., Durlofsky, L. J., 2007: Permeability Upscaling of Fault Zones in the Aztec Sandstone, Valley of Fire State Park, Nevada, with a Focus on Slip Surfaces and Slip Bands. Hydrogeology Journal 15: 1239–1250

Al-Taj, M., 2008: Structural Control on Groundwater Distribution and Flow in Irbid Area, North Jordan. Jordan Journal of Earth and Environmental Sciences *1, 2, 81- 88*

Baker, B. H., 1952: Geology of the Southern Machakos District. Geological Report No 27. Mines and Geology Department. Government Printers, Nairobi

Barhen, J., Berryman, J. G., Borcea, L., Dennis, J., de Groot-Hedlin, C., Gilbert, F., Gill, P., Heinkenschloss, M., Johnson, L., McEvilly, T., More, J., Newman, G., Oldenburg, D., Parker, P., Porto, B., Sen, M., Torczon, V., Vasco, D., and Woodward, N. B., 2000: Optimization and Geophysical Inverse Problems. Ernest Orlando Lawrence Berkeley National Laboratory Report No. 46959

Barongo, J. O., 1989: Application of Transient Airborne Electromagnetic and Ground Resistivity Methods to Geological Mapping in Tropical Terrains. Ph.D. Thesis. Mc Gill University

Billing, M. P., 2008: Structural Geology Third Edition. Prentice Hall of India Private Limited, New Delhi 606pp

Cassinis R, Mazzotti A., 1993: Geophysical Aspects of Areas of Complex Geology — An introduction. Journal of Applied Geophysics 29: 227–245

Chandra, S., Rao, V. A., Krishnamurthy, N. S., Dutta, S., Ahmed, S., 2006: Integrated Studies for Characterization of Lineaments Used to Locate Groundwater Potential Zones in A Hard Rock Region of Karnataka, India. Hydrogeology Journal 14 1042 - 1051

Chikwelu, E. E., and Udensi, E. E., 2013: Direct Current Resistivity Investigation of the Groundwater Potential and Basement Structure in Parts Of Pompo Village, Minna, Nigeria. Journal of Applied Geology and Geophysics 1, 1: 11-19

Coker, J. O., 2012: Vertical electrical sounding (VES) Methods to Delineate Potential Groundwater Aquifers in Akobo Area, Ibadan, South-western, Nigeria. Journal of Geology and Mining Research 4(2): 35-42

Davis, S. N., DeWest, J. W., 1966: Hydrogeology. Wiley, New York 463 pp

Dey, A and Morrison, H. F., 1979a: Resistivity Modeling for Arbitrarily Shaped Two-Deminsional Structures, Geophysics Prospect. 27 106-36 pp

Driscoll, G. F., 2005: Groundwater and Wells. Johnson Filtration System Inc., St. Paul Minnesota 1089pp

Elhag A. B., Elzien S. M., 2013: Structures Controls on Groundwater Occurrence and Flow in Crystalline Bedrocks: A Case Study of the El Obeid area, Western Sudan Global Advanced Research Journal of Environmental Science and Toxicology 2(2): 037-046

Githinji. W. T., 2013: Geological, Geophysical and Geotechnical Evalution of Earth's Subsurface Suitability For Dam Construction: A Case Study of Maira Damsite, Nambale Area Busia County. Msc Thesis University of Nairobi. Unpublished

Griffiths, D. H and Barker, R. D., 1993: Two dimensional resistivity imaging and modeling inareas of complex geology. *Journal of Applied Geophysics,* 29: 211-226

Henriksen, H., Braathen, A., 2006: Effects of fracture lineaments and in-situ rock stresses on groundwater flow in hard rocks: A Case Study from Sunnfjord, Western. Norway Hydrogeology Journal 14: 444–461

Kearey, P., Brooks, M., Hill, I., 2002: An Introduction to Geophysical Exploration, 3rd Edition, Blackwell Science Ltd 262pp

Keller, G. V., Anderson, L. A., and Pritchard, J. I.,1966: Geological Survey Investigations of the Electrical Properties of Crust and Upper Mantle. Geophysics, 31(6):1078 - 1087

Kuria, Z. N., 2011: Seismotectonics of active faults: Magadi fault system, southern Kenya Rift, ITC PhD. Thesis University of Twente

Kuria, Z. N., 2000: Hydrogeology of Lake Nakuru Drainage Basin Using Electrical Resistivity Survey. Msc Thesis University of Nairobi. Unpublished

Lines, L. R., and Treitel, S.,1984: A Review of Least Squared Inversion and its Application to Geophysical Problems. Geophys Prospecting 32: 159-186

Loke, M.H., 1999: Electrical imaging surveys for environmental and engineering studies: A practical guide to 2-D and 3-D surveys, available on www.abem.se

Loke, M.H., 2001: Revised Tutorial: 2-D and 3-D Electrical Imaging Surveys, available on www.geoelectrical.com

Lopez, S. A. P., 1995: One- And Two-Dimensional Interpretation of DC-Resistivity Data. Orkustofnun, Grensasvegur 9, IS-108 Reykjavik, Iceland

Lowrie. W., 2007: Fundamentals of Geophysics 2nd Edition. Cambridge University Press 381pp

MacInnes, S., and Zonge, K.,1996: Two-Dimensional Inversion of Resistivity and IP Data with Topography. Presentation at the 102 Annual Northwest Mining Association Convention. Spokane, Washington

Ministry of Information and Communication, 2012, Konza Technology City Short Term Water Supply Detailed/Provisional Design Report, Volume 1 Main Report pp

Mohammed, N. E., Yaramanci, U., Kheiralla, K. M., Abdelgalil, M. Y., 2011: Assessment of integrated electrical resistivity data on complex aquifer structures in NE Nuba Mountains – Sudan. Journal of African Earth Sciences 60, 5: 337-345

Mulwa. K. J., 2001: Geological and Structural Set-up of Kiserian-Matathia Area and Its Influence on Groundwater Distribution and Flow Msc Thesis University of Nairobi

Mulwa, J.K., Gaciri, S.J., Barongo, J.O., Opiyo-Akech,N., Kianji, G.K., 2005: Geological and Structural Influence on Groundwater Distribution and Flow in Ngong Area, Kenya. *African Journal of Science and Technology Science and Engineering Series* 6, 1: 105 – 115

Mumma, A., Kairu, E. N., Lane, I. M., 2010: Kenya Groundwater Governance Case Study. Final Draft Report for World Bank 81pp

Narayan, S., Dusseault, B., Nobes, C.D., 1994: Inversion Techniques Applied to Resistivity Inverse Problems. Inverse Problem 10: 669-689

Neves, M. A., Norberto, M., 2007: Well productivity controlling factors in crystalline terrains of southeastern Brazil Hydrogeology Journal 15: 471–482

Njoroge, S. N., 2013: Hydrogeological Survey Machakos County. Aqua Well Services

Olayinka, A. l., Amidu, S. A., Oladunjoye, M. A., 2004: Use of Electromagnetic Profiling and Resistivity Sounding for Groundwater Exploration in the Crystalline Basement Area of Igbeti, Southwestern Nigeria. Abstract. Global Journal of Geological Sciences 2(2):243-253

Patella, D and Patella, M. S., 2009: Geophysical Tomography in Engineering Geology: An Overview. The Open Geology Journal 3: 30-38

Per, S., 2007: Lineaments in Groundwater Exploration: A Review of Applications and Limitations. Hydrogeology Journal 15: 71–74

Qarqori, Kh., Rouai, M., Moreau, F., Saracco, G., Dauteuil, O., Hermitte, D., Boualoul, M., Le Carlier de Veslud, C., 2012: Geoelectrical Tomography Investigating and Modeling of Fractures Network around Bittit Spring (Middle Atlas, Morocco). International Journal of Geophysics 2012 13

Sabet, M. A., 1975: Vertical Electrical Resistivity Soundings To Locate Ground Water Resources: Virginia Water Resources Research Center Virginia Polytechnic Institute and State University Blacksburg

Sander, P., 2007: Lineament in Groundwater Exploration; A Review of Applications and Limitations. Hydrogeology Journal 15: 71-74

Sen, M. K., Stoffa, P. L., 2013: Global Optimization Methods in Geophysical Inversion. 2nd Edition Cambridge University 302pp

Silvester, P. P., Ferrari, L. R., 1990: Finite Elements for Electrical Engineers 3rd Edition. Cambridge University

Šumanovac, F and Dominković. S. A., 2007: Determination of Resolution Limits of Electrical Tomography on the Block Model in A Homogenous Environment by Means o Electrical Modelling. Rud.-geol.-naft. zb. 19: 47 – 56

Telford, M. W., Geldart, P. L., Sheriff, E. R., 1990: Applied Geophysics 2nd Edition. Cambridge University Press 770pp

U S Department of Energy., 2000: Electrical Resistance Tomography for Subsurface Imaging; Characterization, Monitoring and Sensor Technology Crosscutting Program and Subsurface Contaminants Focus Area. Innovative Technology Summary Report

Wanjohi A.W., 2013: Characterization of structural control on groundwater using magnetic and electrical resistivity method in Enderit area, Kenya Msc Thesis University of Nairobi. Unpublished

Ward, S. H., 1990a: Geotechnical and Environmental Geophysics. Review and Tutorial, Society of Exploration Geophysicist I: 397

Weiss, M., Rubin, Y., Adar, E., Nativ, R., 2006: Fracture and Bedding Plane Control on Groundwater Flow in a Chalk Aquitard. Hydrogeology Journal 14: 1081–1093

List of Appendices

APPENDIX I

Bore holes Data

BOREHOLE NO.	Latitude	Longitude	Yield (m3/hr)	Drilled depth (M)	WSL	WRL	Control	VES Data
VES2	-1.70166	37.16415	25	185			Profile 10	
VES3	-1.70249	37.15669	8	128				
VES8	-1.69691	37.19574						
VES9	-1.69077	37.18269						
VES10	-1.67016	37.18722	0					
VES12	-1.68225	37.18496	0					
BH 1	-1.68806	37.18194						
BH 2	-1.67972	37.18417						
BH 4	-1.70028	37.15528						
BH 5	-1.70611	37.00444	0				Profile 11	
BH 6	-1.70194	37.16222						
BH 7	-1.69917	37.16333						

BH 8	-1.70339	37.17694	0					
BH 9	-1.70250	37.18417						
BH 10	-1.70583	37.18361	4.3				Profile 5	VES 6
BH 11	-1.70603	37.15439	0				Profile 14	
P100	-1.72211	37.13488		70.4				
P111	-1.67476	37.11429	0	61.31	0	0		
P129	-1.73394	37.12767	6.34	153.9	91.4	5.79		
P132	-1.73717	37.12935		81.08	60.05,70.10	50.9		
P149	-1.73996	37.12809	4.89	107.3	67.06,100.58	57.91		
C12	-1.72195	37.19389	0.5	107	91	44	Profile 2	
C74	-1.74274	37.20206	0.7	61	49	40		
C75	-1.72759	37.20235	0	61	0	0		
C120	-1.68019	37.14408	4.09	158.1	120,100.2,103.6	28.9		
C683	-1.68871	37.18194	0	183	70	56		
C925	-1.74919	37.17924	12	243.8	188.9	140.2		

C2034	-1.74833	37.19660	1.75	94.5	34	25.6		
C2544	-1.73937	37.13332	5.2	97.5		55.8		
C2612	-1.70522	37.16110	1.64	137	51,131	42		
C2613	-1.73814	37.13561	1.31	121	72,92	58,61		
C2912	-1.72166	37.20922	1.75	121	106.1	36.6		
C3399	-1.67317	37.14404		148	112.4	54		
C3416	-1.67508	37.16590	0.55	100	64	51		
C3462	-1.67337	37.12616	0.3		56.4,64	52.4		
C12953	-1.69135	37.16459	1.31	147	56.4	50		
C12963	-1.73525	37.13445	3	106	50,76,94	46		
C13510	-1.68410	37.16672	2	120	72	45.7		
C13511	-1.72577	37.13417	16	126	58,70,88,106	41.2	Profile 13	

APPENDIX II

Borehole VES Models

BOREHOLE VES 2 Model at Profile 10

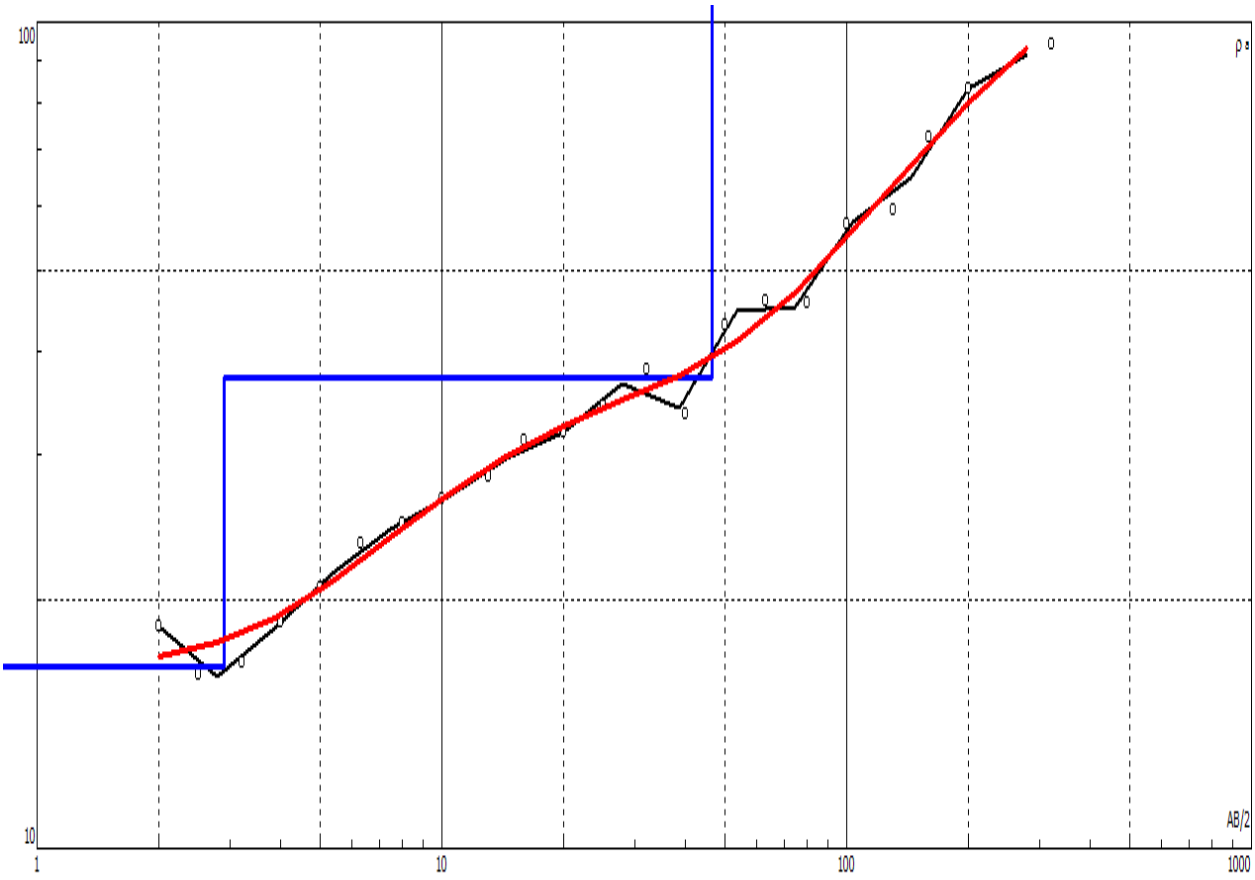

N	ρ	h	d	Alt
1	16.6	2.9	2.9	-2.905
2	37.1	43.6	46.5	-46.49
3	138			

BOREHOLE 10 VES 6 Model at Profile 5

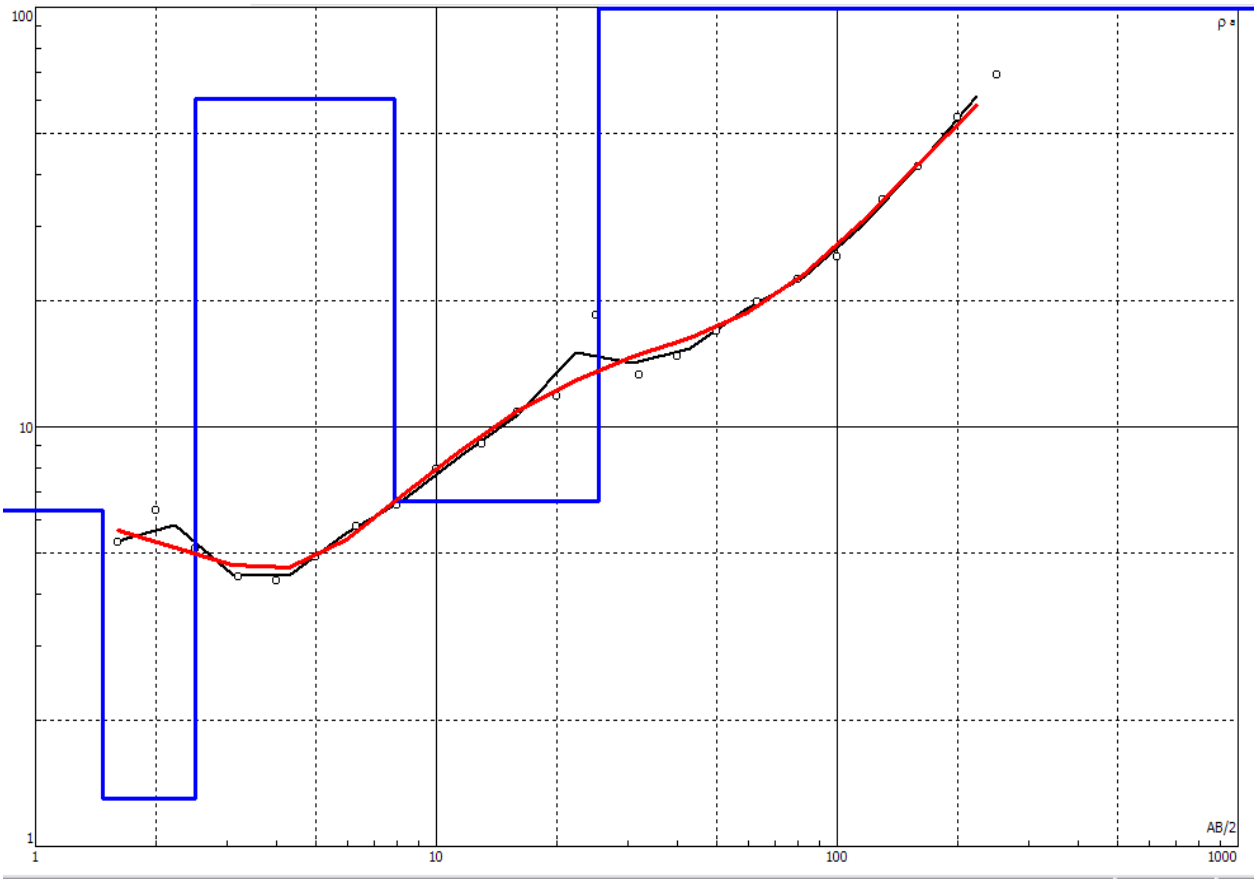

N	ρ	h	d	Alt
1	6.3	1.47	1.47	-1.47
2	1.3	1.04	2.51	-2.51
3	60.5	5.37	7.88	-7.88
4	6.63	17.6	25.5	-25.48
5	9583			

APPENDIX III

Borehole Logs

Borehole log – VES 1 with a Yield of 3.5 m^3/hr

DRILLED DEPTH

From (m)	To (m)	Geological Formation
0	1	Clay soil
1	9	Lateritic soil
9	13	Weathered granitoid gneiss
13	60	Fresh granitoid gneiss
60	64	Weathered biotite gneiss
64	83	Highly weathered biotite gneiss
85	115	Slightly weathered biotite gneiss
115	210	Fresh biotite gneiss

Borehole log – VES 6 with a Yield of 4.3 m^3/hr

DRILLED DEPTH

From (m)	To (m)	Geological Formation
0	0.5	Clay soil
0.5	14	Weathered granitoid gneiss
14	23	Weathered pegmatic quartzite
23	46	Fresh granitoid gneiss
46	78	Fresh biotite gneiss
78	110	Slightly weathered moist felspathic gneiss
110	210	Slightly weathered moist feldspathic-biotite gneiss

Borehole log – VES 6A with a dry borehole

DRILLED DEPTH

From (m)	To (m)	Geological Formation
0	0.5	Clay soil
0.5	14	Weathered granitoid gneiss
14	23	Slightly weathered pegmatic quartzite
23	46	Fresh granitoid gneiss
46	78	Fresh biotite gneiss
78	110	Slightly weathered moist felspathic gneiss
110	210	Slightly weathered moist feldspathic-biotite gneiss

Borehole log – VES 6B with a Yield of 0.9 m^3/hr

DRILLED DEPTH **Geological Formation**

From (m)	To (m)	
0	2	Clay soil
4	9	Lateritic soil
9	23	Slightly fracture granitoid gneiss
23	32	Slightly weathered biotite gneiss
32	69	Slightly fractured biotite gneiss
69	83	Highly weathered wet bitiote gneiss
83	92	Slightly fractured biotite gneiss
92	124	Fresh biotite gneiss

124	129	Slightly fractured biotite gneiss
129	138	Weathered biotite gneiss
138	220	Fresh compact biotite gneiss

Borehole log – VES 10 with a dry borehole

DRILLED DEPTH

From (m)	To (m)	Geological Formation
0	1.5	Clay soil
1.5	18	Fresh quartzite
18	32	Fresh granitoid gneiss
32	50	Slightly weathered granitoid gneiss
50	60	Slightly weathered granitoid gneiss
60	64	Slightly weathered moist biotite gneiss
64	78	Weathered biotite gneiss
78	92	Weathered biotite gneiss
92	152	Fresh biotite gneiss
152	170	Fresh biotite gneiss

Borehole log – VES 12 with a dry borehole

DRILLED DEPTH

From (m)	To (m)	Geological Formation
0	1.5	Clay soil
1.5	4	Weathered granitoid gneiss
4	32	Slightly weathered granitoid gneiss
32	42	Fractured feldspathic gneiss
42	56	Slightly weathered biotite gneiss
56	70	Fractured biotite gneiss
70	78	Fractured moist biotite gneiss
78	124	Fresh biotite gneiss
124	150	Fresh compact biotite gneiss